JOHANNES KEPLER
UNIVERSITÄT LINZ
Netzwerk für Forschung, Lehre und Praxis

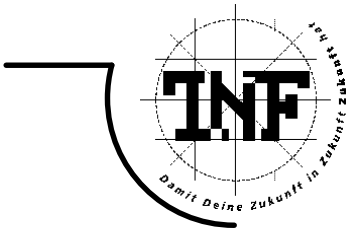

Numerical Simulation of Electrohydrodynamical Problems

Diplomarbeit

zur Erlangung des akademischen Grades

Diplomingenieurin

in der Studienrichtung

Technische Mathematik

Angefertigt am *Institut für Numerische Mathematik*

Betreuung:

Prof. Dr. Joachim Schöberl

Eingereicht von:

Larissa G. Vorhauer

Linz, December, 2007

Abstract

When lacquering in the classical way, i. e., by spraying just with compressed air, half of the material gets lost. Hence new techniques to avoid this exhaustive waste are investigated. This led to different approaches depending on the special needs. Considering automobile industry, charged spraying seems to be a promising idea. Here, corona discharge is used to charge the lacquer droplets in order to govern their motion with the help of an electric field. The aim of this thesis is to develop a simulation tool for this electrohydrodynamic (EHD) flow problem.
Apart from the lacquering and painting of parts, similar problems occur for particle filters such as in chimneys of factories, or in medical laboratory tests, for example to hold enzymes in a place where they can be observed.

The general three dimensional mathematical model of the EHD flow problem is based on Maxwell's equations, especially on Faraday's and Gauss' law. They lead to a non-linear system of partial differential equations for the electric field, the space charge density, and the current density.
For simplicity the corona discharge is treated as a surface process and included in the boundary conditions. The exact location is unknown and depends on the electric field strength what leads to a free boundary problem.

First we consider the diffusion dominated case of the two dimensional EHD problem. This case is numerically easier to treat, but in practice the convection dominates. The stationary case of the model is reformulated according to a Fermi-potential approach which was introduced for semiconductor equations. The obtained free boundary problem is treated in two different ways. The first (intuitive) approach directly iterates the position of the boundary. The second idea introduces the unknown position as a non-linear boundary condition.
A finite element discretization is done and the system of equations is solved with a combination of a Newton's method and a fixed point iteration.

Second we discuss the practically relevant convection dominated case. Therefore we focus on numerical methods for treating convection-diffusion equations. Different methods and stabilizations in primal and mixed formulation are analyzed and discussed. A careful comparison of several finite element methods is done. Roughly speaking, the edge-upwind

stabilization in mixed formulation gives best results as long as the boundary layer is not resolved by the discretization.
Consequently we apply edge-upwind stabilization in mixed variational formulation to the full time-dependent two dimensional EHD problem. Semi-discretization with finite elements is done and the resulting initial value problem for a system of ordinary differential equations is solved by time discretization with the implicit Euler method.

Zusammenfassung

Beim Lackieren mit reiner Druckluft, geht rund die Hälfte des Sprühguts verloren. Aus diesem Grund wird nach neuen Methoden gesucht, um den Verlust zu verringern. Zum Lackieren von Metallteilen, wie in der Automobilindustrie, bietet sich das elektrostatische Sprühen an. Dabei werden, durch eine Coronaentladung, die einzelnen Lacktröpfchen elektrisch aufgeladen, um ihre Bewegung dann mit Hilfe eines elektrischen Feldes beeinflussen zu können. Ziel dieser Arbeit ist die Entwicklung einer Software zur Simulation dieses elektrohydrodynamischen (EHD) Vorgangs.
Diese Methode wird nicht nur beim Lackieren von Werkstücken verwendet. Auch bei Partikelfiltern wie sie in Industrieschornsteinen verwendet werden, oder in medizinischen Labors um zum Beispiel Enzyme an einem Ort zur Untersuchung festzuhalten, wird diese Methode angewandt.

Das allgemeine dreidimensionale mathematische Model des EHD Flusses, wird anhand der Maxwellgleichungen, im Speziellen den Gesetzen von Faraday und Gauss, entwickelt. Das führt auf ein nichtlineares System partieller Differentialgleichungen für das elektrische Feld, die Raumladungsdichte und die Stromdichte.
Die Coronaentladung wird vereinfacht als Oberflächenprozess behandelt und in die Randbedingungen eingebunden. Die genaue Position des Coronaeffekts ist jedoch unbekannt und hängt von der Stärke des elektrischen Feldes ab. Damit ergibt sich ein freies Randwertproblem.

Zuerst betrachten wir den diffusionsdominierten Fall des EHD Problems im Zweidimensionalen. Hier ist die numerische Handhabung einfacher, aber im physikalisch korrekten Fall dominiert die Konvektion. Wir wenden einen Fermi-Potential Ansatz aus dem Forschungsgebiet der Halbleiterphysik auf das stationäre Model an. Das freie Randwertproblem wird auf zwei verschiedene Arten behandelt. Mit einem sehr intuitiven Zugang, bei dem die Position der Randbedingung iteriert wird, und durch die Einführung einer Randbedingung in der eine nichtlineare Abhängigkeit enthalten ist.
Das Problem wird mit Finiten Elementen diskretisiert und das Gleichungssystem mit einer Kombination aus Fixpunkt- und Newtoniteration gelöst.

Dann diskutieren wir den, in der Praxis relevanten, Fall mit dominierender Konvektion. Dazu betrachten wir zuerst numerische Methoden zur Behandlung von Konvektions-

Diffusionsgleichungen. Es werden verschiedene Methoden in primaler und gemischter Formulierung analysiert und diskutiert. Mehrere Finite Elemente Methoden werden miteinander verglichen. Es zeigt sich, dass die Edge-Upwind Stabilizierung in gemischter Formulierung die besten Ergebnisse liefert, solange die Randschicht nicht von der Diskretisierung aufgelöst wird.
Deshalb wird die Edge-Upwind Stabilisierung in gemischter Variationsformulierung auf das vollständige, zeitabhängige EHD Problem im Zweidimensionalen angewandt. Die Semidiskretisierung mit Finiten Elementen ergibt ein Anfangswertproblem für ein System gewöhnlicher Differentialgleichungen das wir mit der impliziten Euler Methode lösen.

Acknowledgments

First of all I want to express my thanks to my supervisor Prof. Joachim Schöberl, for giving me the chance to write this thesis. I am also grateful for inspiring discussions and vital hints during the development of this thesis and the associated implementations.
Furthermore, I am indebted to Sabine Zaglmayr for constructive remarks, her patience in answering all the questions that arose, and her valuable time.
I thank Dr. R. Sonnenschein from *DAIMLER AG, Research and Technology* in Stuttgart for initiating the present work and providing the pictures of the industrial application contained in the introductory Chapter 1.

Moreover I thank Astrid Sinwel and Herbert Egger for various discussions and help in programming and debugging attempts. In addition I thank Martin Huber and Clemens Pechstein for proof-reading. Their comments significantly improved the presentation. Thanks go to Veronika Pillwein for listening and to Tina Sommer for bolstering me.

Above all, special thanks go to Martin Aigner for his support, the moral backup, and the 'Ois wiad guat!'.

For her love and faith in me I am deeply beholden to my mother.

Last but not least I acknowledge the scientific environment of the Institute of Computational Mathematics, chaired by Prof. Ulrich Langer, and the Johann Radon Institute for Applied Mathematics at the Johannes Kepler University Linz. Especially the FWF START-Project Y-192 has to be mentioned for all technical, spatial, and personal support.

Larissa Vorhauer,
Linz, December 2007

Contents

Notations

In this thesis vector fields are denoted via bold face symbols.
The subscript $_h$ is used to keep a discrete entity apart from their continuous analogon.

Notations related to partial differential equations

Ω		open subset of $\mathbb{R}^n$
Γ	$= \partial\Omega$	boundary of the domain Ω
∇f	$= (\frac{\partial f}{\partial x_1}, \ldots, \frac{\partial f}{\partial x_n})$	gradient
$\operatorname{div} \boldsymbol{f}$	$= \sum_{i=1}^{n} \frac{\partial f_i}{\partial x_i}$	divergence of vector field
$\operatorname{curl} \boldsymbol{f}$	$= \nabla \times \boldsymbol{f}$	curl of vector field

Notations related to finite elements

$L_2(\Omega)$	space of square integrable functions on Ω
$H^m(\Omega)$	Sobolev space of L_2-functions with square integrable derivative up to order m
$\|.\|_m$	Sobolev norm of order m
$A(.,.)$	bilinear form
$f(.)$	linear form
V^*	dual space of V
V_h, Q_h	finite element spaces
φ_i	basis functions of V_h
$\mathcal{T}_h$	triangulation of Ω
$\overline{T}$	closure of element $T \subset \Omega$
$\mathring{T}$	interior of element T
$\mathcal{P}^p(T)$	set of polynomials of degree $\leqslant p$ over element T
$(T, \mathcal{P}_T, \Sigma_T)$	physical or global finite element T element domain $\mathcal{P}_T$ space of shape functions Σ_T set of nodal variables
$(\hat{T}, \mathcal{P}_{\hat{T}}, \Sigma_{\hat{T}})$	reference element
$H(\operatorname{div}, \Omega)$	$:= \{\boldsymbol{q} \in [L_2(\Omega)]^d \mid \operatorname{div} \boldsymbol{q} \in L_2(\Omega)\}$
$\mathcal{M}_p(\mathcal{T}_h)$	$:= \{v \in L_2(\Omega) \mid v_{\|_T} \in \mathcal{P}^p(T) \text{ for all } T \in \mathcal{T}_h\}$.
$\mathcal{L}_p(\mathcal{T}_h)$	$:= \{v \in H^1(\Omega) \mid v_{\|_T} \in \mathcal{P}^p(T),\ T \in \mathcal{T}_h\}$ with $p \geqslant 1$.
$\mathcal{RT}_0(T)$	$:= \{\boldsymbol{a} + b\,\boldsymbol{x} \mid \boldsymbol{a} \in \mathbb{R}^2,\ b \in \mathbb{R}\}$, local Raviart-Thomas space of order 0
$\mathcal{RT}_0(\mathcal{T}_h)$	$:= \{v \in [L_2(\Omega)]^2 \mid v \text{ normal continuous },\ v_{\|_T} \in \mathcal{RT}_0(T)\}$.
$\ker b$	$:= \{u \in V \mid b(u, q) = 0 \text{ for all } q \in Q\}$, kernel of b

Notations related to EHD problems

$\boldsymbol{B}$	magnetic flux
$\boldsymbol{E}$	electric field
Φ	electric potential
$\boldsymbol{D}$	electric displacement
ρ	space charge density
ε	electrical permittivity
$\boldsymbol{j}$	electric current density
b	mobility of the ions
$\boldsymbol{V}$	gas velocity
d	ions diffusion coefficient
$\boldsymbol{n}$	outer normal vector
ζ	Fermi potential

Chapter 1

Introduction

This thesis deals with mathematical modeling and numerical simulation of electrohydrodynamical (EHD) flow in air produced by electric corona discharge. The EHD problem is of high interest for many industrial applications. Apart from the lacquering and painting of parts, similar problems occur for particle filters such as in chimneys of factories, or in medical laboratory tests, for example to hold enzymes in a place where they can be observed.

Motivation

A very expensive part of the manufacturing process of cars is the lacquering of the car body. The lacquer itself is a quite expensive hi-tech product.

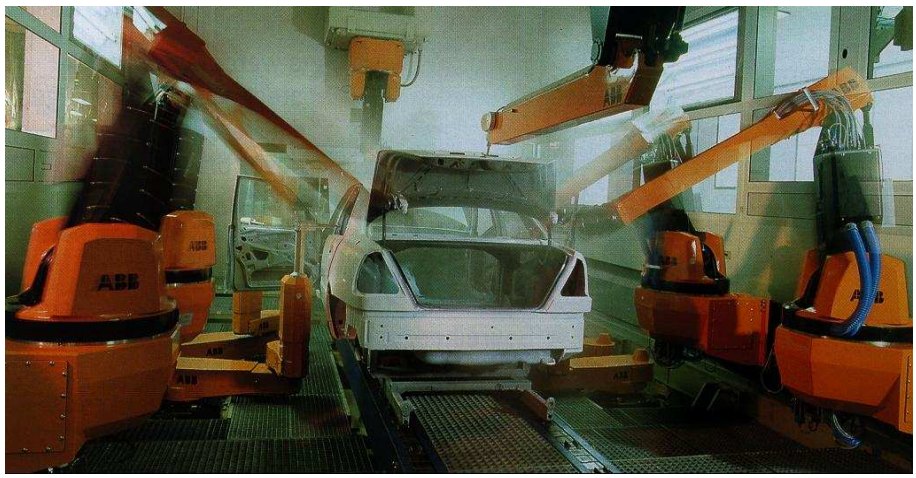

Figure 1.1: Robots already in use in the lacquering line. (Picture provided by DAIMLER AG.)

Therefore a lot of effort is put onto the reduction of wasted material. By just spraying lacquer with compressed air onto the car body about half of it gets lost.

One way of optimizing the recovery of the lacquer is the technique of charged spraying. The idea is to govern a flow with the help of electric fields. The benefits of charged spraying are among others more uniform coverage of target surfaces due to the mutual repulsion of the charged droplets and enhanced adhesion and deposition [26]. Owing to the advantages of this technology it is of high interest for companies. Some of them implemented it already in the lacquering line (cf. Figure 1.1). For the purpose of optimizing the efficiency of charged spraying even more, various settings need to be tested. Therefore simulations, containing a large number of different physical and chemical models to describe the complex process, are required.

Experimental setup

Various settings have been tested in experiments to investigate their effects. We consider the following experiment, which can be used for comparison to simulation results.
In order to minimize undesired effects the experiment takes place in a room where everything is electrically neutral (Figure 1.2), except the target (car door) and parts of the headpiece.

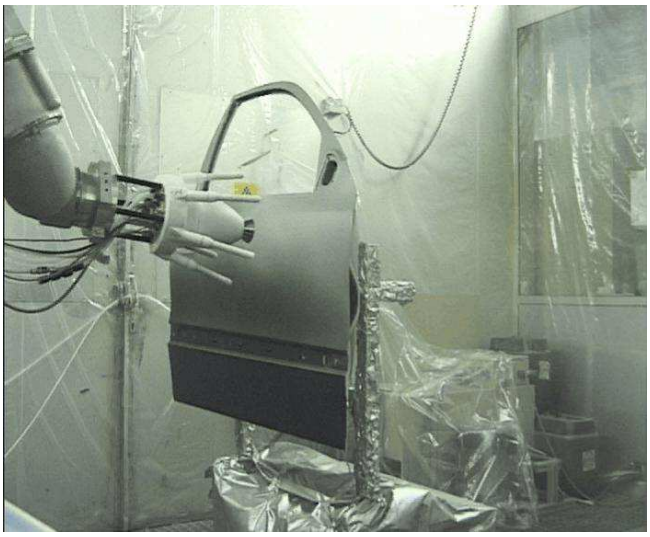

Figure 1.2: Experimental setup. (Picture provided by DAIMLER AG.)

Figure 1.3 shows a closer look at the headpiece, a typical vaporizer. The bell in the center has inlets for the lacquer. Due to the rotation of the bell, the lacquer is evaporated into droplets. A collection of fine fibers on the rim of the bell allows to influence the size of the droplets. Air inlets are arranged in a circle around the bell. The air supports the evaporation by the pneumatic force and the air entrainment transports the lacquer droplets towards the target [26]. When the airflow is deflected by the target, it drags along the small lacquer particles, for which the momentum is not enough to reach the surface of the

target. The efficency of the lacquering process can be increased by adding an additional force which makes the particles reach the target.

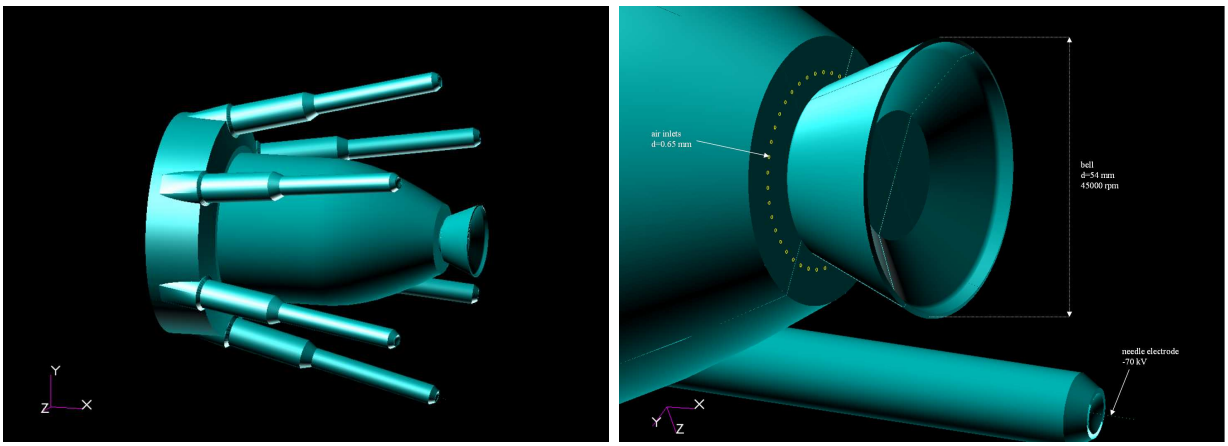

Figure 1.3: Close-up to the Ecobell-vaporizer. (Pictures provided by DAIMLER AG.)

One possibility of handling this problem is the already mentioned charged spraying. If the particles are ions (charged particles) one can influence their flow with an electric field. The electric field is built up by six electrodes which are arranged around the bell (cf. Figure 1.3).
Due to the high voltage applied to the electrode and the comparable small radius of the peak of the needle the air near the peak is ionized since electrons are split off the air molecules [11]. This effect is called corona discharge. While the positively charged ions are attracted by the electrodes the free electrons bind to the lacquer particles. Because of the positive voltage between target and needle, the Coulomb force drags the negatively charged lacquer particles towards the target.

Summing up, the whole carriage process is composed of

- the airflow,
- the ions carriage with self consistent electric field,
- and the particle movement.

A combination of several mathematical models is needed for the description of this process, e. g. the continuity equation as well as Navier-Stokes-equations for the flow and much more besides. It is computationally not feasible to resolve the very turbulent flow by Navier-Stokes-equations. Figure 1.4 shows a snapshot of the particle allocation during the lacquering process. Therefore especially the small vortices are additionally modeled as a stochastic process.

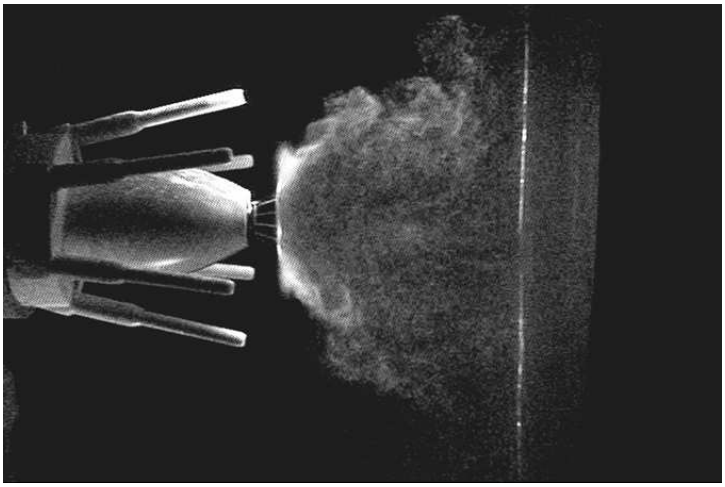

Figure 1.4: Ecobell-vaporizer in use; standard adjustment. (Picture provided by DAIMLER AG.)

Electric subproblem

From the whole carriage process described above we single out the electric subproblem causing the electrohydrodynamic (EHD) flow. Important quantities to describe the electric subproblem are the electric field, the space charge density and the current density. A crucial point concerns the boundary conditions for the space charge density on the corona electrode. Therefore we are especially interested in what happens around the needle.
A simplified model of the corona effect is to treat the corona discharge as a surface process and therefore incorporate it as a boundary condition. This is done by neglecting the thickness of the ionization layer and considering only the negative lacquer ions, moving with a constant mobility [2]. In the following we assume that there are no other forces on the ions than the electric field. The mass of the lacquer particles and their binding process with the free electrons are also neglected and only the flow of the charges is taken into account. So the unknowns of this model are the electric field and the space charge density.

We will see that even this subproblem is already a rather complex assignment due to nonlinear equations and boundary conditions.

The task of this thesis is to model and simulate the previously mentioned electric subproblem. The goal is to develop an appropriate numerical approach for solving the electric subproblem.

Organization of this thesis

- **Chapter 2: Problem Formulation**
  The mathematical model is derived from the physical background. The corresponding

governing equations for a general three dimensional setup are presented. We develop a simplified two-dimensional mathematical model and by means of a schematic computational domain the according boundary conditions are designed.

- **Chapter 3: Basic Concepts**
  We provide a brief summary of the numerical treatment of elliptic partial differential equations. In the course of a variational framework for the primal formulation we give an overview of the basic definitions and numerical realization of the finite element method (FEM). Furthermore we present a variational framework of mixed (dual) formulations. In this context we state some basics of the approximation properties of conforming FEM for mixed formulations to enable a-priori error estimates.

- **Chapter 4: The EHD Problem - The Fermi-Potential-Approach**
  The mathematical model can be transformed and treated in different ways. We apply an approach of the research field of semiconductor equations. The governing equations of the problem and the boundary conditions are reformulated according to the Fermi-potential ansatz. Two different approaches to treat the free boundary are described. Finally the numerical results are presented.

- **Chapter 5: The Convection-Diffusion Problem**
  In this chapter we concentrate on convection-diffusion problems. We analyze different methods and stabilizations in primal and mixed formulation and discuss them by means of a one dimensional example. These computations are done in the software package MATLAB.

- **Chapter 6: The EHD Problem with Edge-Upwind Stabilization**
  The whole time-dependent electrohydrodynamic system of equations is analyzed. An upwind scheme in mixed variables is applied. Semidiscretization with finite elements and time discretization with implizite Euler is done. Finally numerical results are given.

The implementation of the algorithms and the computations contained in the present work are done in the software package netgen/ngsolve (see www.hpfem.jku.at).

Chapter 2

Problem Formulation

Starting with the physical model of the electric subproblem, we derive the corresponding mathematical model. Accordingly we introduce the governing physical laws for a general three dimensional setup.

2.1 System of governing equations

The calculation of the electric field and the space charge density is the crucial step in the electrohydrodynamic (EHD) flow simulation.
Due to an electric corona discharge, electrons are injected from the ionization layer and form the space charge in the air gap between the two electrodes.
The model is based on Maxwell's equations, especially on Faraday's and Gauss' law.

We consider the electro-quasi-static case, where the magnetic flux $\boldsymbol{B}$ does not change with time. Due to Faraday's law of induction $-\frac{\partial \boldsymbol{B}}{\partial t} = \operatorname{curl} \boldsymbol{E}$ the curl of the electric field vanishes

$$\operatorname{curl} \boldsymbol{E} = 0.$$

In this case the electric field $\boldsymbol{E}$ can be characterized as a gradient field and can be described by the electric potential Φ as

$$\boldsymbol{E} = -\nabla\Phi. \tag{2.1}$$

Gauss' law states that the electric flux through a closed surface is determined by the electric charge enclosed in this surface. In differential form this reads as

$$\operatorname{div} \boldsymbol{D} = \rho, \tag{2.2}$$

where ρ denotes the space charge density and $\boldsymbol{D}$ the vector valued electric displacement.

The air between the electrodes is assumed to be a linear, homogeneous and isotropic material. The according constitutive law describes the relation be the electric field $\boldsymbol{E}$ and its displacement $\boldsymbol{D}$

$$\boldsymbol{D} = \varepsilon \boldsymbol{E}. \tag{2.3}$$

The electrical permittivity ε is in general a 3×3 tensor. For isotropic media it simplifies to a scalar. If the material is furthermore supposed to be linear, the permittivity ε is also independent of the electric field $\boldsymbol{E}$.

Therefore Gauss' law can be reformulated as

$$\operatorname{div} \varepsilon \boldsymbol{E} = \rho. \tag{2.4}$$

With the special form of the electric field (2.1), equation (2.4) yields the Poisson equation for the electric potential Φ, i. e.

$$-\operatorname{div} \varepsilon \nabla \Phi = \rho. \tag{2.5}$$

Next we discuss the electric current due to the moving charges.
The charge conservation law states that a change of the charge density in time in a certain domain has to lead to an in- or outflow of charges, and so implies electric currents. Therefore the electric current density $\boldsymbol{j}$ and the space charge density ρ are related via

$$\frac{\partial \rho}{\partial t} + \operatorname{div} \boldsymbol{j} = 0. \tag{2.6}$$

The electric current density consists of three main macroscopic contributions.
The first one arises from charged particles, which are accelerated by the Coulomb force and move towards the target. This causes a drift current expressed by $b \nabla \Phi \rho$ where b denotes the mobility of the ions.
Of course the movement of the charged particles is also influenced by the movement of the ambient gas. This transport caused by the flowing gas implies a current $\boldsymbol{V}\rho$ where $\boldsymbol{V}$ is the gas velocity.
The fact that charged particles tend to achieve a steady state causes a diffusion current given by $-d \nabla \rho$, where d denotes the diffusion coefficient of the ions.
Taking everything into account we get

$$\boldsymbol{j} = \underbrace{b \nabla \Phi \rho}_{\text{drift}} + \underbrace{\boldsymbol{V}\rho}_{\text{transport}} - \underbrace{d \nabla \rho}_{\text{diffusion}}. \tag{2.7}$$

We want to decouple equation (2.7) from the flow calculation. As mentioned in [25] it can be assumed that the drift velocity of ions in our application is about two orders of magnitude higher than the typical velocity $\boldsymbol{V}$ of the gas flow.
Therefore we can neglect the second term and equation (2.7) simplifies to

$$\boldsymbol{j} = b \nabla \Phi \rho - d \nabla \rho. \tag{2.8}$$

Remark 2.1. Equation (2.8) can also be derived from the Boltzmann equation formulated for one type of charge carriers, e. g. electrons. This can be done by moment methods (cf. [15], Chapter 2.3). The Boltzmann equation describes the evolution of a particle distribution (dependent on space, velocity, and time) in a fluid. It is used e. g. to study how a fluid transports physical quantities such as charged particles, and to derive transport properties.
A feature of the moment methods is the reduction of independent variables from seven (space, velocity, time) to only four (space, time). This is done by introducing the moments of the distribution function with respect to the velocity. Equations for the moments can be derived by multiplying the Boltzmann equation by powers of the velocity and integrating over the velocity space. The lowest order moments are related to physical quantities in a simple way and the resulting equations of the moment methods represent conservation laws. This system can be reduced to a drift diffusion model for the current density. In [15] this is used to derive a simple drift-diffusion model for semiconductor equations.

Summing up, we obtain the following non-linear system of partial differential equations

$$
\begin{aligned}
-\operatorname{div} \varepsilon \nabla \Phi &= \rho && && (2.9)\\
\frac{\partial \rho}{\partial t} + \operatorname{div} \boldsymbol{j} &= 0 && \text{for } (x,t) \in \Omega \times (0,T) && (2.10)\\
\boldsymbol{j} &= b \nabla \Phi \, \rho - d \nabla \rho, && && (2.11)
\end{aligned}
$$

for the unknowns Φ (electric potential), ρ (space charge density), and $\boldsymbol{j}$ (current density). Note the non-linear dependency in the drift term in (2.11). Assuming a steady state equation (2.10) reduces to

$$\operatorname{div} \boldsymbol{j} = 0 \qquad \text{for } x \in \Omega. \tag{2.12}$$

2.2 Boundary conditions

For technical simplification we reduce our mathematical model to two dimensions and investigate the following problem setting. From now on we consider the schematic computational domain shown in Figure 2.1, which describes the air surrounding the electrode and the target as our domain of interest. The electrode and the target are resolved by the boundary. The electrode is modeled in form of a needle. Its boundary is split into two parts $\Gamma_{co} \cup \Gamma_{el \setminus co} = \Gamma_{el}$. We have to treat the peak of the needle Γ_{co} separately, because in a subarea of this region the corona discharge occurs. The shaft of the needle $\Gamma_{el \setminus co}$ is insulated. The target is represented by the boundary Γ_{ta}. We truncate the two dimensional plane by introducing the artificial boundary Γ_{out}. Considering the physics behind the problem we are able to state the appropriate boundary conditions. On each boundary we need a condition for either the potential Φ or the normal component of the electric displacement $\boldsymbol{D}$ as well as one for either the space charge density ρ or the normal current density $\boldsymbol{j}$.
In the following we refer to the outer normal vector of the boundary by $\boldsymbol{n}$.

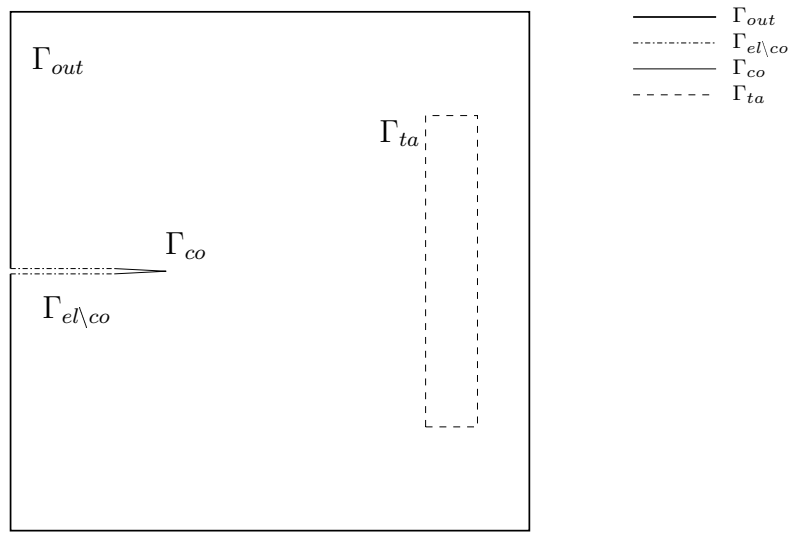

Figure 2.1: Computational domain.

Boundary conditions for the potential

The boundary conditions on the potential are straightforward. If we truncate the computational domain Ω far enough from the needle and the target, we are allowed to assume no charges near the boundary. Consequently we impose Neumann boundary conditions on the outer boundary, i. e.

$$\varepsilon \nabla \Phi \cdot \boldsymbol{n} = 0 \qquad \text{on } \Gamma_{out}. \tag{2.13}$$

Furthermore we know the values for the potential at the target and the electrode. The target is grounded, hence the potential there has to be zero. At the needle a negative voltage is applied, and we fix the potential to $\Phi_e < 0$ with respect to ground. The appropriate boundary conditions for this case are Dirichlet conditions on the target and on the electrode,

$$\Phi = \quad 0 \qquad \text{on } \Gamma_{ta}, \tag{2.14}$$

$$\Phi = \quad \Phi_e \qquad \text{on } \Gamma_{el} = \Gamma_{co} \cup \Gamma_{el\backslash co}. \tag{2.15}$$

Boundary conditions for the space charge density

Analog to the Neumann boundary condition for the potential on the outer boundary Γ_{out}, we assume that no electric current flows in normal direction of Γ_{out}, i. e.

$$\boldsymbol{j} \cdot \boldsymbol{n} = 0 \qquad \text{on } \Gamma_{out}. \tag{2.16}$$

The remaining boundary conditions for the space charge density are more involved. From physics we know that the charges of the particles are neutralized at Γ_{ta}. The space charge density ρ does not change with respect to the outer normal direction to this boundary, i. e.

$$\nabla \rho \cdot \boldsymbol{n} = 0 \qquad \text{on } \Gamma_{ta}. \tag{2.17}$$

With these two equations and the relation between current density and space charge density (2.8), we can reformulate the boundary conditions for the variable of interest. If we multiply equation (2.8) by the normal vector $\boldsymbol{n}$ we get

$$\boldsymbol{j} \cdot \boldsymbol{n} = b\,\nabla\Phi\,\rho \cdot \boldsymbol{n} - d\,\nabla\rho \cdot \boldsymbol{n}.$$

The diffusion term vanishes on Γ_{ta} according to equation (2.17). Hence, the boundary condition for the current density is

$$\boldsymbol{j} \cdot \boldsymbol{n} = b\,\nabla\Phi\,\rho \cdot \boldsymbol{n} \qquad \text{on } \Gamma_{ta}. \tag{2.18}$$

Setting up the boundary conditions for the space charge density on the electrode is much more sophisticated and requires a more detailed discussion of the corona discharge, which will lead to a free-boundary condition.

In the 'active' region $\Gamma_{co,a} \subset \Gamma_{co}$, where the corona effect occurs, the corona onset, the generated free electrons follow the direction of the electric field and therefore $\boldsymbol{j} \cdot \boldsymbol{n} > 0$ holds. On the remaining 'inactive' part of Γ_{co}, lets call it $\Gamma_{co,i} := \Gamma_{co} \backslash \Gamma_{co,a}$, $\boldsymbol{j} \cdot \boldsymbol{n} = 0$ has to be fulfilled. Because of the insulation this is also fulfilled on $\Gamma_{el \backslash co}$. Summarizing this, we get

$$\left.\begin{array}{ll} \boldsymbol{j} \cdot \boldsymbol{n} = 0 & \text{on } \Gamma_{el} \backslash \Gamma_{co,a} \\ \boldsymbol{j} \cdot \boldsymbol{n} > 0 & \text{on } \Gamma_{co,a} \end{array}\right\} \Rightarrow \boldsymbol{j} \cdot \boldsymbol{n} \geqslant 0 \qquad \text{on } \Gamma_{el}. \tag{2.19}$$

From the mathematical point of view a boundary condition for the charge density or the current density is needed on the injector Γ_{co}, but physically the corona discharge depends on the electric field strength [2]. On the boundary the vector field $\boldsymbol{E}$ can be decomposed into a normal $E_n \boldsymbol{n}$ and a tangential $\boldsymbol{E}_\tau$ component

$$\boldsymbol{E} = E_n \boldsymbol{n} + \boldsymbol{E}_\tau.$$

Since $\boldsymbol{E} = -\nabla\Phi$ and Φ is constant on the boundary Γ_{el} (2.15), the tangential part $\boldsymbol{E}_\tau$ vanishes, i. e. $\boldsymbol{E}_\tau = 0$. Since in our special problem setting (with $\Phi_e < 0$) E_n is a positive scalar and we obtain $|\boldsymbol{E}| = E_n$.
In general, the electric field increases proportionally to the voltage. But Kaptzov's hypothesis [9] states that the electric field preserves its value at the corona onset, after the corona effect is initiated. Hence there exists a threshold strength of the electric field E_{co} for the corona onset, i. e.

$$\left.\begin{array}{ll} E_n = E_{co} & \text{on } \Gamma_{co,a} \\ E_n < E_{co} & \text{on } \Gamma_{el} \backslash \Gamma_{co,a} \end{array}\right\} \Rightarrow E_n \leqslant E_{co} \qquad \text{on } \Gamma_{el}, \tag{2.20}$$

but the corona onset $\Gamma_{co,a}$ is a free boundary. We point out that one of the inequalities (2.19) and (2.20) is always sharp. Therefore we can write

$$(\boldsymbol{j} \cdot \boldsymbol{n})\,(E_n - E_{co}) = 0 \qquad \text{on } \Gamma_{el}. \tag{2.21}$$

A further discussion of the corona discharge will be done in the context of the two different approaches for handling this effect and is postponed to Section 4.3.1 on page 31.

Summarizing, we have to face two challenges in our problem. First, the non-linearity of the system (2.9)-(2.11) of partial differential equations. Secondly, the free boundary value problem due to the effect of the corona discharge.

Chapter 3

Basic Concepts

This chapter contains a brief summary of the numerical treatment of elliptic partial differential equations. Therefore a variational framework of the primal formulation in use is presented at the beginning. The corresponding existence and uniqueness result and the needed function spaces L_2 and H^1 are also outlined.
In the course of the primal formulation we give an overview of the basic analysis, the design, and the numerical realization of the finite element method (FEM). We dwell on the FEM and some essential definitions as the Galerkin approximation, the construction of the finite dimensional space $V_h \subset V$, the triangulation $\mathcal{T}_h$, and the finite element itself. Furthermore some basics of the approximation properties of conforming FEM for the primal formulation are stated.
In the second part of this chapter a variational framework of mixed (dual) formulations is presented. The corresponding existence and uniqueness results as well as the additionally needed function space $H(\mathrm{div})$ are discussed. The general definitions of the FEM also apply here. In this context we shortly introduce the lowest-order Raviart-Thomas element which is $H(\mathrm{div})$-conforming. Some basics of the approximation properties of conforming FEM for mixed formulations are stated to enable a-priori error estimates.
Finally, we list some fundamental formulas which we make use of in subsequent chapters.

3.1 Variational framework and FEM discretization for primal formulations

As a simple example we consider the Poisson problem

$$-\Delta u = f \qquad \text{in } \Omega \subset \mathbb{R}^d \tag{3.1}$$

with Dirichlet boundary conditions

$$u = 0 \qquad \text{on } \Gamma. \tag{3.2}$$

Now we derive the variational formulation as follows. We multiply (3.1) by a suitable test function and integrate over the domain Ω. Integration by parts yields

$$\int_\Omega \nabla u \cdot \nabla v \, dx = \int_\Omega f \, v \, dx. \tag{3.3}$$

Existence of the integrals is ensured if we require $|\nabla u|^2$, $|\nabla v|^2$, $|f|^2$, and $|v|^2$ to be integrable. This leads us to the natural function spaces of this variational formulation which are subject of the next definition.

Definition 3.1. Function spaces. *We define the Hilbert spaces*

$$L_2(\Omega) := \{v \mid \int_\Omega v^2 \, dx < \infty\},$$
$$H^1(\Omega) := \{v \in L_2(\Omega) \mid \nabla v \in [L_2(\Omega)]^d\},$$

with their corresponding scalar products

$$(u, v)_0 := \int_\Omega uv \, dx,$$
$$(u, v)_1 := (\nabla u, \nabla v)_0 + (u, v)_0,$$

respectively. The corresponding norms are referred to as $\|.\|_0$ and $\|.\|_1$. Additionally we define a function space with essential boundary conditions

$$H_0^1(\Omega) := \{v \in H^1(\Omega) \mid v_{|\Gamma} = 0\}.$$

Motivated by (3.3) we introduce the following abstract form of variational problems.

Find $u \in V$ such that

$$A(u, v) = f(v) \qquad \text{for all } v \in V, \tag{3.4}$$

where $A(.,.)$ is a bilinear form and $f(.)$ a linear form. In the following we state some definitions and well known results for further usage. For proofs we refer the reader to [3] and [4].

3.1.1 Existence and Uniqueness

Definition 3.2. *A bilinear form $A(.,.)$ on a normed linear space H is said to be*

1. coercive *if there exists a constant $\alpha_1 > 0$ such that*

$$A(v, v) \geqslant \alpha_1 \|v\|_H^2 \qquad \textit{for all } v \in H$$

2. continuous (bounded) *if there exists a constant* $\alpha_2 > 0$ *such that*

$$|A(u,v)| \leqslant \alpha_2 \|u\|_H \|v\|_H \qquad \textit{for all } u, v \in H$$

Theorem 3.3. (Lax-Milgram) *Given a real Hilbert space* $(V,(.,.))$*, a continuous linear functional* $f \in V^*$ *and a continuous, coercive bilinear form* $A : V \times V \to \mathbb{R}$*, there exists a unique solution* $u \in V$ *such that*

$$A(u,v) = f(v) \qquad \textit{for all } v \in V$$

and u *satisfies*

$$\|u\|_V \leqslant \frac{1}{\alpha_1} \|f\|_{V^*}.$$

3.1.2 The Galerkin Approximation

In general, problems of the form (3.4) can not be solved analytically. Instead approximative techniques have to be used. A well known concept for constructing discrete approximations of the exact solution of variational problem (3.4) is the concept of conforming discretization methods. There the infinit-dimensional problem is restricted to a finite-dimensional subspace V_h of V. This leads to a Galerkin approximation where (3.4) is replaced by the discret variational problem

Find $u_h \in V_h$ such that

$$A(u_h, v_h) = f(v_h) \qquad \text{for all } v_h \in V_h. \tag{3.5}$$

Corollary 3.4. *Replacing the Hilbert space* V *by a (closed) finite dimensional subspace* $V_h \subset V$ *does not change the existence and uniqueness results obtained by Lax-Milgram theorem 3.3.*

Let $\{\varphi_i\}_{i=1,\ldots,N_h}$ be a basis of V_h. Then we can expand any $v_h \in V_h$ in terms of this basis,

$$v_h(x) = \sum_{i=1}^{N_h} v_i \, \varphi_i(x).$$

Owing to the linearity of $A(.,.)$ and $f(.)$, it is enough to test the discrete variational problem (3.5) only with the basis functions. With the definitions

$$\underline{\underline{A}}_h := (A(\varphi_i, \varphi_j))_{1 \leqslant i,j \leqslant N_h}, \quad \underline{u}_h := (u_i)_{1 \leqslant i \leqslant N_h}, \quad \text{and} \quad \underline{f}_h := (f(\varphi_j))_{1 \leqslant j \leqslant N_h}$$

the original discrete variational problem (3.5) is equivalent to the Galerkin system

$$\underline{\underline{A}}_h \underline{u}_h = \underline{f}_h. \tag{3.6}$$

3.1.3 Basic concepts of the Finite Element Method

For a more detailed but easily accessible discussion of the finite element methods we refer the reader to [3], [6] and [4].

The finite element method (FEM) is a special Galerkin method that follows certain principles in the construction of the subspaces V_h. The three major aspects of this construction are as follows

- A triangulation $\mathcal{T}_h$ is established, covering the domain $\overline{\Omega} \subset \mathbb{R}^d$, i. e. $\overline{\Omega}$ is written as a finite union of sub domains $T \in \mathcal{T}_h$ with the properties stated below.
- The functions in the finite element space V_h are chosen to be piecewise polynomials, i. e. $v_{h|_T} \in \mathcal{P}^p(T)$ for $p \in \mathbb{N}$, $T \in \mathcal{T}_h$.
- A basis $\{\varphi_i\}$ of V_h with local support is used, i. e. each basis function φ_i is non-zero only on a few elements.

Due to the local support of the basis functions φ_i the matrix $\underline{\underline{A}}_h$ of the Galerkin system (3.6) is sparse. Hence iterative solvers can be applied for efficiency and fast solving.

The Triangulation

We assume the domain Ω to be an open, bounded domain with a Lipschitz continuous boundary.

Definition 3.5. *$\mathcal{T}_h$ is called a triangulation of $\Omega \subset \mathbb{R}^d$, if it consists of subsets T which satisfy the following conditions.*

1. *The triangulation $\mathcal{T}_h$ is a covering of Ω:*

$$\overline{\Omega} = \bigcup_{T \in \mathcal{T}_h} T.$$

2. *Each element T is a closed domain with a nonempty connected interior:*

$$\forall\, T \in \mathcal{T}_h : T = \overline{\mathring{T}}, \mathring{T} \neq \varnothing \text{ and } T \text{ is connected.}$$

3. *Each element T has a Lipschitz-continuous boundary:*

$$\forall\, T \in \mathcal{T}_h : \partial T \text{ is Lipschitz-continuous.}$$

4. *The elements are non-overlapping, i. e.*

$$\mathring{T}_i \cap \mathring{T}_j = \varnothing \quad \text{for } i \neq j.$$

5. *The intersection $T_i \cap T_j$ of two distinct elements ($i \neq j$) is either empty, a vertex, an edge or a face (if $d = 3$) of both elements:*

$$\forall\, T_i, T_j \in \mathcal{T}_h : i \neq j \Rightarrow T_j \cap T_j = \begin{cases} \varnothing, \\ \textit{vertex}, \\ \textit{edge}, \\ \textit{face}. \end{cases}$$

Throughout this thesis we consider quasi-uniform triangulations according to the following definitions (cf. [6]).

Definition 3.6. *A family of triangulations $\mathcal{T}_h$ is called* regular *if there exists a constant $\kappa > 0$ such that every $T \in \mathcal{T}_h$ contains a ball with radius r_T satisfying*

$$\frac{h_T}{r_T} \leqslant \kappa \quad \textit{for all } T \in \bigcup \mathcal{T}_h,$$

where h_T denotes half the diameter of T and if the quantity

$$h = \max_{T \in \mathcal{T}_h} h_T$$

approaches zero.

Definition 3.7. *A family of triangulations $\mathcal{T}_h$ satisfies an* inverse assumption *if there exists a constant $\nu > 0$ such that*

$$\frac{h}{h_T} \leqslant \nu \quad \textit{for all } T \in \bigcup \mathcal{T}_h.$$

Definition 3.8. *A regular family of triangulations that satisfies an inverse assumption is called* quasi-uniform.

The Finite Element

According to [4] we follow Ciarlet's specification [6] of a finite element. It contains three basic definitions for the construction of a finite element.

Definition 3.9. *Let*

1. *the* element domain *$T \subseteq \mathbb{R}^n$ be a bounded closed set with nonempty interior and piecewise smooth boundary,*
2. *the space of* shape functions *$\mathcal{P}_T$ be a finite dimensional space of functions on T, and*
3. *the set of* nodal variables *$\Sigma_T = \{N_1^T, \ldots, N_k^T\}$, also referred to as degrees of freedom, be a basis for $\mathcal{P}_T^*$, where $\mathcal{P}_T^*$ denotes the dual space of $\mathcal{P}_T$.*

Then we call the triple $(T, \mathcal{P}_T, \Sigma_T)$ a finite element.

Definition 3.10. *Let $(T, \mathcal{P}_T, \Sigma_T)$ be a finite element. The basis $\{\varphi_1, \ldots, \varphi_k\}$ of $\mathcal{P}_T$ is called the* nodal basis *of $\mathcal{P}_T$, if it is dual to the set of nodal variables Σ_T, i. e. $N_i(\varphi_j) = \delta_{ij}$.*

The reference element and its transformation

The finite element $(T, \mathcal{P}_T, \Sigma_T)$ is also called physical or global finite element. For practical implementation and simplification of design and analysis of the FE-method the mapping idea is used. First one constructs a local basis (shape functions) on the reference element $(\hat{T}, \mathcal{P}_{\hat{T}}, \Sigma_{\hat{T}})$. Here $\hat{T}$ is of simple shape (e. g. the unit triangle in 2D, see Figure 3.1). Furthermore the functions are mapped onto the physical element $T \in \mathcal{T}_h$ by a conforming transformation. One of the advantages of this approach is the possibility to perform many computations (e. g., numerical integration, derivation) a-priori on the reference element.

The transformations of the reference element to physical elements have to be continuously differentiable bijections. A special case of such transformations are the affine linear maps. They ensure that polynomials are mapped to polynomials of the same degree. This simplifies the analysis of the finite element method.

The entirety of the considerations above can be summarized with the following definition for finite element spaces.

Definition 3.11. *A family of finite element spaces V_h on triangulations $\mathcal{T}_h$ of $\Omega \subset \mathbb{R}^d$ is called an* affine family*, if there exists an element $(\hat{T}, \mathcal{P}_{\hat{T}}, \Sigma_{\hat{T}})$ with the following properties:*

- *For all $T_j \in \bigcup \mathcal{T}_h$ there exists an affine mapping $F_j : \hat{T} \to T_j$, such that for every $v \in V_h$ the restriction onto T_j is of the form*

  $$v(x) = p(F_j^{-1}x) \qquad \text{with } p \in \mathcal{P}_{\hat{T}}.$$

  The mapping is affine, i. e.,

  $$F_j(\hat{\boldsymbol{x}}) := \boldsymbol{b}_j + B_j\,\hat{\boldsymbol{x}} \qquad \text{with } B_j \in \mathbb{R}^d_d,\ \boldsymbol{b}_j \in \mathbb{R}^d.$$

- *Moreover all functionals $\ell \in \Sigma_T$ are of the form $\ell(v) = \hat{\ell}(p)$ with $p = v \circ F$ and $\hat{\ell} \in \Sigma_{\hat{T}}$.*

For more details on such transformations we refer the reader to the standard FEM literature as mentioned at the beginning of Section 3.1.3. From now on we consider only affine families of triangular elements.

Conforming finite element space

If $V_h \subset V$ holds, V_h is a conforming finite element space. We introduce the classical lowest-order finite element used for H^1-conforming methods.

Definition 3.12. *(The linear H^1-conforming finite element.) The classical lowest-order H^1-conforming finite element for the simplex $T \in \mathbb{R}^d$ (a segment for $d = 1$ and a triangle for $d = 2$), is defined by*

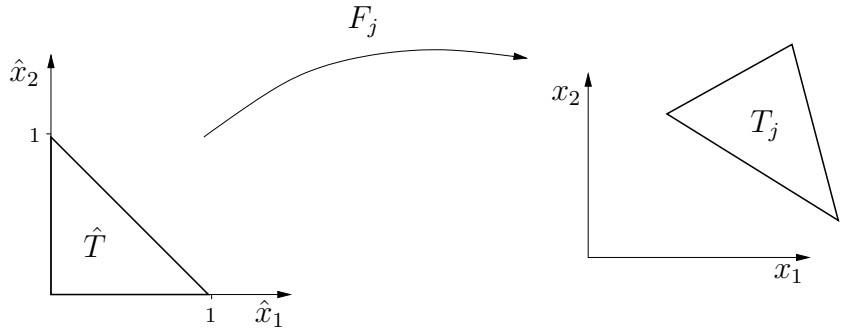

Figure 3.1: The mapping of a reference element $\hat{T}$ to a physical element T_j in 2D.

- *the local space* $\mathcal{P}_T = P^1(T)$ *of dimension* $\dim(P^1(T)) = d + 1$,
- *the* $(d + 1)$ *vertex-based degrees of freedom (dofs), which corresponds to point-evaluation at the vertices, i. e.*

$$N_i^V \quad : \quad v \to v(V_i) \quad \textit{for all } V_i \in \mathcal{V}_T,$$

where $\mathcal{V}_T$ *denotes the local set of vertices belonging to the element* T*.*

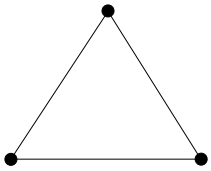

Figure 3.2: The 2-dimensional nodal H^1-conforming finite element. The dots illustrate the degrees of freedom.

The corresponding global space is continuous and piecewise linear (such that $V_h \subset H^1(\Omega)$)

$$V_h = \mathcal{L}_1(\mathcal{T}_h) := \{v \in L_2(\Omega) \mid v \text{ continuous}, \ v_{|_T} \in \mathcal{P}^1(T) \text{ for all } T \in \mathcal{T}_h\}.$$

Remark 3.13. Basis functions.
The corresponding nodal basis are the well known hat functions (see Figure 3.3 for 1D) defined as $v_{|_T} \in \mathcal{P}_1(T)$ *with* $v_j(V_i) = \delta_{ij}$*.*

More general we consider $V_h^p \subset V$ continuous and piecewise polynomial of degree p

$$V_h^p = \mathcal{L}_p(\mathcal{T}_h) := \{v \in H^1(\Omega) \mid v_{|_T} \in \mathcal{P}^p(T), \ T \in \mathcal{T}_h\} \quad \text{with } \ p \geqslant 1.$$

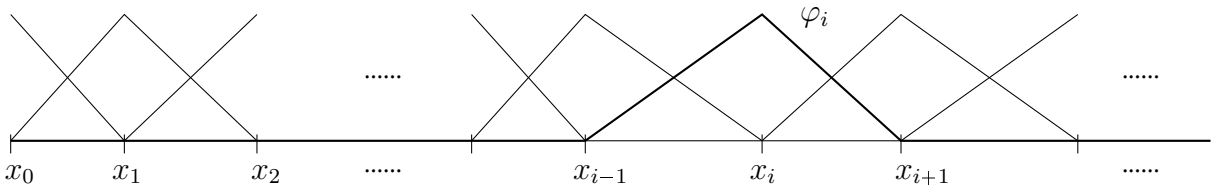

Figure 3.3: Hat functions: Lowest-order basis function in one dimension for H^1-conforming function space.

3.1.4 Approximation properties of conforming FEM

For a coercive problem the Lax-Milgram theorem states the existence of a unique solution $u \in V$ of (3.4). Due to conformity $V_h \subset V$ it also states existence of a unique discrete solution $u_h \in V_h$ of (3.5). Céa's Lemma states that the energy norm of the discretization error $\|u - u_h\|_V$ is proportional to the approximation error.

Lemma 3.14. (Céa) *Suppose that the variational problem* (3.4) *fulfills the assumptions of Lax-Milgram (Theorem 3.3). Let $u \in V$ denote the exact solution of* (3.4).
Let V_h be a subspace of the Hilbert space V and $u_h \in V_h$ the solution of the discrete problem (3.5).
Then the discretization error $u - u_h$ *can be estimated by the* approximation error *as follows:*

$$\|u - u_h\|_V \leqslant \frac{\alpha_2}{\alpha_1} \inf_{v_h \in V_h} \|u - v_h\|_V,$$

where α_2 is the continuity constant and α_1 the coercivity constant of $A(.,.)$ on V.

Up to a constant factor we obtain the best approximation within the function space V_h in the energy norm. Now the accuracy of the approximation depends on the choice of the function space and its interpolation properties for the solution u.

According to the embedding theorems $H^m(\Omega) \subset C^0(\Omega)$ for $m > \frac{d}{2}$ (see [1]), i. e., every $v \in H^m$ can be identified with a continuous function. Thus the interpolation operator π_h is well defined and $v_h = \pi_h v \in V_h$ is the continuous and piecewise linear function which coincides with v at the nodes x_i.
The interpolation error $\|u - \pi_h u\|_V$ is obviously an upper bound for the best approximation error.

Theorem 3.15. (Approximation theorem) *Let $\mathcal{T}_h$ be a quasi-uniform triangulation of Ω. Corresponding to this triangulation let $m \geqslant 1$ and define the mesh-dependent semi norm and the mesh-dependent norm*

$$|v|_{m,h} := \sqrt{\sum_{T \in \mathcal{T}_h} |v|^2_{m,T}}, \qquad \|v\|_{m,h} := \sqrt{\sum_{T \in \mathcal{T}_h} \|v\|^2_{m,T}}.$$

Then we obtain for the interpolation with piecewise polynomials of degree $p \geqslant 1$ with a constant $C = C(\Omega, \kappa, p)$

$$\|u - \pi_h u\|_{m,h} \leqslant C\, h^{n-m} |u|_{n,h} \quad \textit{for } u \in C(\Omega),\ u \in H^n(T),\ T \in \mathcal{T}_h \tag{3.7}$$

with $0 \leqslant m \leqslant n \leqslant p+1$.

Certainly $\|v\|_{m,h} = \|v\|_{m,\Omega}$ for $v \in H^m(\Omega)$. Of course the semi norm $|.|_{n,h}$ on the right hand side of (3.7) can be replaced by the full norm $\|.\|_{n,h}$. Therefore the Approximation Theorem 3.15 can also be written as

$$\|u - \pi_h u\|_{m,h} \leqslant C\, h^{n-m} \|u\|_{n,h} \quad \text{for } u \in C(\Omega),\ u \in H^n(T),\ T \in \mathcal{T}_h$$

with $0 \leqslant m \leqslant n \leqslant p+1$. Especially, for any $u \in H^{p+1}(\Omega)$ there exists an interpolant $\pi_h u \in V_h$ such that the interpolation error in $L_2(\Omega)$ and $H^1(\Omega)$ can be estimated as

$$\|u - \pi_h u\|_0 \leqslant Ch^{p+1} \|u\|_{p+1}, \tag{3.8}$$

$$\|u - \pi_h u\|_1 \leqslant Ch^{p} \|u\|_{p+1}. \tag{3.9}$$

3.2 Variational framework and FEM discretization for mixed formulations

We want to formulate the second order equation forming the Poisson problem (3.1) as a system of first order equations.

$$\nabla u = \boldsymbol{p}, \tag{3.10a}$$

$$\operatorname{div} \boldsymbol{p} = -f. \tag{3.10b}$$

This formulation has the advantage that the flux $\boldsymbol{p}$ becomes an explicit side product.
Now we proceed similar as described for (3.1). Multiplying by suitable test functions $\boldsymbol{q}$ and v, integrating over the domain and integrating by parts in (3.10a) yields the dual mixed formulation

$$\begin{aligned} \int_\Omega \boldsymbol{p}\,\boldsymbol{q}\,dx \quad + \int_\Omega \operatorname{div}\boldsymbol{q}\, u\,dx &= 0 && \text{for all } \boldsymbol{q}, \\ \int_\Omega \operatorname{div}\boldsymbol{p}\, v\,dx &= -\int_\Omega f\, v\,dx && \text{for all } v. \end{aligned} \tag{3.11}$$

In order to ensure the existence of all integrals, we have to identify suitable function spaces for u, v, $\boldsymbol{p}$ and $\boldsymbol{q}$. All of them have to be square integrable and for $\boldsymbol{p}$ and $\boldsymbol{q}$ also their divergences have to be in $L_2(\Omega)$. Therefore $\boldsymbol{p}, \boldsymbol{q} \in H(\operatorname{div}, \Omega)$ with the following definition.

Definition 3.16. Function space. *We define the vector-valued Hilbert space*

$$H(\mathrm{div}, \Omega) := \{\boldsymbol{q} \in [L_2(\Omega)]^d \mid \mathrm{div}\, \boldsymbol{q} \in L_2(\Omega)\}$$

with its corresponding scalar product

$$(\boldsymbol{p}, \boldsymbol{q})_{\mathrm{div}} := (\mathrm{div}\, \boldsymbol{p}, \mathrm{div}\, \boldsymbol{q})_0 + (\boldsymbol{p}, \boldsymbol{q})_0.$$

The corresponding norm is referred to as $\|.\|_{\mathrm{div}}$.

Problems of the form (3.11) are called saddle-point problems and can be specified as a mixed problem of the following general type.

Find $u \in V$ and $p \in Q$ such that

$$\begin{aligned} a(u, v) + b(v, p) &= f(v) && \text{for all } v \in V, \\ b(u, q) &= g(q) && \text{for all } q \in Q. \end{aligned} \tag{3.12}$$

As a notation remark we want to state here, that the mixed variational problem (3.12) can also be formulated with the help of a compound space.

Find $(u, p) \in V \times Q$ such that

$$B(u, p\,;\, v, q) = \tilde{f}(v, q) \qquad \text{for all } (v, q) \in V \times Q \tag{3.13}$$

with

$$\begin{aligned} B(u, p\,;\, v, q) &:= a(u, v) + b(u, q) + b(v, p), \\ \tilde{f}(v, q) &:= f(v) + g(q). \end{aligned} \tag{3.14}$$

For proofs and further details on the results stated in this section we refer the reader to [3], [5] and [17].

3.2.1 Existence and Uniqueness

The following result for mixed formulations is the analogon to the result of the Lax-Milgram Theorem for primal formulations.

Theorem 3.17. (Brezzi) *Let V and Q be real Hilbert spaces, $f \in V^*$, $g \in Q^*$ and the bilinear forms $a : V \times V \to \mathbb{R}$ and $b : V \times Q \to \mathbb{R}$ fulfill the following properties:*

1. *The bilinear forms are* bounded, *i. e. there exist constants $\alpha_2, \beta_2 > 0$ with*

$$\begin{aligned} |a(v, w)| &\leqslant \alpha_2 \|v\|_V \|w\|_V && \text{for all } v, w \in V, \\ |b(v, q)| &\leqslant \beta_2 \|v\|_V \|q\|_Q && \text{for all } v \in V, \text{ for all } q \in Q. \end{aligned}$$

2. $a(.,.)$ *is* $\ker b$-coercive*, i. e. there exists a constant* $\alpha_1 > 0$ *with*

$$|a(v,v)| \geqslant \alpha_1 \|v\|_V^2 \qquad \text{for all } v \in \ker b, \tag{3.15}$$

where $\ker b := \{u \in V \mid b(u,q) = 0 \ \text{for all } q \in Q\}$.

3. $b(.,.)$ *satisfies the* inf-sup condition *also called* Ladyshenskaja-Babuška-Brezzi condition (LBB-condition)*, i. e. there exists a constant* $\beta_1 > 0$

$$\inf_{q\in Q} \sup_{v\in V} \frac{b(v,q)}{\|v\|_V \|q\|_Q} \geqslant \beta_1. \tag{3.16}$$

Then there exists a unique solution $(u,p) \in V \times Q$ *of* (3.12) *satisfying the a-priori estimates*

$$\|u\|_V \leqslant \frac{1}{\alpha_1}\|f\|_{V^*} + \frac{1}{\beta_1}\left(1 + \frac{\alpha_2}{\alpha_1}\right)\|g\|_{Q^*},$$
$$\|p\|_Q \leqslant \frac{1}{\beta_1}\left(1 + \frac{\alpha_2}{\alpha_1}\right)\|f\|_{V^*} + \frac{\alpha_2}{\beta_1^2}\left(1 + \frac{\alpha_2}{\alpha_1}\right)\|g\|_{Q^*}.$$

3.2.2 Conforming finite element spaces

One of the most commonly used finite element for $H(\mathrm{div})$-conforming methods is the lowest-order Raviart-Thomas element.

Definition 3.18. *The lowest order Raviart-Thomas element (of order* $k = 0$*) on a triangle* T *is defined by*

- *the local space* $\mathcal{RT}_0(T) := \{\boldsymbol{a} + b\,\boldsymbol{x} \mid \boldsymbol{a} \in \mathbb{R}^2,\, b \in \mathbb{R}\}$ *with* $\dim(\mathcal{RT}_0(T)) = 3$,
- *the total flux over each edge* $E_\alpha \in \mathcal{E}_T$*, i. e.*

$$N_\alpha \ : \ \boldsymbol{v} \to \int_{E_\alpha} \boldsymbol{v}\cdot\boldsymbol{n}\,dx \qquad \alpha = 1,2,3,$$

where $\mathcal{E}_T$ *denotes the local set of edges belonging to the element* T.

The global space is defined as

$$\mathcal{RT}_0(\mathcal{T}_h) := \{v \in [L_2(\Omega)]^2 \mid v \text{ normal continuous },\ v_{|_T} \in \mathcal{RT}_0(T)\}.$$

The continuity of the normal component at the element boundaries assures conformity $\mathcal{RT}_0(\mathcal{T}_h) \subset H(\mathrm{div},\Omega)$.
The global basis functions for $H(\mathrm{div},T)$ are constructed by a conforming transformation of the basis functions on the reference element $\hat{T}$. The Piola transformation (also called contravariant transformation) preserves curl-fields and is a $H(\mathrm{div})$-conforming

transformation (cf. [5]).

For high-order Raviart-Thomas elements, their form functions and error estimates in a graspable presentation we refer the reader to [24].

Next, we introduce the classical lowest-order finite element for discretizing L_2-functions.

Definition 3.19. *The lowest-order L_2-conforming finite element on a simplex T is defined by*

- *the local space $\mathcal{P}_T = \mathcal{P}^0(T)$ of dimension $\dim(\mathcal{P}^0(T)) = 1$,*
- *one degree of freedom, which corresponds to the integral over the element, i. e.*

$$N_0 \quad : \quad v \to \int_T v \, dx.$$

The global space is defined as

$$\mathcal{M}_0(\mathcal{T}_h) := \{v \in L_2(\Omega) \mid v_{|_T} \in \mathcal{P}^0(T) \text{ for all } T \in \mathcal{T}_h\}.$$

Figure 3.4: (left hand side) The 2-dimensional lowest order Raviart-Thomas element. The arrows refer to the degrees of freedom. (right hand side) The 2-dimensional L_2-conforming lowest-order finite element. The dot illustrates the degree of freedom.

3.2.3 Approximation properties of conforming FEM

Now we apply a conforming Galerkin approximation to the variational problem (3.12). Therefore we choose finite-dimensional spaces $V_h \subset V$ and $Q_h \subset Q$ and restrict problem (3.12) to $V_h \times Q_h$. We consider the discrete variational problem

Find $(u_h, p_h) \in V_h \times Q_h$ such that

$$\begin{aligned} a(u_h, v_h) + b(v_h, p_h) &= f(v_h) \qquad \text{for all } v_h \in V_h, \\ b(u_h, q_h) &= g(q_h) \qquad \text{for all } q_h \in Q_h. \end{aligned} \tag{3.17}$$

Theorem 3.20. *Suppose that the variational problem* (3.12) *fulfills the assumptions of Brezzi's Theorem 3.17. Let* $(u,p) \in V \times Q$ *denote the exact solution to* (3.12).
Let the discrete spaces $V_h \subset V$ *and* $Q_h \subset Q$ *fulfill the following assumptions.*

1. *The bilinear form* $a(.,.)$ *is* $\ker b_h$*-coercive with a constant* $\alpha' > 0$ *and* $\alpha' \neq \alpha'(h)$, *where* $\ker b_h := \{v_h \in V_h \mid b(v_h, q_h) = 0 \ \text{for all}\ q_h \in Q_h\}$.
2. *The bilinear form* $b(.,.)$ *fulfills the inf-sup condition with a constant* $\beta' > 0$ *and* $\beta' \neq \beta'(h)$
$$\sup_{v_h \in V_h} \frac{b(v_h, p_h)}{\|v_h\|_V} \geqslant \beta' \|p_h\|_Q \qquad \text{for all } p_h \in Q_h.$$

Denote by $(u_h, p_h) \in V_h \times Q_h$ *the unique solution of the discrete problem* (3.17).
Then the discretization errors $u - u_h$ *and* $p - p_h$ *can be estimated by the sum of the approximation errors as follows:*

$$\|u - u_h\|_V + \|p - p_h\|_Q \leqslant c \left[\inf_{v_h \in V_h} \|u - v_h\|_V + \inf_{q_h \in Q_h} \|p - q_h\|_Q \right].$$

In general $\ker b_h \not\subset \ker b$. In the special case where $\ker b_h \subset \ker b$ enhanced estimate can be given.

Theorem 3.21. *Suppose that the assumptions of Theorem 3.20 are fulfilled. Furthermore let* u_h *be the solution of* (3.17) *and let* $\ker b_h \subset \ker b$, *i. e. for all* $v_h \in V_h$ *holds*

$$\text{if } \ b(v_h, q_h) = 0 \ \text{ for all } q_h \in Q_h \quad \Rightarrow \quad b(v_h, q) = 0 \ \text{ for all } q \in Q.$$

Then the discretization errors $u - u_h$ *can be estimated by*

$$\|u - u_h\|_V \leqslant c \inf_{v_h \in V_h} \|u - v_h\|_V$$

Remark 3.22. *The mixed form* (3.11) *of the Poisson problem with* $\boldsymbol{p}_h \in \mathcal{RT}_0(\mathcal{T}_h)$ *and* $u_h \in \mathcal{M}_0(\mathcal{T}_h)$ *fulfills the assumptions of Theorem 3.21. Note that the naming of variables is opposite to the general theory.*

3.3 Formulas of fundamental importance

This section contains a brief collection of some important formulas and definitions used later on.

Green's formula:
$$\int_\Omega \nabla v \cdot \nabla w \, dx = \int_\Gamma v \, \frac{\partial w}{\partial n} \, ds - \int_\Omega v \, \Delta w \, dx \tag{3.18}$$

ε-inequality: also called Young inequation

$$|ab| \leqslant \frac{1}{2\varepsilon}a^2 + \frac{\varepsilon}{2}b^2 \tag{3.19}$$

Inverse estimate for finite element functions $v_h \in V_h \subset H^1$

$$\|\nabla v_h\|_0^2 \leqslant C^2 h^{-2} \|v_h\|_0^2 \tag{3.20}$$

Also applies elementwise.

Chapter 4

The EHD Problem with a Fermi-Potential Approach

We introduce a Fermi-potential approach motivated by semiconductor physics. The resulting free boundary problem is treated with two different approaches. The first one is quite natural while the second one is numerically easier to use. Later on iterative solution strategies for the non-linear coupled problem are pointed out. A 2D FEM-discretization is done and the numerical results for the diffusion-dominated problem are presented.

4.1 The Fermi-potential approach

In the following we consider the non-linear system of the stationary governing equations (2.9), (2.11) and (2.12) derived in Chapter 2. This system is of a similar structure as a simplified form of the drift-diffusion equations describing the charge carriers in semiconductors (see [16]; Chapter 6.2).

Remark 4.1. The Fermi-potential approach. The Fermi-potential approach is used in the theory on charge carrier statistics in semiconductors [10]. For electrons, the probability that a certain state of energy is occupied is described by the Fermi-Dirac distribution. For non-degenerated semiconductors at room temperature it is justified to replace the Fermi-Dirac distribution by the Maxwell-Boltzmann distribution. Integration over the states yields the Fermi-potential approach for the space charge density. For more details within the context of semiconductors we recommend the reader to [15], [14], [21] and [23].

From the Fermi-potential approach (cf. [12]) we obtain an exponential ansatz for the space charge density

$$\rho = -\rho_0 \, e^{\frac{b}{d}(\Phi - \zeta)}, \tag{4.1}$$

where ζ denotes the Fermi-potential. The parameter ρ_0 denotes the space charge density if a voltage corresponding to the Fermi-potential is applied, i. e., $\Phi = \zeta$. The constants b

and d are the mobility and the diffusion coefficient introduced in Chapter 2. Using

$$\begin{aligned} \nabla\rho &= -\rho_0 e^{\frac{b}{d}(\Phi-\zeta)}\frac{b}{d}\nabla(\Phi-\zeta) \\ &= \rho\frac{b}{d}(\nabla\Phi-\nabla\zeta), \end{aligned} \tag{4.2}$$

equation (2.11) simplifies to

$$\begin{aligned} \boldsymbol{j} &= b\nabla\Phi\,\rho - d\,\rho\frac{b}{d}(\nabla\Phi-\nabla\zeta) \\ &= b\,\rho\,\nabla\zeta. \end{aligned} \tag{4.3}$$

The System of governing equations

Consequently, the simplified system reads as

$$-\operatorname{div}(\varepsilon\nabla\Phi) = \rho \qquad \text{for } x\in\Omega, \tag{4.4}$$

$$-\operatorname{div}(b\,\rho\nabla\zeta) = 0 \qquad \text{for } x\in\Omega, \tag{4.5}$$

with the exponential ansatz for the space charge density

$$\rho = -\rho_0\, e^{\frac{b}{d}(\Phi-\zeta)}. \tag{4.1}$$

The non-linearity is now hidden in ρ. For a fixed ρ the system is linear in Φ and ζ.

Next, we have to adapt the boundary conditions to the Fermi-potential approach. We start from the general description of the imposed boundary conditions formulated in Section 2.2. The boundary conditions for the electric potential remain unchanged. Boundary conditions for the Fermi-potential can be imposed by adjusting the boundary conditions for either the space charge density or the current density.

Boundary conditions on the outer boundary

The Neumann boundary conditions $\boldsymbol{j}\cdot\boldsymbol{n}=0$ on the outer boundary can easily be reformulated for the Fermi-potential ζ. Providing equation (4.3) we can write

$$b\,\rho\nabla\zeta\cdot\boldsymbol{n} = 0 \qquad \text{on } \Gamma_{out}. \tag{4.6}$$

Boundary conditions on the target

Since the space charge density does not change with respect to the outer normal direction on Γ_{ta}, i. e.,

$$\nabla\rho\cdot\boldsymbol{n} = \frac{b}{d}\,\rho\,(\nabla\Phi-\nabla\zeta)\cdot\boldsymbol{n} = 0 \qquad \text{on } \Gamma_{ta},$$

we obtain

$$b\,\rho\nabla\zeta\cdot\boldsymbol{n} = b\,\rho\nabla\Phi\cdot\boldsymbol{n} \qquad \text{on } \Gamma_{ta}. \tag{4.7}$$

So, both potentials have the same normal flux on the target. A further interpretation is

$$\boldsymbol{j} \cdot \boldsymbol{n} = -b\rho \boldsymbol{E} \cdot \boldsymbol{n}.$$

Thus the current density in normal direction is equal to the negative drift current in normal direction and no diffusion takes place.

Remark 4.2. The non-linear system (2.9)–(2.11) together with the boundary conditions on the electrode Γ_{el} (especially (2.19) and (2.20)) can be transformed to a variational inequality. By introducing the Fermi-potential the reformulation as variational inequality is much more complicated. Therefore we used a different approach.

Summing up, the Fermi-potential approach for the EHD problem leads to the following classical formulation:

Find Φ and ζ such that

$$\begin{aligned} -\operatorname{div}(\varepsilon \nabla \Phi) &= \rho \quad \text{in } \Omega, \\ -\operatorname{div}(b\,\rho \nabla \zeta) &= 0 \quad \text{in } \Omega, \end{aligned}$$

with $\rho = -\rho_0 \, e^{\frac{b}{d}(\Phi - \zeta)}$ and the boundary conditions

$$\begin{aligned} \varepsilon \nabla \Phi \cdot \boldsymbol{n} &= 0 && \text{on } \Gamma_{out}, \\ \Phi &= 0 && \text{on } \Gamma_{ta}, \\ \Phi &= \Phi_e && \text{on } \Gamma_{el}, \\ b\,\rho \nabla \zeta \cdot \boldsymbol{n} &= 0 && \text{on } \Gamma_{out}, \\ b\,\rho \nabla \zeta \cdot \boldsymbol{n} &= b\,\rho \nabla \Phi \cdot \boldsymbol{n} && \text{on } \Gamma_{ta}, \\ b\,\rho \nabla \zeta \cdot \boldsymbol{n} &= 0 && \text{on } \Gamma_{el} \backslash \Gamma_{co,a}, \\ b\,\rho \nabla \zeta \cdot \boldsymbol{n} &= j_{co}(\boldsymbol{E}) && \text{on } \Gamma_{co,a}. \end{aligned}$$

The treatment of the free boundary $\Gamma_{co,a}$ and the unknown value $j_{co}(\boldsymbol{E})$ is postponed to Section 4.3.

4.2 Variational framework

The analysis of the partial differential equations is commonly done within a variational framework. In the following we first introduce the appropriate spaces and then derive a variational (weak) formulation of our system of partial differential equations. The natural function space V for a variational formulation of Poisson equations is the Sobolev space $H^1(\Omega)$ (see Definition 3.1).
The essential (Dirichlet) boundary conditions are incorporated in the test and ansatz space:

$$\begin{aligned} V_0 = \quad H^1_{0,D}(\Omega) \quad &:= \{u \in H^1(\Omega) \mid u_{|\Gamma_{el} \cup \Gamma_{ta}} = 0\} \\ V_g = \quad H^1_{g,D}(\Omega) \quad &:= \{u \in H^1(\Omega) \mid u_{|\Gamma_{el}} = g \quad \wedge \quad u_{|\Gamma_{ta}} = 0\} \end{aligned}$$

We multiply equation (4.4) by a test function $w \in V_0$, integrate over Ω, and obtain

$$\int_\Omega -\operatorname{div}(\varepsilon\,\nabla\Phi)\,w\,dx = \int_\Omega \rho\,w\,dx \qquad \text{for all } w \in V_0.$$

Integration by parts on the left hand side leads to

$$\int_\Omega \varepsilon\,\nabla\Phi\cdot\nabla w\,dx - \int_{\partial\Omega} \varepsilon\,\nabla\Phi\cdot\boldsymbol{n}\,w\,ds = \int_\Omega \rho\,w\,dx \qquad \text{for all } w \in V_0.$$

Handling equation (4.5) the same way, but with a test function $v \in V$, we obtain the following system of equations:

Find $\Phi \in V_g$ and $\zeta \in V$ such that

$$\int_\Omega \varepsilon\,\nabla\Phi\cdot\nabla w\,dx - \int_{\partial\Omega} \varepsilon\,\nabla\Phi\cdot\boldsymbol{n}\,w\,ds = \int_\Omega \rho\,w\,dx \qquad \text{for all } w \in V_0, \tag{4.8}$$

$$\int_\Omega b\rho\,\nabla\zeta\cdot\nabla v\,dx - \int_{\partial\Omega} b\rho\,\nabla\zeta\cdot\boldsymbol{n}\,v\,ds = 0 \qquad \text{for all } v \in V, \tag{4.9}$$

with $\rho = -\rho_0\, e^{\frac{b}{d}(\Phi-\zeta)}$.

In the next step we incorporate the boundary conditions. The boundary term of the first equation (4.8) equals to

$$-\int_{\partial\Omega} \varepsilon\,\nabla\Phi\cdot\boldsymbol{n}\,w\,ds = -\int_{\Gamma_{el}\cup\Gamma_{ta}} \varepsilon\,\nabla\Phi\cdot\boldsymbol{n}\,\underbrace{w}_{=0}\,ds - \int_{\Gamma_{out}} \underbrace{\varepsilon\,\nabla\Phi\cdot\boldsymbol{n}}_{=0}\,w\,ds = 0.$$

The boundary term of the second equation (4.9) can be written as

$$\begin{aligned} -\int_{\partial\Omega} b\rho\,\nabla\zeta\cdot\boldsymbol{n}\,v\,ds &= -\int_{\Gamma_{el}\cup\Gamma_{ta}} b\rho\,\nabla\zeta\cdot\boldsymbol{n}\,v\,ds - \int_{\Gamma_{out}} b\rho\,\underbrace{\nabla\zeta\cdot\boldsymbol{n}}_{=0}\,v\,ds \\ &= -\int_{\Gamma_{el}} b\rho\,\nabla\,\zeta\cdot\boldsymbol{n}\,v\,ds - \int_{\Gamma_{ta}} b\rho\,\nabla\,\Phi\cdot\boldsymbol{n}\,v\,ds. \end{aligned}$$

Since $b\rho\,\nabla\zeta\cdot\boldsymbol{n} = \boldsymbol{j}\cdot\boldsymbol{n} = 0$ on $\Gamma_{el}\backslash\Gamma_{co,a}$ the term at this boundary vanishes. Only the boundary condition on $\Gamma_{co,a}$ remains

$$-\int_{\partial\Omega} b\rho\,\nabla\zeta\cdot\boldsymbol{n}\,v\,ds = -\int_{\Gamma_{co,a}} b\rho\,\nabla\zeta\cdot\boldsymbol{n}\,v\,ds - \int_{\Gamma_{ta}} b\rho\,\nabla\,\Phi\cdot\boldsymbol{n}\,v\,ds.$$

By incorporating these boundary terms into the equations (4.8) and (4.9) we obtain our problem in weak formulation.

Find $\Phi \in V_g$ and $\zeta \in V$ such that

$$\int_\Omega (\varepsilon \nabla\Phi \cdot \nabla w)\, dx - \int_\Omega \rho\, w\, dx = 0 \qquad \text{for all } w \in V_0, \quad (4.10)$$

$$\int_\Omega b\rho\, \nabla\zeta \cdot \nabla v\, dx - \int_{\Gamma_{co,a}} \underbrace{b\rho\, \nabla\zeta \cdot \boldsymbol{n}}_{=j_{co}(\boldsymbol{E})}\, v\, ds - \int_{\Gamma_{ta}} b\rho\, \nabla\Phi \cdot \boldsymbol{n}\, v\, ds = 0 \qquad \text{for all } v \in V. \quad (4.11)$$

In this coupled system (coupled via the boundary term) the free boundary $\Gamma_{co,a}$ as well as the boundary value $j_{co}(\boldsymbol{E})$ on $\Gamma_{co,a}$ are still unknown.

4.3 Solution strategies

First we present two approaches for locating the free boundary $\Gamma_{co,a}$. Throughout these two methods we assume the space charge density ρ to be fixed. The first approach suggests itself while the second is a bit smarter and easier to handle numerically.
Thereafter some iterative solution strategies for the non-linear coupled EHD problem with the space charge density $\rho(\Phi, \zeta)$ are presented.

4.3.1 The localization of the free boundary

First approach (An iteration for locating $\Gamma_{co,a}$)
When solving the coupled system (4.10) and (4.11) the main problem is, that the location of $\Gamma_{co,a}$ is unknown as well as the boundary value $j_{co}(\boldsymbol{E})$ on $\Gamma_{co,a}$. In order to motivate an iterative procedure we recall the physics of the corona effect.

Remark 4.3. (Occurrence on Γ_{co}.) If the local electric field exceeds the threshold it causes ionization. The generated ions induce an electric current which attenuates the local electric field. Therefore the electric field strength can not increase further.

The following iterative procedure (Algorithm 4.4) is a realization of this process.
We solve the coupled system with an initial setting for the location of $\Gamma_{co,a}$ and the corresponding boundary conditions. Where the computed electric field exceeds the threshold E_{co} we adapt the boundary condition by adding a surface current density to locally compensate the electric field.

Algorithm 4.4. ***Locating*** $\Gamma_{co,a}$

Initial settings: iteration index $r = 0$ *and*
corona onset $\Gamma^0_{co,a} = \varnothing$.

while (location of $\Gamma^r_{co,a}$ *changes too much)*

- *Find* Φ^r, ζ^r *by solve non-linear system* (4.10), (4.11) *with* $\Gamma^r_{co,a}$ *and* $b\rho\,\nabla\zeta^r \cdot \boldsymbol{n} = j^r_{co}$ *on* $\Gamma^r_{co,a}$
- *Update corona onset:*
  $\Gamma^{r+1}_{co,a} \hat{=}$ *part of* Γ_{co} *where* $|\nabla\Phi^r \cdot \boldsymbol{n}| = E^r_n \geqslant E_{co}$
  and compute new surface current density:
  $j^{r+1}_{co} = j^r_{co} + s(r)\ max((E^r_n - E_{co}), 0) \quad$ *on* $\Gamma^{r+1}_{co,a}$
- $r = r + 1$

end

In each step of the iteration we determine the corona onset $\Gamma^{r+1}_{co,a}$ by means of the strength of the electric field calculated in the previous interation. The boundary value j^r_{co} denotes the corresponding normal current throughout the iteration. If the value of the electric field exceeds the threshold E_{co} somewhere on Γ_{el} during an iteration step, we increase local the electric surface current density, in order to compensate the surplus of the electric field. The scaling factor s of the additional current density depends on the iteration step r to be able to keep changes small late in the iteration.
We point out that following this approach in each step a non-linear system has to be solved.

Second approach (A smart boundary condition on Γ_{co})
In order to simplify the algorithm and to avoid the iteration for the location of $\Gamma_{co,a}$ (Algorithm 4.4) we reconsider the boundary conditions of the current density on the whole electrode Γ_{el}.
Instead of locating the boundary $\Gamma_{co,a}$, we state a boundary condition dependent on E_n. We approximate $\boldsymbol{j} \cdot \boldsymbol{n}$ on Γ_{el} by the piecewise linear function $K_r(E_n)$

$$\boldsymbol{j} \cdot \boldsymbol{n} \approx K_r(E_n) = \begin{cases} \alpha_F(E_n - E_{co}) & \text{for } E_n \geqslant E_{co} \\ 0 & \text{else} \end{cases} \qquad \text{on } \Gamma_{el} \tag{4.12}$$

with an appropriate choice for the slope α_F. This function is illustrated in Figure 4.1 (blue line). Under ideal conditions, meaning enough surrounding atoms which can be ionized and that the local potential is independent of the ionization process, the current density would be infinite as pictured in Figure 4.1 (magenta line).

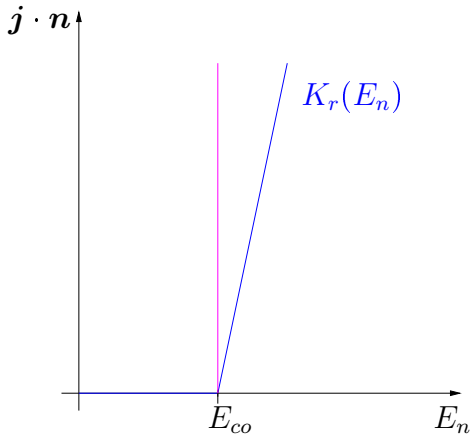

Figure 4.1: The approximate $K_r(E_n)$ (blue) models the surface current density $\boldsymbol{j} \cdot \boldsymbol{n}$ on the electrode. The straight line (magenta) describes the ideal case.

For a slope $\alpha_F \to \infty$ the function $K_r(E_n)$ approximates the idealized model of the current density. We incorporate this boundary condition into our variational framework and exchange (4.10), (4.11) by the following system:

Find $\Phi \in V_g$ and $\zeta \in V$ such that

$$\int_\Omega (\varepsilon \nabla \Phi \cdot \nabla w - \rho\, w)\, dx = 0 \qquad \forall\, w \in V_0, \tag{4.13}$$

$$\int_\Omega b\rho\, \nabla \zeta \cdot \nabla v\, dx - \int_{\Gamma_{el}} K_r(-\nabla \Phi \cdot \boldsymbol{n})\, v\, ds - \int_{\Gamma_{ta}} b\rho\, \nabla \Phi \cdot \boldsymbol{n}\, v\, ds = 0 \qquad \forall\, v \in V. \tag{4.14}$$

4.3.2 Iterative solution strategies for the non-linear coupled EHD problem

In the following we discuss some non-linear solution strategies which will result in a combination of a Newton's method [18] and a fixed point iteration [18]. For a better readability we describe the non-linear problem in the following abstract framework.

Find $\Phi \in V_g$ and $\zeta \in V$ such that

$$\langle A(\Phi, \zeta), (w, v) \rangle = f(w, v) \qquad \text{for all } w \in V_0, v \in V \tag{4.15}$$

with the bilinear form

$$\langle A(\Phi, \zeta), (w, v) \rangle := A[\Phi, \zeta](\Phi, \zeta; w, v)$$

where

$$\begin{aligned} A[\Phi^*,\zeta^*](\Phi,\zeta;w,v) &= \int_\Omega (\varepsilon\nabla\Phi\cdot\nabla w + \rho_0 e^{\frac{b}{d}(\Phi^*-\zeta^*)} w)\,dx \\ &\quad - \int_\Omega \rho_0 e^{\frac{b}{d}(\Phi^*-\zeta^*)}\, b\,\nabla\zeta\cdot\nabla v\,dx \\ &\quad - \int_{\Gamma_{el}} K_r(-\nabla\Phi\cdot\boldsymbol{n})\,v\,ds + \int_{\Gamma_{ta}} \rho_0 e^{\frac{b}{d}(\Phi^*-\zeta^*)}\, b\,\nabla\Phi\cdot\boldsymbol{n}\,v\,ds, \end{aligned} \tag{4.16}$$

and the right hand side

$$f(w,v) = 0.$$

For applying Newton's method we need the Gateaux derivatives of the operator A in the direction $u \in V_0$ [22].

Definition 4.5. *The Gateaux derivative $F'(x)$ of a given operator $F(x)$ in a direction v is defined as*

$$F'(x)v := \lim_{t\to 0}\frac{1}{t}\left[F(x+tv) - F(x)\right].$$

Hence, the Gateaux derivatives of the operator A are given by

$$\begin{aligned} \left\langle \frac{\partial A}{\partial\Phi}(\Phi,\zeta)\,u,(w,0)\right\rangle &= \lim_{t\to 0}\frac{1}{t}[\langle A(\Phi+t\,u,\zeta),(w,0)\rangle - \langle A(\Phi,\zeta),(w,0)\rangle] \\ &= \int_\Omega \varepsilon\nabla u\cdot\nabla w + \rho_0 e^{\frac{b}{d}(\Phi-\zeta)}\frac{b}{d}u\,w\,dx \end{aligned}$$

and

$$\begin{aligned} \left\langle \frac{\partial A}{\partial\zeta}(\Phi,\zeta)\,u,(0,v)\right\rangle &= \lim_{t\to 0}\frac{1}{t}[\langle A(\Phi,\zeta+t\,u),(0,v)\rangle - \langle A(\Phi,\zeta),(0,v)\rangle] \\ &= \int_\Omega -\rho_0 e^{\frac{b}{d}(\Phi-\zeta)} b\,\nabla u\cdot\nabla v + \rho_0 e^{\frac{b}{d}(\Phi-\zeta)}\frac{b^2}{d}\,u\,\nabla\zeta\cdot\nabla v\,dx \\ &\quad - \int_{\Gamma_{ta}} \rho_0 e^{\frac{b}{d}(\Phi-\zeta)}\frac{b^2}{d}\,u\,\nabla\Phi\cdot\boldsymbol{n}\,v\,ds. \end{aligned}$$

Algorithm - Newton's method for Φ and a fixed point iteration for ζ

First of all, we solve the problem (4.15) using Newton's method for Φ (cf. [18]). According to the requirements of this method we need monotony of the operator $A(\,.\,,\zeta)$.

Lemma 4.6. *The operator $A(\,.\,,\zeta)$ is monoton.*

Proof. We use zero as a testfunction for ζ. Let $x, y \in V$.

$$\begin{aligned}\langle A(x,\zeta) - A(y,\zeta), (x,0) - (y,0)\rangle = \\ \int_\Omega (\varepsilon \nabla x \cdot \nabla x + \rho_0 e^{\frac{b}{d}(x-\zeta)} x)\, dx - \int_\Omega (\varepsilon \nabla y \cdot \nabla x + \rho_0 e^{\frac{b}{d}(y-\zeta)} x)\, dx \\ - \int_\Omega (\varepsilon \nabla x \cdot \nabla y + \rho_0 e^{\frac{b}{d}(x-\zeta)} y)\, dx + \int_\Omega \varepsilon \nabla y \cdot \nabla y + \rho_0 e^{\frac{b}{d}(y-\zeta)} y)\, dx = \\ \int_\Omega (\varepsilon(\nabla x - \nabla y)^2\, dx + \int_\Omega (x-y)(\rho_0 e^{\frac{b}{d}(x-\zeta)} - \rho_0 e^{\frac{b}{d}(y-\zeta)}) \geqslant 0\end{aligned}$$

□

Due to the monotony of the operator $A(\,.\,,\zeta)$, a global solution with respect to Φ exists and Newton's method converges towards this global solution. But the monotony of the operator $A(\Phi,\,.\,)$ can not be shown. Due to that Newton's method for ζ might converge towards a local solution. Hence we use a fixed point iteration which guarantees convergence to solve the equation for ζ (cf. Algorithm 4.8). For Φ we use a modified Newton method (cf.[19]) with a variable step size τ obtained by linesearch (cf. Algorithm 4.7).

Algorithm 4.7. (Newton's method for Φ)

for $l = 0, \ldots, N_\Phi$

find $u \in V_0$ *such that*
$\left\langle \frac{\partial A}{\partial \Phi}(\Phi^{k,l}, \zeta^{k,0})\, u, (w,0) \right\rangle = f(w,0) - \left\langle A(\Phi^{k,l}, \zeta^{k,0}), (w,0) \right\rangle \quad$ *for* $w \in V$
for τ *obtained by linesearch*
$\Phi^{k,l+1} = \Phi^{k,l} + \tau\, u$

end

Algorithm 4.8. (Fixed point iteration for ζ)

for $l = 0, \ldots, N_{\zeta,F}$

find $u \in V$ *such that* ($v_0 \in V_0$)
$A[\Phi^{k+1,0}, \zeta^{k,l}](\Phi^{k+1,0}, u; 0, v_0) = f(0, v_0) - A[\Phi^{k+1,0}, \zeta^{k,l}](\Phi^{k+1,0}, \zeta^{k,l}; 0, v_0)$
$\zeta^{k,l+1} = \zeta^{k,l} + \tau\, u$

end

Algorithm 4.9.

for $k = 0, \ldots, \#$*(non-linear iterations)*

Newton's method for Φ *(Algorithm 4.7)*

$\Phi^{k+1,0} = \Phi^{k,N_\Phi+1}$

Fixed point iteration for ζ *(Algorithm 4.8)*

$\zeta^{k+1,0} = \zeta^{k,N_\zeta+1}$

end

Modified Algorithm

On account of the well known slow convergence of the fixed point iteration due to very small damping parameters, we try another method for finding a solution for the Fermi-potential ζ. We already mentioned that Newton's method might not find the global minimum when solving the equation for ζ. But with a reasonable initial guess for ζ, close enough to the global minimum, Newton's method results in fast convergence.

Algorithm 4.10.

for $k = 0, \ldots, \#$*(non-linear iterations)*

Newton's method for Φ *(Algorithm 4.7)*

$\Phi^{k+1,0} = \Phi^{k,N_\Phi+1}$

get initial guess for Newton's method from
Fixed point iteration for ζ *(Algorithm 4.8 with e. g.* $N_{\zeta,F} = 5$*)*

Newton's method for ζ *(Algorithm 4.11)*

$\zeta^{k+1,0} = \zeta^{k,N_\zeta+1}$

end

Algorithm 4.11. (Newton's method for ζ)

for $l = 0, \ldots, N_{\zeta,N}$

find $u \in H^1$ *such that*

$$\left\langle \frac{\partial A}{\partial \zeta}(\Phi^{k,0}, \zeta^{k,l})(u), (0, v) \right\rangle = f(0, v) - \left\langle A(\Phi^{k,0}, \zeta^{k,l}), (0, v) \right\rangle$$

$$\zeta^{k,l+1} = \zeta^{k,l} + u$$

end

Therefore we use some steps of the fixed-point-iteration to get a useful initial guess for ζ. We assume that this is a good enough startin value for Newton's method.
In numerical experiments we observe better convergence compared to the pure fixed point iteration.

4.4 Numerical Results

4.4.1 Parameters

Most of the parameters are given physical constants, namely

- the permittivity of the ambient gas $\varepsilon = 8.85 \cdot 10^{-11}\ As/Vm$ $(8.85 \cdot 10^{-12} As/Vm)$,
- the mobility of ions $b = 2.1 \cdot 10^{-4}\ m^2/Vs$ and
- the ions diffusion coefficient d in m^2/s.

The correct value of the diffusion coefficient would be $d = 5.4 \cdot 10^{-6}\ m^2/s$ which causes numerical problems. We believe that finite elements with upwind stabilization should be able to treat also this realistic diffusion parameter. The diffusion coefficient is the one, which changes in the later given examples. The parameters on the boundary are

- the potential at the electrode $\Phi_e = -70\ kV$ and
- the threshold strength of the electric field $E_{co} = 10^4\ V/m$.

In this two dimensional model of the tip the singularities of the electric field are much weaker as in 3D. Therefore we have to lower the threshold E_{co} in order to be reached. The physically correct value in three dimensions depends on temperature, pressure and the composition of the surrounding gas (air). A plausible value is $E_{co} = 1.2 \cdot 10^6\ V/m$.
Further parameters needed for the computation are

- the slope of $K_r(E_n)$, i. e., $\alpha_F = 10^{-15}$ and finally
- the scaling parameter of the space charge density $\rho_0 = 10^{-11}$.

4.4.2 Computations

The following details are for a calculation done with an Dual Intel Xeon, 2.8 GHz processor. The inner iterations were limited to a maximum number of steps. These are 10 steps for the inner iteration for Φ and 50 steps for the inner iteration for ζ. Most of the time, the iteration for Φ converged faster (after 1-3 iteration steps). As a stopping criterion for the outer iteration we use the sum of the relative updates for Φ and ζ, i. e.,

$$\frac{\|\Phi^{k,0} - \Phi^{k+1,0}\|_{l_2}}{\|\Phi^{k+1,0}\|_{l_2}} + \frac{\|\zeta^{k,0} - \zeta^{k+1,0}\|_{l_2}}{\|\zeta^{k+1,0}\|_{l_2}} < 1 \cdot 10^{-11}$$

and thereby obtain the following results (see Table 4.4.2).

diffusion coefficient d (m^2/s)	computing time (sec)	number of outer loops
2.0	68.2	4
1.5	67.9	4
0.5	68.8	4
0.09	132.0	4

Table 4.1: Computing time and interation numbers for varied diffusion coefficient.

As a first example we discuss the results for the diffusion coefficient $d = 0.5\ m^2/s$. The electric potential Φ for $d = 0.5\ m^2/s$ can be seen in Figure 4.2. As expected, it shows a smooth transition from the negative potential at the needle towards the zero potential at the target.

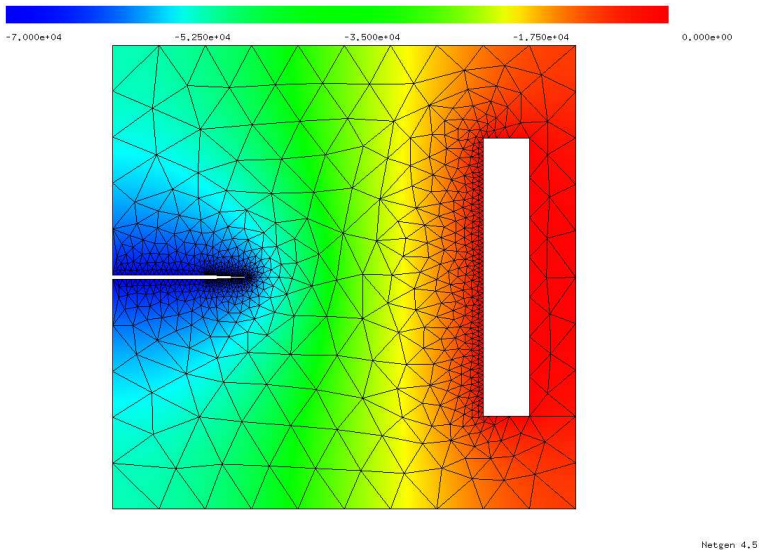

Figure 4.2: The electric potential Φ for diffusion coefficient $d = 0.5$.

The results for the Fermi potential ζ look quite similar to the electric potential Φ. The difference $(\Phi - \zeta) = c_1 \log \rho - c_2$ is the crucial factor in the computation of ρ (cf. Figure 4.3), since the remaining parameters are constants.

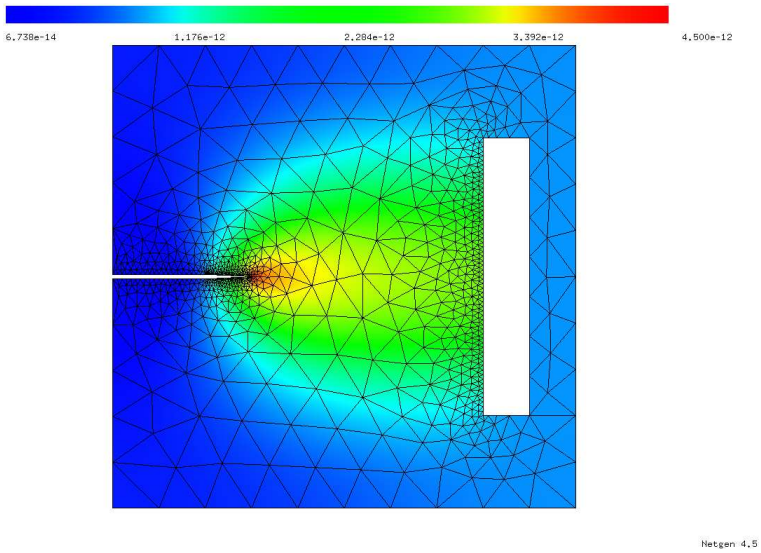

Figure 4.3: The space charge density ρ for diffusion coefficient $d = 0.5$.

Due to the corona effect, free electrons are generated next to the peak of the electrode. These charges move towards the target. The steady state of the space charge density can be seen in Figure 4.3. The highest concentration occurs in the center, on the shortest distance between needle and target. The concentration decreases further outside.

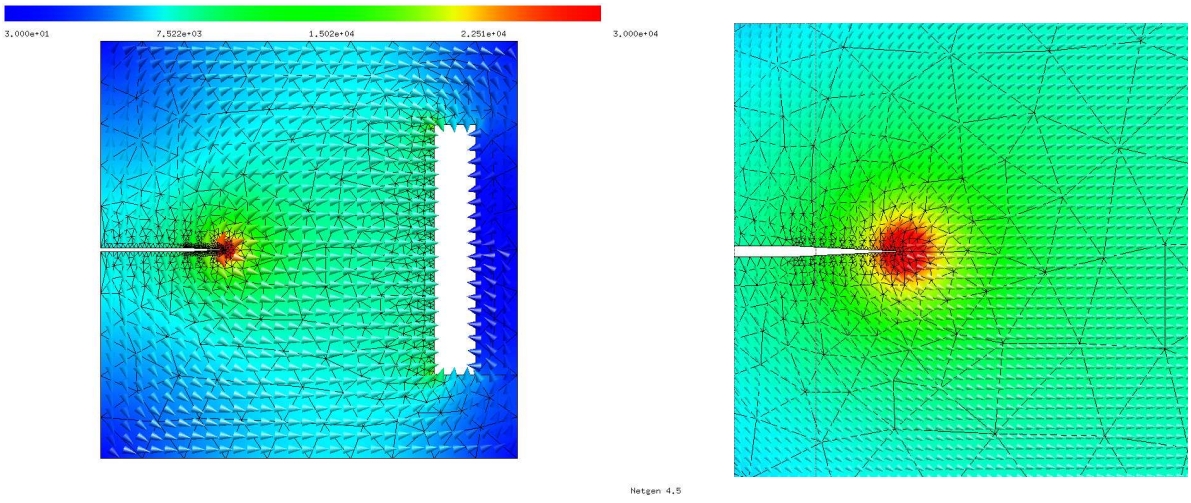

Figure 4.4: The electric field $\boldsymbol{E}$ on the whole domain (left) and zoomed onto the peak of the needle (right) for diffusion coefficient $d = 0.5$.

The resulting electric field is shown in Figure 4.4. Only the re-entrant corners of the target, where the derivative has a singularity, cause slightly higher values.
Finally the according current density $\boldsymbol{j}$ for diffusion coefficient $d = 0.5\ m^2/s$ calculated by $\boldsymbol{j} = b\,\rho\,\nabla\zeta$ is shown in Figure 4.5.

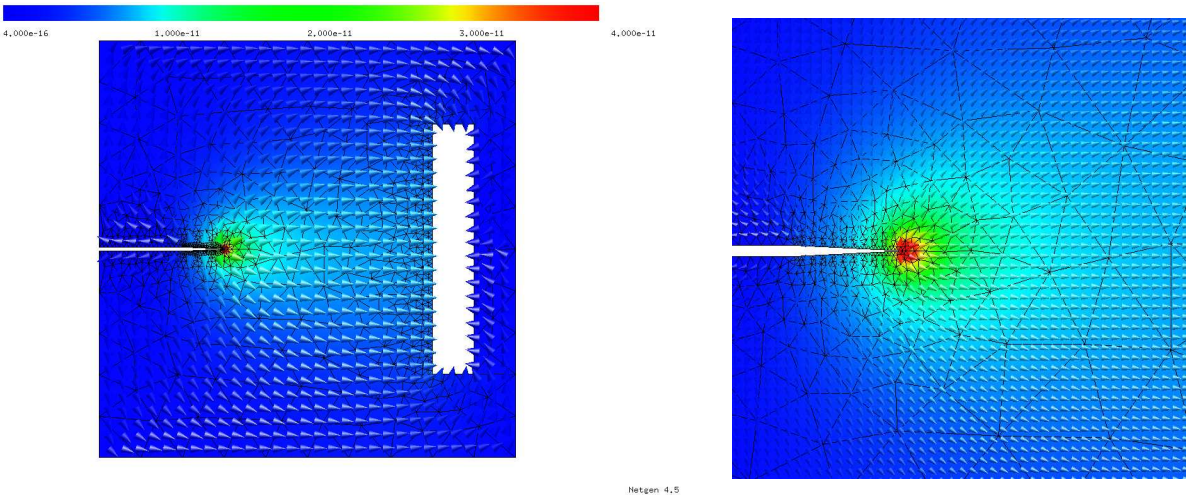

Figure 4.5: The current density $\boldsymbol{j}$ on the whole domain (left) and zoomed onto the peak of the needle (right) for diffusion coefficient $d = 0.5$.

The second example we consider, are the results for the diffusion coefficient $d = 0.09\ m^2/s$.

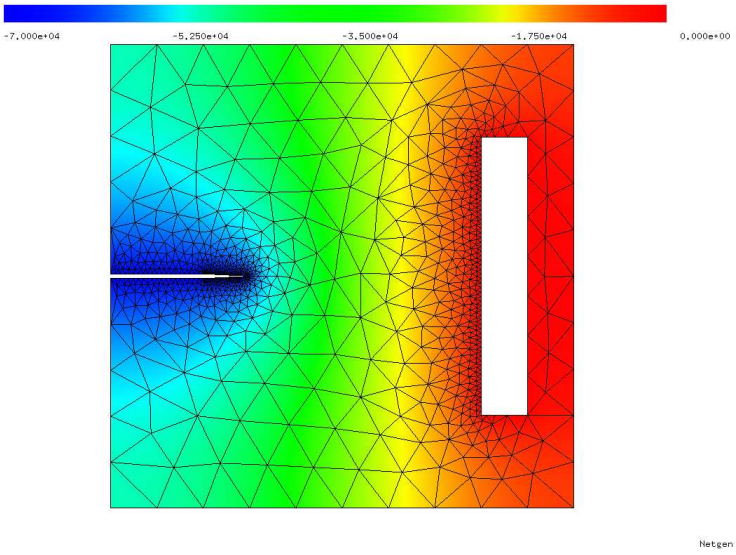

Figure 4.6: The electric potential Φ for diffusion coefficient $d = 0.09$.

The results for the Fermi potential ζ for $d = 0.09\ m^2/s$ look again quite similar to the

electric potential Φ (see Figure 4.6).

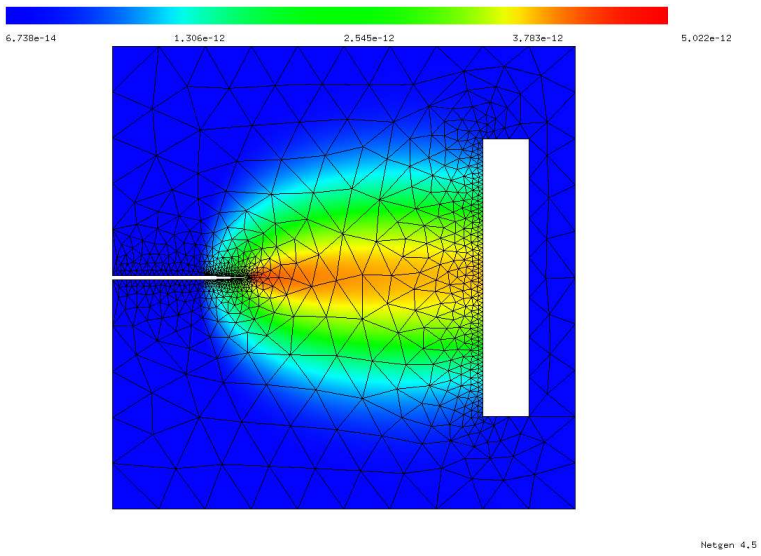

Figure 4.7: The space charge density ρ for diffusion coefficient $d = 0.09$.

The steady state of the space charge density ρ can be seen in Figure 4.7. The highest concentration again occurs in the center, on the shortest distance between needle and target. Note that obviously less diffusion takes place (compared to Figure 4.3) and thus the concentration reaches higher values near the peak of the needle.
The resulting electric field is shown in Figure 4.8 and the current density $\boldsymbol{j}$ is pictured in Figure 4.9.

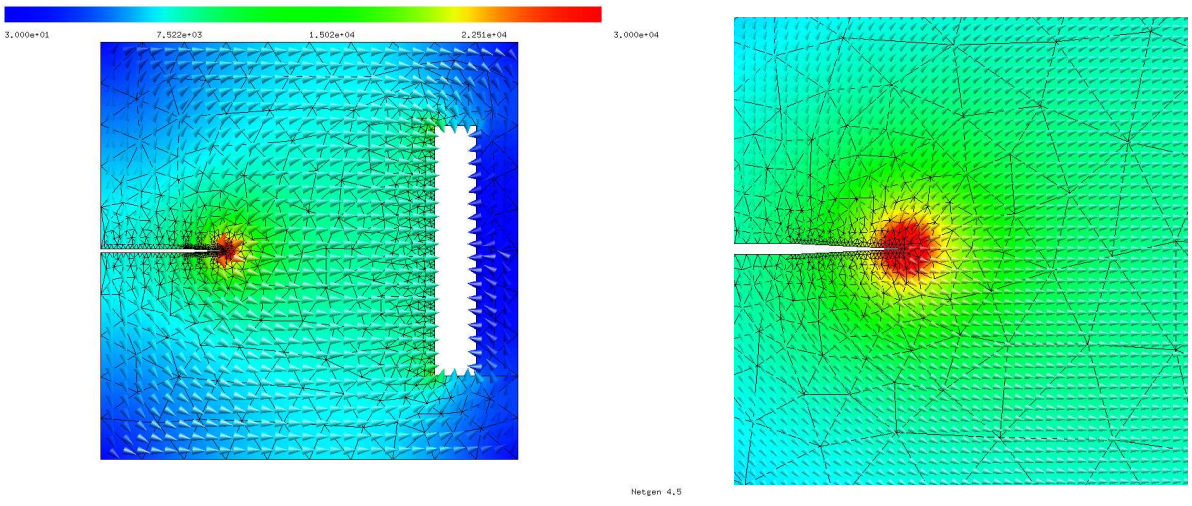

Figure 4.8: The electric field $\boldsymbol{E}$ on the whole domain (left) and zoomed onto the peak of the needle (right) for diffusion coefficient $d = 0.09$.

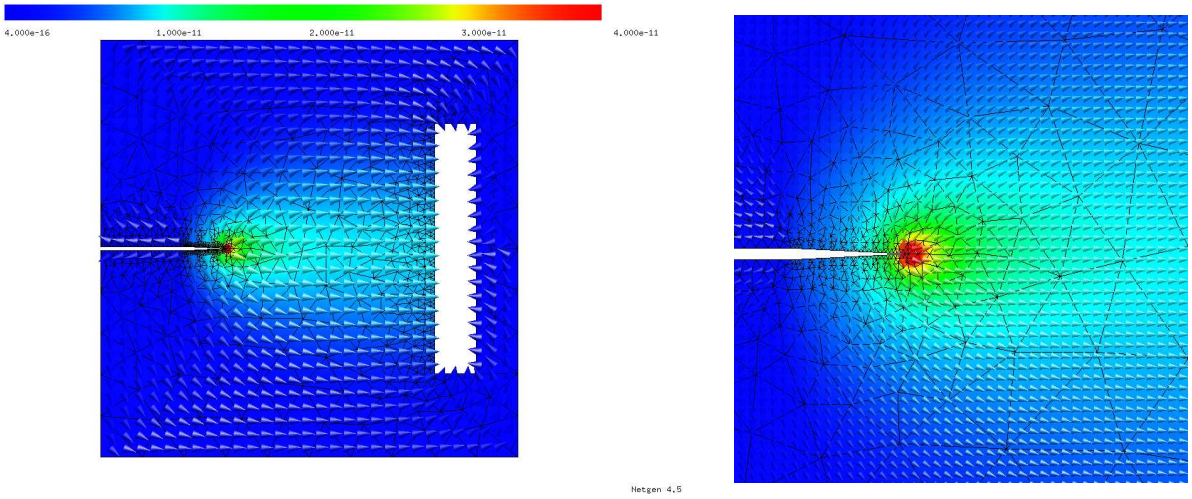

Figure 4.9: The current density $\boldsymbol{j}$ on the whole domain (left) and zoomed onto the peak of the needle (right) for diffusion coefficient $d = 0.09$.

Numerical tests revealed that $d = 0.09$ is the smallest working diffusion coefficient. For every smaller coefficient d the method diverges. This motivates to study methods for the convection dominated case.

Chapter 5

The Convection-Diffusion Problem

We shall now have another look at the system of equations (2.9)–(2.11) which we want to analyze:

$$\begin{aligned} -\operatorname{div} \varepsilon \nabla \Phi &= \rho \\ \frac{\partial \rho}{\partial t} + \operatorname{div} \boldsymbol{j} &= 0 \qquad\qquad \text{for } (\boldsymbol{x}, t) \in \Omega \times (0, T) \\ \boldsymbol{j} &= b \nabla \Phi \, \rho - d \nabla \rho. \end{aligned}$$

In this section we will concentrate on the convection-diffusion part (2nd and 3rd equation) in our EHD problem. Taking Φ as fixed we define the constant $\hat{\boldsymbol{b}} := b \nabla \Phi$. Substituting $\boldsymbol{j} = \hat{\boldsymbol{b}} \, \rho - d \nabla \rho$ in $\frac{\partial \rho}{\partial t} + \operatorname{div} \boldsymbol{j} = 0$ one obtains

$$\frac{\partial \rho}{\partial t} + \operatorname{div}(\hat{\boldsymbol{b}} \, \rho - d \nabla \rho) = 0. \tag{5.1}$$

If $\hat{\boldsymbol{b}}$ is divergence free and d is constant this simplifies to

$$\frac{\partial \rho}{\partial t} + \hat{\boldsymbol{b}} \cdot \nabla \rho - d \, \Delta \rho = 0. \tag{5.2}$$

This equation has obviously the form of a convection-diffusion problem as already treated in [8] for example. In order to analyze some existing methods (cf. outline below) we consider a simplified version of this convection-diffusion problem. An analysis of the variational formulation of the problem will be done, to ensure a unique solution. Some finite element methods will be formulated and a-priori error estimates will be done.

In content and structure the following chapter sticks roughly to the book of Claes Johnson [8], especially to Chapter 9 about hyperbolic problems.

For a general introduction into this sophisticated issue, we consider convection-diffusion problems of the form

$$\frac{\partial u}{\partial t} - \operatorname{div}(a \nabla u - \boldsymbol{b} \, u) + c \, u = f \qquad \text{for } (\boldsymbol{x}, t) \in \Omega \times (0, T), \tag{5.3}$$

where $\Omega \subset \mathbb{R}^d$ is a polygonal bounded domain and u a scalar field representing for example a concentration. Furthermore $a \geqslant 0$ is a diffusion coefficient, $\boldsymbol{b} = (b_1, \ldots, b_d)^T$ a vector field in $\mathbb{R}^d$ with $\operatorname{div} \boldsymbol{b} = 0$ and $c \in \mathbb{R}$ an absorption coefficient. With small or vanishing diffusion term these problems have mainly hyperbolic character. The numerical solution of problems with dominating diffusion by using standard conforming finite element methods (cf., e. g. [3]) is well understood. Also the treatment of the hyperbolic limit ($a = 0$) via discontinuous Galerkin methods (cf. [8]). However, the numerical solution of problems with dominant convection, but non-negligible diffusion, is difficult. Standard finite element methods for hyperbolic problems do not work well in cases where the exact solution is not smooth. For instance a step-like discontinuity in the exact solution causes in general large spurious oscillations in the finite element solution. These oscillations emanating of the jump reach far into the domain and therefore the finite element solution will be fairly different from the exact solution everywhere. On the other hand, classical artificial diffusion methods [8] excessively smear out a sharp front. Hence, these methods are lacking in either stability or accuracy. These difficulties are possible to overcome by modified non-standard finite element methods with satisfactory convergence properties. Techniques like the streamline diffusion method and the discontinuous Galerkin method have high order accuracy and good stability properties. Recently, a high interest in this research field can be observed (cf. [7]).
In the following we compare standard methods and some recently developed techniques and give a one dimensional example. Therefore we discuss solution methods for scalar problems of the following form:

Find $u \in V$ such that

$$\begin{aligned} \frac{\partial u}{\partial t} - \operatorname{div}(a \nabla u - \boldsymbol{b}\, u) + c\, u &= f && \text{for } (\boldsymbol{x}, t) \in \Omega \times (0, T), \\ u(\boldsymbol{x}, 0) &= u_0(\boldsymbol{x}) && \text{for } \boldsymbol{x} \in \Omega, \\ &+ \text{B.C.} && \text{for } (\boldsymbol{x}, t) \in \Gamma \times (0, T). \end{aligned} \tag{5.4}$$

For a constant diffusion coefficient a and a divergence free vector field $\boldsymbol{b}$ this can be formulated as follows (instationary case):

Find $u \in V$ such that

$$\begin{aligned} \frac{\partial u}{\partial t} - a\, \Delta u + \boldsymbol{b} \cdot \nabla u + c\, u &= f && \text{for } (\boldsymbol{x}, t) \in \Omega \times (0, T), \\ u(\boldsymbol{x}, 0) &= u_0(\boldsymbol{x}) && \text{for } \boldsymbol{x} \in \Omega, \\ &+ \text{B.C.} && \text{for } (\boldsymbol{x}, t) \in \Gamma \times (0, T). \end{aligned} \tag{5.5}$$

The coefficients $a \geqslant 0$, $\boldsymbol{b} = (b_1, \ldots, b_d)^T$ and c depend smoothly on $(\boldsymbol{x}, t)$. Usually one has to assume that

$$\frac{1}{2} \operatorname{div} \boldsymbol{b} + c \geqslant \alpha \qquad \in \Gamma \times (0, T), \tag{5.6}$$

where $\alpha \geqslant 0$ in general. This condition ensures the stability of the problem (5.5) for all $a \geqslant 0$. For a small coefficient a, equation (5.6) can be relaxed (see, e. g. [8]). Since we have a divergence free vector field $\boldsymbol{b}$ the condition (5.6) reduces to $c \geqslant 0$.

In particular in the stationary case problem (5.5) simplifies to

Find $u \in V$ such that

$$\begin{aligned} -a\,\Delta u + \boldsymbol{b} \cdot \nabla u + c\,u &= f && \text{for } \boldsymbol{x} \in \Omega, \\ &+ \text{B.C.} && \text{for } \boldsymbol{x} \in \Gamma. \end{aligned} \tag{5.7}$$

In this case the coefficients of condition (5.6) depend smoothly on $\boldsymbol{x}$. The condition ensures the stability of the problem for all $\alpha > 0$. Due to the divergence free vector field $\boldsymbol{b}$ the condition (5.6) reduces to $c > 0$ for the stationary case.
The stationary model problem is a linear equation of mixed elliptic hyperbolic type. We assume that a is small, which means that (5.7) has mainly hyperbolic nature.

5.1 Outline

For a small coefficient a the problem (5.7) is mainly governed by the hyperbolic influences. Therefore we start viewing the purely hyperbolic case. We study the analysis and numerical treatment.
Back at the convection-diffusion equation we study the resulting boundary layers and consider a simplified model problem with constant coefficients and Dirichlet boundary conditions. There exists a straight forward extension to variable coefficients and other boundary conditions.

We shall consider the following finite element methods:

- Standard Galerkin (cf. Section 5.4)
- Streamline Upwind Petrov Galerkin (SUPG) (cf. Section 5.5)
- Discontinuous Galerkin (DG) (cf. Section 5.6)
- Standard Galerkin for mixed formulation (cf. Section 5.7)
- Streamline edge-upwind for mixed formulation (cf. Section 5.8)

The Standard Galerkin method and the SUPG method apply to stationary equations of mixed elliptic hyperbolic type of the form (5.7) with small diffusion coefficient. In contrast, the Discontinuous Galerkin method was originally designed for purely hyperbolic problems of the form (5.5) and (5.7) with diffusion coefficient $a = 0$. Nowadays it is also

established as non-conforming method for $a > 0$.

In the following we restrict ourselves to the stationary case. For the time dependent problem (5.5) we refer the reader to the time discontinuous streamline diffusion method presented in Chapter 9.9 in [8].

Remark 5.1. *Consider the time-dependent purely hyperbolic problem:*

$$\frac{\partial u}{\partial t} + \boldsymbol{b}(\boldsymbol{x}) \cdot \nabla u + c\, u = 0 \qquad \text{for } (\boldsymbol{x}, t) \in \Omega \times (0, T). \tag{5.8}$$

Replacing t by x_0 and setting $b_0 \equiv 1$ this can also be written as

$$\sum_{i=0}^{n} b_i \frac{\partial u}{\partial x_i} + c\, u = 0 \tag{5.9}$$

and therefore as an equation of the same type as the static version. Hence we can treat this equation in the same way as the stationary case.

5.2 Preliminaries

In the following the numerical analysis is done for $\Omega \subset \mathbb{R}^d$, $d = 1, 2, 3$. In the sequel we compare the different methods by applying them to the following one dimensional example. The according results are displayed in the figures contained in this chapter.

Example 5.2. *Find $u \in V$ such that*

$$\begin{aligned} -a\, u'' + b\, u' &= 1 \qquad \text{for } x \in (0, 1), \\ u(0) &= 1, \\ u(1) &= 0. \end{aligned} \tag{5.10}$$

The exact solution of the problem is given by

$$u(x) = \frac{1}{b}\, x + \frac{(1 + b)(e^{-\frac{b}{a}} - e^{\frac{b}{a}(x-1)})}{(b - e^{-\frac{b}{a}})} + 1 \tag{5.11}$$

and is illustrated in Figure 5.1.

Throughout this chapter we discuss two model problems.

Problem 5.3. ***Convection-diffusion problem*** *Let Ω be a bounded convex polygonal domain in $\mathbb{R}^d$, $d = 1, 2, 3$ with boundary $\Gamma = \partial\Omega$. We shall consider the following stationary boundary value problem with $c = 1$ and Dirichlet boundary condition:*

$$\begin{aligned} -a\, \Delta u + \boldsymbol{b} \cdot \nabla u + u &= f \qquad \text{for } \boldsymbol{x} \in \Omega, \\ u &= g \qquad \text{for } \boldsymbol{x} \in \Gamma, \end{aligned}$$

where a is a small positive constant, and $\boldsymbol{b} \cdot \nabla u$ denotes the derivative in the $\boldsymbol{b}$-direction.

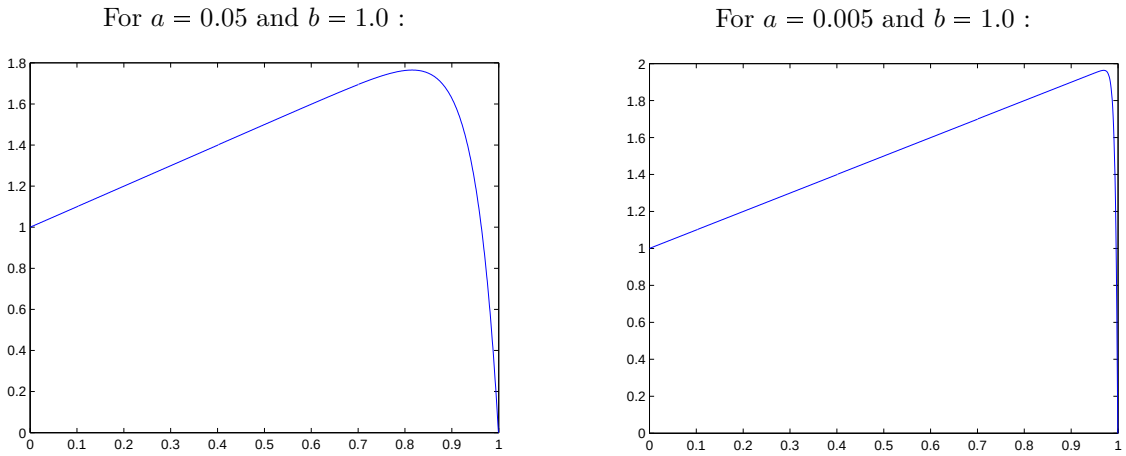

Figure 5.1: The exact solution for Example 5.2 for different parameters a and b.

Problem 5.4. ***Hyperbolic problem*** *The corresponding purely hyperbolic problem is obtained by setting* $a = 0$.

$$\begin{aligned} \boldsymbol{b} \cdot \nabla u + u &= f \qquad \text{for } \boldsymbol{x} \in \Omega, \\ u &= g \qquad \text{for } \boldsymbol{x} \in \Gamma_-, \end{aligned}$$

where Γ_- *denotes the inflow boundary defined by* $\Gamma_- := \{\boldsymbol{x} \in \Gamma \mid \boldsymbol{n}(\boldsymbol{x}) \cdot \boldsymbol{b} < 0\}$. *In contrast to the convection-diffusion problem which contains derivatives of second order, it is enough for the reduced problem to prescribe the boundary values only on* Γ_-.

For the following discussion we use the notations

$$\begin{aligned} (v, w) &:= \int_\Omega vw \, dx, \\ \|v\|_0 &:= \|v\|_{L_2(\Omega)}, & \|v\|_s &:= \|v\|_{H^s(\Omega)}, \\ \langle v, w \rangle_{\boldsymbol{b}} &:= \int_\Gamma vw \, \boldsymbol{n} \cdot \boldsymbol{b} \, ds, & \langle v, w \rangle_{\boldsymbol{b},\,||} &:= \int_\Gamma vw \, |\boldsymbol{n} \cdot \boldsymbol{b}| \, ds, \\ \langle v, w \rangle_{\boldsymbol{b},\,-} &:= \int_{\Gamma_-} vw \, \boldsymbol{n} \cdot \boldsymbol{b} \, ds, & \langle v, w \rangle_{\boldsymbol{b},\,+} &:= \int_{\Gamma_+} vw \, \boldsymbol{n} \cdot \boldsymbol{b} \, ds, \end{aligned}$$

where $\Gamma_+ = \Gamma \backslash \Gamma_- = \{\boldsymbol{x} \in \Gamma \mid \boldsymbol{n}(\boldsymbol{x}) \cdot \boldsymbol{b} \geqslant 0\}$. Notice that by Green's formula it follows that

$$(\boldsymbol{b} \cdot \nabla v, w) = \langle v, w \rangle_{\boldsymbol{b}} - (v, \boldsymbol{b} \cdot \nabla w). \tag{5.12}$$

We assume that $\{\mathcal{T}_h\}$ is a family of quasi-uniform triangulations $\mathcal{T}_h = \{T\}$ of Ω with mesh size h. An appropriate finite element space is

$$V_h = \mathcal{L}_p(\mathcal{T}_h) := \{v \in H^1(\Omega) \mid v_{|_T} \in \mathcal{P}^p(T),\ T \in \mathcal{T}_h\} \quad \text{with } p \geqslant 1$$

for a given integer $p > 0$. Differently speaking V_h is the space of continuous and piecewise polynomial functions of degree p.

5.3 Boundary layers

For a better understanding of boundary layers we briefly study the stationary hyperbolic ($a = 0$) equation (5.7) with homogeneous right hand side ($f = 0$)

$$\boldsymbol{b}(\boldsymbol{x}) \cdot \nabla u(\boldsymbol{x}) + c\, u(\boldsymbol{x}) = 0 \qquad \text{for } \boldsymbol{x} \in \Omega. \tag{5.13}$$

The parameterized curves $\boldsymbol{x}(s) = (x_1(s), \ldots, x_d(s))$ represent the streamlines of the velocity field $\boldsymbol{b}(\boldsymbol{x}) = (b_1(\boldsymbol{x}), \ldots, b_d(\boldsymbol{x}))$. Such a curve $\boldsymbol{x}(s)$ is a solution of the system of ordinary differential equations

$$\frac{dx_i}{ds} = b_i(\boldsymbol{x}(s)) \qquad i = 1, \ldots, d,$$

and is called characteristic curve (or simply characteristic) of the problem (5.13).

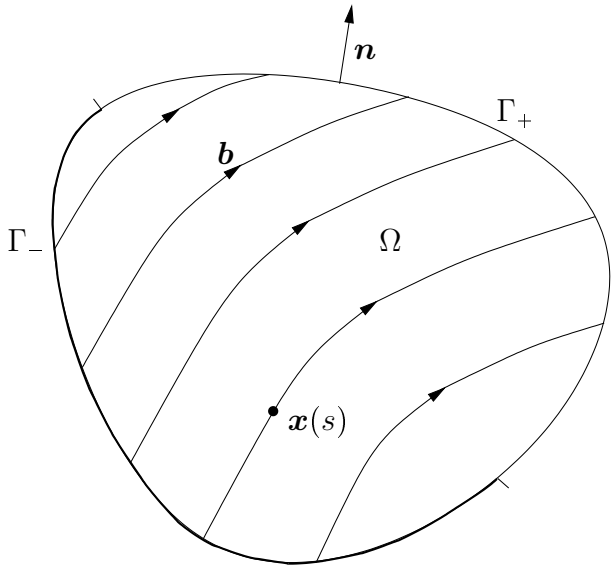

Figure 5.2: (Originally from JOHNSON [8] Fig.9.1)

If $\boldsymbol{b}$ is Lipschitz-continuous, i. e., there exists a constant C such that

$$|\boldsymbol{b}(\boldsymbol{x}) - \boldsymbol{b}(\boldsymbol{y})| \leqslant C|\boldsymbol{x} - \boldsymbol{y}| \quad \text{for all } \boldsymbol{x}, \boldsymbol{y} \in \Omega,$$

it can be shown that only one characteristic function $\boldsymbol{x}(s)$ passes through a given point $\bar{\boldsymbol{x}} \in \Omega$. In other words, there exists a unique function $\boldsymbol{x}(s)$, such that

$$\begin{aligned} \frac{dx_i}{ds} &= b_i(\boldsymbol{x}) \qquad i = 1, \ldots, d, \\ \boldsymbol{x}(0) &= \bar{\boldsymbol{x}}. \end{aligned}$$

Using the chain rule, the derivative of $u(\boldsymbol{x}(s))$ with respect to s can be expressed as

$$\frac{d}{ds}(u(\boldsymbol{x}(s))) = \sum_{i=1}^{d} \frac{\partial u}{\partial x_i}\frac{dx_i}{ds} = \sum_{i=1}^{d} \frac{\partial u}{\partial x_i} b_i(\boldsymbol{x}) = \boldsymbol{b}(\boldsymbol{x}) \cdot \nabla u(\boldsymbol{x}).$$

Together with the stationary hyperbolic partial differential equation (5.13) we obtain the ordinary differential equation

$$\frac{d}{ds}(u(\boldsymbol{x}(s))) + c\,u(\boldsymbol{x}(s)) = 0. \tag{5.14}$$

This makes it particularly simple to compute u along a given characteristic. Granted that u is known at one point of a characteristic, u can be obtained by integrating (5.14) along $\boldsymbol{x}(s)$. Considering a concrete example this means: If u is known on the inflow boundary Γ_- (compare figure 5.2), u can be determined in each point $\boldsymbol{x} \in \Omega$ by starting at the inflow boundary and integrating along the corresponding characteristic curve.
This explains why effects (e. g. jump discontinuities of u) that appear on the inflow boundary are propagated just along the characteristics.
Hence, if boundary data are discontinuous and have, e. g. a jump, then solution u of Problem 5.4 is discontinuous with a jump across the characteristic (with starting point at the jump on the inflow boundary).

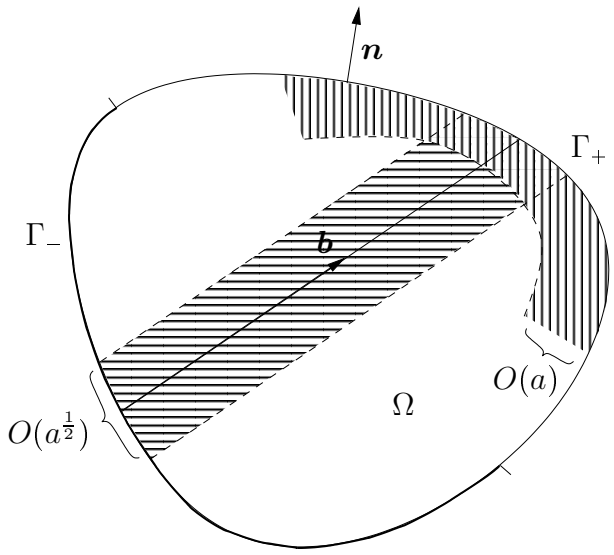

Figure 5.3: The characteristics of the reduced problem Problem 5.4 are straight lines parallel to $\boldsymbol{b}$. The corresponding layers are schematically pictured. (Originally from JOHNSON [8] Fig.9.4)

Adding a diffusion term ($a > 0$) results in the equation of Problem 5.3. The solution u of this convection-diffusion equation has to be continuous in Ω. Thus a discontinuity at the

boundary spreads out in a region of width $O(a^{\frac{1}{2}})$ (see Figure 5.3) around the characteristic. Such thin regions where u or derivatives of u rapidly change are called layers.
Solving the hyperbolic equation Problem 5.4 gives certain values of u on the outflow boundary $\Gamma_+ = \Gamma \backslash \Gamma_-$. If they differ from the given boundary values g on Γ_+ of the convection-diffusion problem the solution of Problem 5.3 reveals a boundary layer of width $O(a)$ (see Figure 5.3).

5.4 Standard Galerkin

The variational formulation for Problem 5.3 is given by:

Find $u \in H_0^1(\Omega)$ such that

$$A(u, v) = f(v) \qquad \text{for all } v \in H_0^1(\Omega) \tag{5.15}$$

with bilinear form and linear form defined as

$$\begin{aligned} A(w, v) &:= (a \nabla w, \nabla v) + (\boldsymbol{b} \cdot \nabla w + w, v), \\ f(v) &:= (f, v) - (g, v). \end{aligned}$$

With a conforming finite element space

$$V_{0,h} = \{v \in V_h \mid v_{|\Gamma=0}\} \subset H_0^1(\Omega)$$

the standard Galerkin method for (5.15) leads to the discretized problem

Find $u_h \in V_{0,h}$ such that

$$A(u_h, v_h) = f(v_h) \qquad \text{for all } v_h \in V_{0,h}. \tag{5.16}$$

Standard Galerkin for hyperbolic problem (*Problem 5.4*)

First we analyze the stability of the reduced Problem 5.4. We consider the standard Galerkin method with weakly imposed boundary conditions:

Find $u_h \in V_h \subset H^1(\Omega)$ such that

$$B(u_h, v_h) = \tilde{f}(v_h) \qquad \text{for all } v_h \in V_h, \tag{5.17}$$

with bilinear form and linear form defined as

$$\begin{aligned} B(w, v) &:= (\boldsymbol{b} \cdot \nabla w + w, v) - \langle w, v \rangle_{\boldsymbol{b}, -}, \\ \tilde{f}(v) &:= (f, v) - \langle g, v \rangle_{\boldsymbol{b}, -}. \end{aligned}$$

The stability of the discrete variational problem (5.17) is the result of the following property of the bilinear form $B(.,.)$:

Lemma 5.5. *For any $v \in H^1(\Omega)$ we have*

$$B(v,v) = \|v\|_0^2 + \frac{1}{2}\langle v, v\rangle_{\boldsymbol{b},||}.$$

Proof. This can easily be verified (cf. [8], Lemma 9.1, p.179) using Green's formula

$$(\boldsymbol{b}\cdot\nabla v, v) = \langle v, v\rangle_{\boldsymbol{b}} - (v, \boldsymbol{b}\cdot\nabla v), \tag{5.12}$$

which yields

$$(\boldsymbol{b}\cdot\nabla v, v) = \frac{1}{2}\langle v, v\rangle_{\boldsymbol{b}} = \frac{1}{2}\langle v, v\rangle_{\boldsymbol{b},+} + \frac{1}{2}\langle v, v\rangle_{\boldsymbol{b},-}.$$

Hence,

$$\begin{aligned} B(v,v) &= \|v\|_0^2 + \frac{1}{2}\langle v, v\rangle_{\boldsymbol{b},+} + \frac{1}{2}\langle v, v\rangle_{\boldsymbol{b},-} - \langle v, v\rangle_{\boldsymbol{b},-} \\ &= \|v\|_0^2 + \frac{1}{2}\langle v, v\rangle_{\boldsymbol{b},+} - \frac{1}{2}\langle v, v\rangle_{\boldsymbol{b},-} \\ &= \|v\|_0^2 + \frac{1}{2}\langle v, v\rangle_{\boldsymbol{b},||} \end{aligned}$$

where we used that $\boldsymbol{n}\cdot\boldsymbol{b} \geqslant 0$ on Γ_+ and $\boldsymbol{n}\cdot\boldsymbol{b} < 0$ on Γ_-. □

The lower bound for $B(v,v)$ needed for existence and uniqueness of the solution is provided by Lemma 5.5. Next we are interested in an a-priori error estimate.

Theorem 5.6. *If u satisfies Problem 5.4 and $u_h \in V_h$ is the solution of* (5.17)*, then there exists a constant C such that*

$$\|u - u_h\|_0 + \langle u - u_h, u - u_h\rangle_{\boldsymbol{b}} \leqslant Ch^p\|u\|_{p+1}. \tag{5.18}$$

Proof. Confer [8] (Theorem 9.1, p.180). □

The error estimate (5.18) indicates that if the exact solution u of the hyperbolic problem (Problem 5.4) is smooth enough (i. e., $u \in H^{p+1}(\Omega)$) in such a way that $\|u\|_{p+1}$ is finite, then the standard Galerkin method converges at a rate of $O(h^p)$. Since the optimal rate would be $O(h^{p+1})$ this performance is quite satisfactory. But in general the solution u is not smooth enough, e. g. for u discontinuous $\|u\|_1 = \infty$. In this case estimate (5.18) is obviously useless.

Standard Galerkin for convection-diffusion problem (*Problem 5.3*)

In order to show the stability of Problem 5.3 we prove an a-priori error estimate for the discrete variational problem (5.16). Hence, we first have a look at (5.15) and show in the following that the bilinear form $A(.,.)$ and the linear form $f(.)$ fulfill the requirements for Lax Milgram (cf. Theorem 3.3).
The continuity of the bilinear form (with constant $\gamma > 0$) and the linear form is easy to show and therefore left to the reader. It remains to show that the bilinear form $A(.,.)$ is coercive on V.

Provided that $a(\boldsymbol{x}) \geqslant a = \text{constant} > 0$, $c(\boldsymbol{x}) \geqslant c = \text{constant} > 0$ almost everywhere and $\|b_i\|_\infty \leqslant \tilde{b} = \text{constant} < \infty$ for all $i = 1, \ldots, d$ there holds the following calculation. In order to keep this proof more general we replace $c = 1$ again by a general c. The bilinear form is therefore given as

$$A(v,v) = \int_\Omega a|\nabla v|^2\,dx + \int_\Omega \boldsymbol{b}\cdot\nabla v\, v\,dx + \int_\Omega c\,v^2\,dx.$$

Note that the sign of the second term can either be positiv or negativ. We use its negativ absolute value as a lower estimate.

$$\begin{aligned}
A(v,v) &\geqslant \int_\Omega a|\nabla v|^2\,dx - |\int_\Omega \boldsymbol{b}\cdot\nabla v\, v\,dx| + \int_\Omega c\,v^2\,dx \\
&\geqslant a\|\nabla v\|_0^2 - \tilde{b}\|\nabla v\|_0\|v\|_0 + c\|v\|_0^2 && \text{(C.S.)} \\
&\geqslant a\|\nabla v\|_0^2 - \tilde{b}\left(\frac{1}{2\epsilon}\|\nabla v\|_0^2 + \frac{\epsilon}{2}\|v\|_0^2\right) + c\|v\|_0^2 && (|ab| \leqslant \frac{1}{2\varepsilon}a^2 + \frac{\varepsilon}{2}b^2) \\
&= (a - \frac{\tilde{b}}{2\epsilon})|v|_1^2 + (c - \frac{\tilde{b}\epsilon}{2})\|v\|_0^2 \\
&\geqslant \min(a - \frac{\tilde{b}}{2\epsilon}, c - \frac{\tilde{b}\epsilon}{2})\|v\|_1^2.
\end{aligned}$$

Summing up, coercivity on V, i. e.,

$$A(v,v) \geqslant \alpha\|v\|_1^2 \qquad \text{for all } v \in V$$

is fulfilled with $\alpha = \min(a - \frac{\tilde{b}}{2\epsilon}, c - \frac{\tilde{b}\epsilon}{2}) > 0$, but only if the bound $\tilde{b}$ fulfills $\tilde{b} < \sqrt{4ac}$.
The coercivity completes the assumptions of Lax-Milgram theorem 3.3, hence existence and uniqueness of the exact solution as well as of the Galerkin solution u_h are ensured. Finally the a-priori error estimate is left to be shown.

Theorem 5.7. *If u_h satisfies* (5.16) *and u satisfies problem 5.3, then there exists a constant $\widetilde{C}$ such that*

$$\|u - u_h\|_1 \leqslant \widetilde{C}h^r\|u\|_{r+1} \tag{5.19}$$

with $\widetilde{C} = \frac{\gamma}{\alpha}C$ and $\alpha = min(a, 1)$. Where γ is the continuity constant of the bilinear form $A(.,.)$, i. e., $|A(v,w)| \leqslant \gamma\,\|v\|\,\|w\|$.

Proof. We choose the arbitrary function v_h in Theorem 3.14 equal to the interpolant $\pi_h u$ of u. Using the estimate (3.9) leads to the desired statement. □

Obviously for a small diffusion coefficient $a \ll 1$ the constant $\widetilde{C}$ becomes arbitrary large.

See example 5.2:

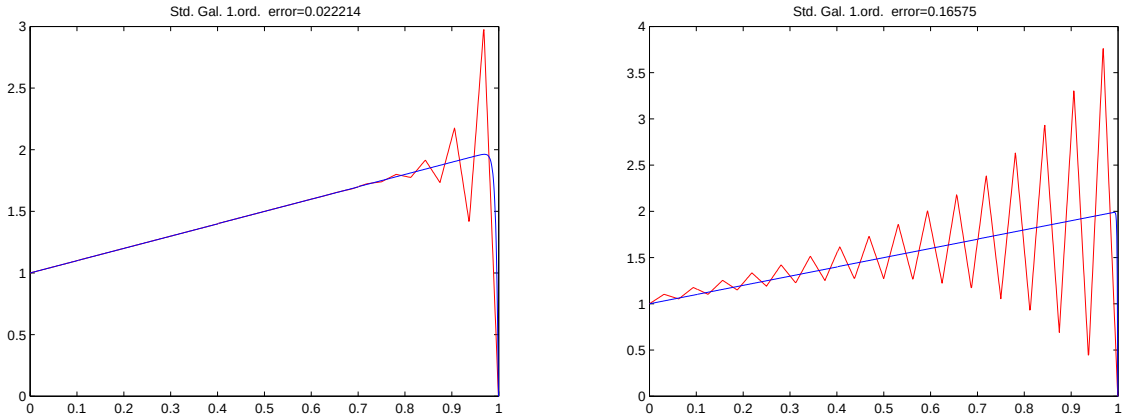

For $a = 0.005$ and $b = 1.0$. For $a = 0.001$ and $b = 1.0$.

Figure 5.4: The solution (red) for Example 5.2 using standard Galerkin method and linear elements with the same discretization for two different diffusion coefficients. (Versus exact solution (blue).)

It can be observed, that standard finite element methods for convection-diffusion problems with small diffusion coefficient a do not give reasonable results in cases where the exact solution is not smooth. If the exact solution has, e. g. a jump discontinuity, the finite element solution will in general exhibit large incorrect oscillations even far from the jump and will then be fairly far from the exact solution everywhere.

It is also important how fine the mesh is. For the discretization parameter $h \leqslant \frac{a}{b}$ this method will perform well. But for $h \gg \frac{a}{b}$ there may occur unmeant oscillations, destroying the solution. We illustrate this effects with Example 5.2. We especially observe what happens to the results when decreasing h from $h > \frac{a}{b}$ to $h < \frac{a}{b}$ (cf. Figure 5.5).

For a small diffusion coefficient a the solution $u(x)$ of Example 5.2 is close to a straight line except in a layer at the boundary ($x = 1$). This layer where u decays from 1 to 0 is of width $O(a)$.
Summing up, the effects that can be observed are either a bad approximation at the boundary layer (too broad layer) or oscillations at the boundary layer which spread out. The smaller a, the thinner the boundary layer, which causes numerical problems (oscillations) for $a \to 0$ (cf. Figure 5.4). Increasing the order gives better results but it

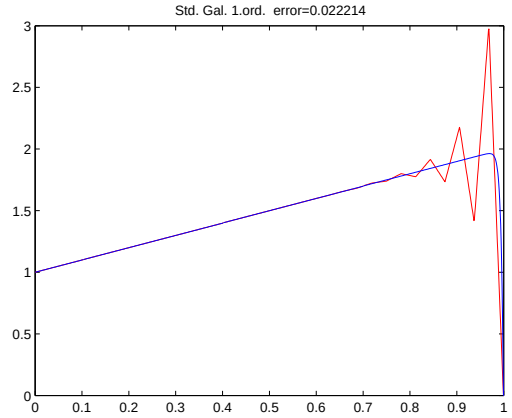

For $a = 0.005$ and $b = 1.0$ with $h = 0.0312$.

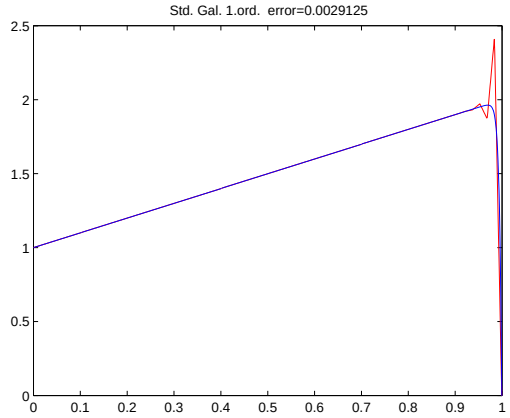

For $a = 0.005$ and $b = 1.0$ with $h = 0.0156$.

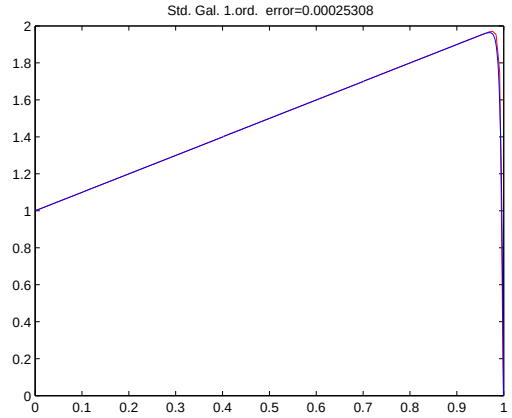

For $a = 0.005$ and $b = 1.0$ with $h = 0.0078$.

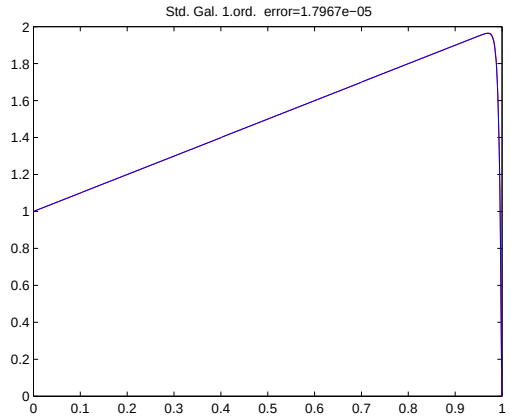

For $a = 0.005$ and $b = 1.0$ with $h = 0.0039$.

Figure 5.5: The solution (red) for Example 5.2 using standard Galerkin method and linear elements decreasing the mesh width h from $h > a$ to $h < a$. (Versus exact solution (blue).)

does not change the appearance of the negative effects at the boundary layer (cf. Figure 5.6). It does not even get significant better, since the main part of the model problem can be perfectly approximated by linear elements.

Applying the standard Galerkin method with piecewise linear functions on a uniform mesh (mesh width h) to example 5.2, we obtain a system of equations

$$-\frac{a}{h^2}[u_{i+1} - 2u_i + u_{i-1}] + \frac{b}{2h}[u_{i+1} - u_{i-1}] = 0, \qquad i = 1, \ldots, N-1$$
$$u_0 = 1, \; u_n = 0$$

where u_i are the values of the finite element approximation u_h at the grid points

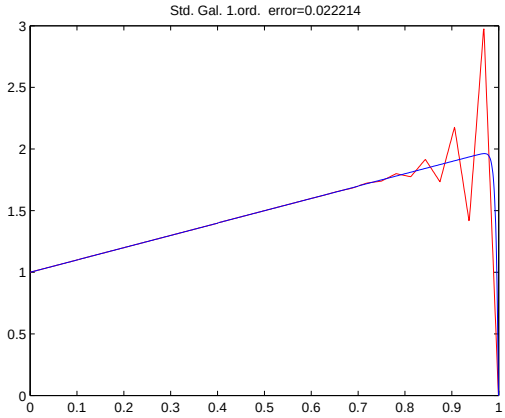

For $a = 0.005$ and $b = 1.0$ with $h = 0.0312$.

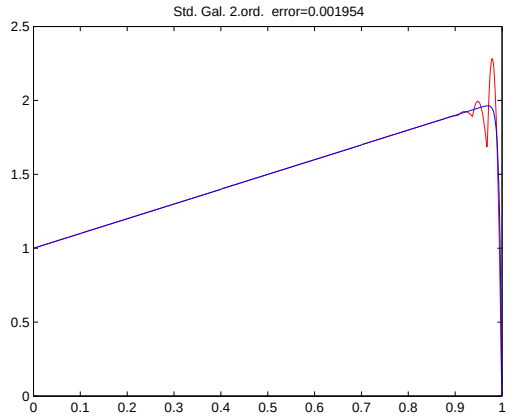

For $a = 0.005$ and $b = 1.0$ with $h = 0.0312$.

Figure 5.6: The solution (red) for Example 5.2 using standard Galerkin method and elements of first and second order with the same discretization.

$x_i = ih,\ i = 0, 1, \ldots, N$. The diagonal block of the matrix of the diffusion term contains a, contrary to the matrix of the convection term. Therefore we lose the M-matrix property of the stiffness matrix.

Remark 5.8. *With the help of adaptive error estimators or additional knowledge about the boundary layer, the boundary layer could be resolved with, e. g. geometric refinement. In our model case this could be done by bisecting the last element recursively.*

5.5 Streamline-Upwind Petrov-Galerkin (SUPG)

We observed that for a coarse discretization the standard Galerkin method has difficulties to obtain good approximations. These difficulties can be overcome, by solving a modified problem. This modified problem should be near the original with diffusion term $-a\Delta u$. The main idea is to modify the diffusion term by introducing a certain amount of extra diffusion acting directly in streamline direction. It turns out that it is sufficient to add a term $-\delta_a(\boldsymbol{b} \cdot \nabla(\boldsymbol{b} \cdot \nabla u))$ with $\delta_a = h - a$. Such a modified artificial diffusion method results in a discrete variational problem that can be written as:

$$\begin{aligned} &\text{Find } u_h \in V_{0,h} \text{ such that} \\ &(a\,\nabla u_h, \nabla v_h) + \delta_a(\boldsymbol{b} \cdot \nabla u_h, \boldsymbol{b} \cdot \nabla v_h) + (\boldsymbol{b} \cdot \nabla u_h + u_h, v_h) = (f, v_h) \\ &\qquad\qquad\qquad\qquad\qquad\qquad\qquad\qquad\qquad\qquad \text{for all } v_h \in V_{0,h}. \end{aligned} \tag{5.20}$$

In this way no crosswind diffusion (perpendicular to the streamlines) is introduced. Unfortunately this corresponds to an $O(h)$-perturbation of the exact solution of the original prob-

lem. However, there exists a possibility to introduce the modifying term $\delta_a(\boldsymbol{b}\cdot\nabla u_h, \boldsymbol{b}\cdot\nabla v_h)$ without such a perturbation. In a first approach we apply this technique (SUPG) to Problem 5.4.

SUPG for the hyperbolic problem (*Problem 5.4*)

We start from the discrete variational problem (5.17) gained from the standard Galerkin method with weakly imposed boundary conditions. The test functions are chosen of the special form $v_h + h\,\boldsymbol{b}\cdot\nabla v_h$. Thereby we obtain the discrete formulation of the streamline diffusion method:

Find $u_h \in V_h$ such that

$$\begin{aligned}(\boldsymbol{b}\cdot\nabla u_h + u_h, v_h + h\,\boldsymbol{b}\cdot\nabla v_h) - (1+h)\langle u_h, v_h\rangle_{\boldsymbol{b},-} = \\ (f, v_h + h\,\boldsymbol{b}\cdot\nabla v_h) - (1+h)\langle g, v_h\rangle_{\boldsymbol{b},-} \qquad \text{for all } v_h \in V_h.\end{aligned} \tag{5.21}$$

This formulation is consistent with Problem 5.4 since relation (5.21) is still true when replacing u_h by the exact solution u. But it prevents an $O(h)$-perturbation as (5.20). For the analysis we introduce the formulation

Find $u_h \in V_h$ such that

$$B_m(u_h, v_h) = \tilde{f}_m(v_h) \qquad \text{for all } v_h \in V_h, \tag{5.22}$$

with bilinear form and linear form defined as

$$\begin{aligned}B_m(w,v) &:= (\boldsymbol{b}\cdot\nabla w + w, v + h\,\boldsymbol{b}\cdot\nabla v) - (1+h)\langle w, v\rangle_{\boldsymbol{b},-},\\ \tilde{f}_m(v) &:= (f, v + h\,\boldsymbol{b}\cdot\nabla v) - (1+h)\langle g, v\rangle_{\boldsymbol{b},-}.\end{aligned}$$

The proof of an a-priori error estimate will be done in the following norm

$$\|v\|_{\boldsymbol{b}} := \left(h\|\boldsymbol{b}\cdot\nabla v\|_0^2 + \|v\|_0^2 + \frac{1+h}{2}\langle v, v\rangle_{\boldsymbol{b},||}\right)^{\frac{1}{2}}.$$

This norm is chosen according to the proof of the stability property of the bilinear form $B_m(.,.)$.

Lemma 5.9. *For any $v \in H^1(\Omega)$ we have*

$$B_m(v,v) = \|v\|_{\boldsymbol{b}}^2.$$

The error estimate for the streamline diffusion method can then be formulated as following.

Theorem 5.10. *If u_h satisfies (5.21) and u satisfies Problem 5.4, then there exists a constant C such that*

$$\|u - u_h\|_{\boldsymbol{b}} \leqslant Ch^{r+\frac{1}{2}}\|u\|_{r+1}. \tag{5.23}$$

Proof. Confer [8] (p.183 f.). □

This error estimate (5.23) states that

$$\begin{aligned} \|u - u_h\|_0 &\leqslant Ch^{r+\frac{1}{2}}\|u\|_{r+1}, \\ \|(\boldsymbol{b}\cdot\nabla u - \boldsymbol{b}\cdot\nabla u_h)\|_0 &\leqslant Ch^{r}\|u\|_{r+1}. \end{aligned}$$

This means that the L_2-error is half a power of h from being optimal, and the L_2-error of the derivative in streamline direction is optimal. This sounds somewhat better than the estimates (5.18) for the standard Galerkin method in the case of a smooth solution. In this method effects are propagated approximately as in the continuous problem, i. e.,essentially along the characteristics. One can prove [8] that the effect of for example a jump in the exact solution across a characteristic will be limited to a narrow region around the characteristic.

Remark 5.11. *For the continuous problem Problem 5.4 (for simplicity with $g = 0$) the following stability estimate can be done*

$$\sqrt{\langle u, u\rangle_{\boldsymbol{b},||}} + \|u\|_0 + \|\boldsymbol{b}\cdot\nabla u\|_0 \leqslant C\|f\|_0.$$

First we gain control of the terms $\sqrt{\langle u, u\rangle_{\boldsymbol{b},||}}$ and $\|u\|_0$. Using $B(u,u) = \tilde{f}(u)$ with $g = 0$ and Lemma 5.5 gives us the start.

$$\begin{aligned} \|u\|_0^2 + \frac{1}{2}\langle u, u\rangle_{\boldsymbol{b},||} = (f,u) &\leqslant \|f\|_0\|u\|_0 \leqslant \frac{1}{2}(\|f\|_0^2 + \|u\|_0^2), \\ \|u\|_0^2 + \frac{1}{2}\langle u, u\rangle_{\boldsymbol{b},||} - \frac{1}{2}\|u\|_0^2 &\leqslant \frac{1}{2}\|f\|_0^2, \\ \|u\|_0^2 + \langle u, u\rangle_{\boldsymbol{b},||} &\leqslant \|f\|_0^2, \end{aligned}$$

which leads to $\sqrt{\langle u, u\rangle_{\boldsymbol{b},||}} + \|u\|_0 \leqslant \overline{c}\,\|f\|_0$. The control of $\boldsymbol{b}\cdot\nabla u$ follows by using $\boldsymbol{b}\cdot\nabla u = f - u$, i. e.,

$$\begin{aligned} \|\boldsymbol{b}\cdot\nabla u\|_0 = \|f - u\|_0 &\leqslant \|f\|_0 + \|u\|_0 \\ &\leqslant \|f\|_0 + \|u\|_0 + \sqrt{\langle u, u\rangle_{\boldsymbol{b},||}} \\ &\leqslant (1 + \overline{c})\,\|f\|_0 \end{aligned}$$

The corresponding stability estimate for the streamline diffusion method is obtained by using Lemma 5.9 with $v = u_h$ and reads $\|u_h\|_{\boldsymbol{b}} \leqslant C\|f\|$ or

$$\sqrt{\langle u_h, u_h\rangle_{\boldsymbol{b},||}} + \|u_h\|_0 + \sqrt{h}\|\boldsymbol{b}\cdot\nabla u_h\|_0 \leqslant C\|f\|_0.$$

In the discrete case the control of $\|u_h\|_0$ does not give any control of the streamline derivative $\|\boldsymbol{b}\cdot\nabla u_h\|_{\boldsymbol{b}}$. Only a partial control is build in through the modified test function. But the estimate is weaker than the above mentioned estimate for the continuous problem.

SUPG for the convection-diffusion problem (*Problem 5.3*)

Multiplying Problem 5.3 with the test function $v+\delta\boldsymbol{b}\cdot\nabla v$ where $v \in H_0^1(\Omega)$ and integrating over the domain, we obtain

$$\begin{aligned}(a\,\nabla u, \nabla v) - \delta(a\,\Delta u, \boldsymbol{b}\cdot\nabla v) + (u + \boldsymbol{b}\cdot\nabla u, v+\delta\boldsymbol{b}\cdot\nabla v) = \\ (f, v + \delta\boldsymbol{b}\cdot\nabla v) \qquad \text{for all } v \in V,\end{aligned} \tag{5.24}$$

where partial integration was done on the term $-a(\Delta u, v)$. The positive parameter δ has to be specified which will be done below. Formulating the discrete analogue of this relation the term $(\Delta u_h, \boldsymbol{b}\cdot\nabla v_h)$ is not well defined. In order to give this term a suitable meaning we define

$$(\Delta u_h, \boldsymbol{b}\cdot\nabla v_h) \equiv \sum_{T\in\mathcal{T}_h}\int_T \Delta u_h \boldsymbol{b}\cdot\nabla v_h dx, \tag{5.25}$$

which is well defined since the integrals over the interior of each triangle T is well defined. Consequently the streamline diffusion method for Problem 5.3 reads as

Find $u_h \in V_{0,h}$ such that

$$\begin{aligned}(a\,\nabla u_h, \nabla v_h) - \delta(a\,\Delta u_h, \boldsymbol{b}\cdot\nabla v_h) + (u_h + \boldsymbol{b}\cdot\nabla u_h, v_h+\delta\boldsymbol{b}\cdot\nabla v_h) = \\ (f, v_h + \delta\boldsymbol{b}\cdot\nabla v_h),\end{aligned} \tag{5.26}$$

where $\delta = \bar{C}h$ if $a < h$ with $\bar{C}$ sufficiently small (see Remark 5.12 below), and $\delta = 0$ if $a \geqslant h$. This formulation is consistent and the error estimate (5.23) and the results from (5.21) can be extended to this discrete variational formulation (5.26) with $a < h$.

Remark 5.12. *Now we investigate the stability estimate for* (5.26) *in the case* $a < h$. *We aim to prove that the additional term* $-\delta(a\,\Delta u_h, \boldsymbol{b}\cdot\nabla v_h)$ *does not harm the stability result obtained by introducing the term* $\delta(\boldsymbol{b}\cdot\nabla u_h, \boldsymbol{b}\cdot\nabla v_h)$. *We have for* $v \in V_{0,h}$

$$\begin{aligned}
|\delta(a\,\Delta v, \boldsymbol{b}\cdot\nabla v)| &= |a\delta\sum_{T\in\mathcal{T}_h}\int_T \Delta v\,\boldsymbol{b}\cdot\nabla v dx| \\
&= |a\delta\sum_{T\in\mathcal{T}_h} -\int_T \nabla v\nabla(\boldsymbol{b}\cdot\nabla v)dx| && \textit{part.int., } v_{|\Gamma} = 0 \\
&\leqslant a\delta\sum_{T\in\mathcal{T}_h} |\int_T \nabla v\nabla(\boldsymbol{b}\cdot\nabla v)dx| \\
&\leqslant a\sum_{T\in\mathcal{T}_h} [\|\nabla v\|_0\,\delta\|\nabla(\boldsymbol{b}\cdot\nabla v)\|_0] && \textit{C.S.} \\
&\leqslant a\sum_{T\in\mathcal{T}_h}\left[\frac{1}{2}\|\nabla v\|_0^2 + \frac{1}{2}\delta^2\|\nabla(\boldsymbol{b}\cdot\nabla v)\|_0^2\right] && ab \leqslant \frac{1}{2}(a^2+b^2) \\
&\leqslant a\sum_{T\in\mathcal{T}_h}\left[\frac{1}{2}\|\nabla v\|_0^2 + \frac{1}{2}\delta^2 C^2 h_T^{-2}\|\boldsymbol{b}\cdot\nabla v\|_0^2\right] && \textit{inverse estimate} \\
&\leqslant \frac{1}{2}a\|\nabla v\|_0^2 + \frac{1}{2}a\delta C^2 h^{-2}\delta\|\boldsymbol{b}\cdot\nabla v\|_0^2.
\end{aligned}$$

Now the bilinear form associated with (5.26) *(we refer to it as* $A_m(.,.)$*) can be estimated by*

$$A_m(v,v) \geqslant \frac{1}{2}a\|\nabla v\|_0^2 + \|v\|_0^2 + (1 - \frac{1}{2}a\delta C^2 h^{-2})\delta\|\boldsymbol{b}\cdot\nabla v\|_0^2 \qquad \textit{for all } v \in V_{0,h},$$

which yields the desired stability result

$$A_m(v,v) \geqslant \frac{1}{2}(a\|\nabla v\|_0^2 + \delta\|\boldsymbol{b}\cdot\nabla v\|_0^2 + \|v\|_0^2) \qquad \textit{for all } v \in V_{0,h},$$

$\bar{C}$ *has to be chosen small enough to fulfill*

$$a\delta C^2 h^{-2} = a\bar{C}hC^2h^{-2} \leqslant C^2\bar{C} < 1. \tag{5.27}$$

Summing up, the discrete variational formulation (5.26) gained from the idea of the Streamline-Upwind Petrov-Galerkin method is one possibility of constructing an high-order accurate method for Problem 5.3 with good stability properties.

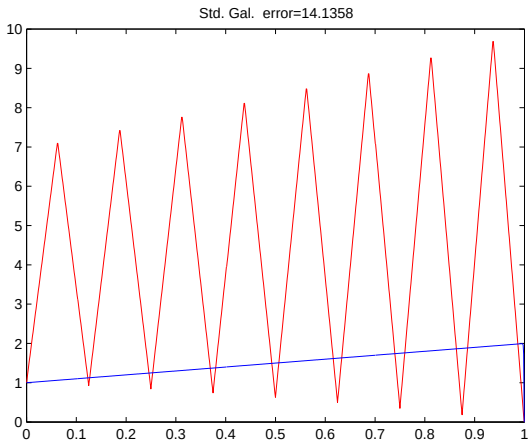

Solved with std. Gal. for $a = 0.0005$ and $b = 1.0$ with $h = 0.0625$.

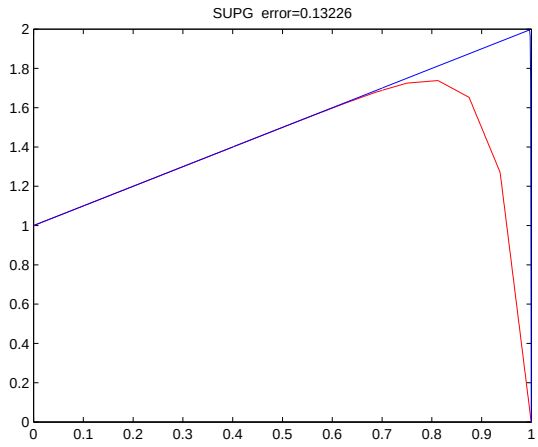

Solved with SUPG for $a = 0.0005$ and $b = 1.0$ with $h = 0.0625$.

Figure 5.7: The solutions (red) for Example 5.2 using linear elements and the same discretization for both methods.

The numerical experiments for Example 5.2 as shown in Figure 5.7 confirm that especially for coarse discretizations no oscillations occur using the SUPG method. The approximate solution generated by the SUPG method has at least some qualitative commonplaces with the true solution. It recovers the shape of the exact solution much better even though the boundary layer is smeared out. For a finer discretization the solution converges towards the exact solution (cf. Figure 5.8) and from the moment on when the discretization resolves the boundary layer it is identical to the solution of the standard Galerkin method which then is as good as possible.

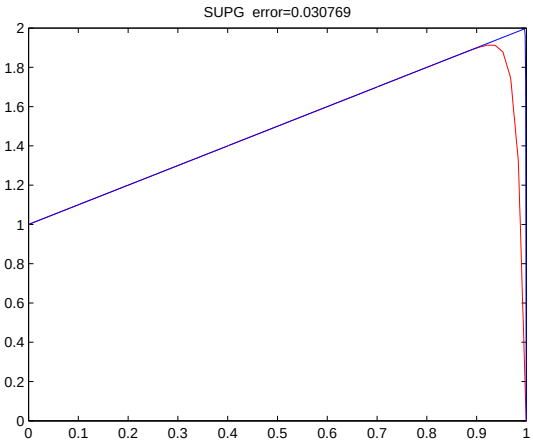

Solved with SUPG for $a = 0.0005$ and $b = 1.0$ with $h = 0.0156$.

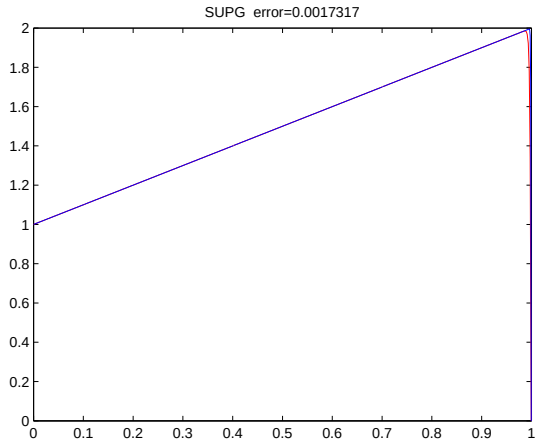

Solved with SUPG for $a = 0.0005$ and $b = 1.0$ with $h = 0.0039$.

Figure 5.8: The solutions (red) for Example 5.2 using linear elements converges to the exact solution.

5.6 Discontinuous Galerkin (DG)

The discontinuous Galerkin method is based on the following finite element space

$$V_h = \{v \in L_2(\Omega) \mid v_{|_T} \in \mathcal{P}^p(T) \text{ for all } T \in \mathcal{T}_h\},$$

which contains no continuity requirements across inter element boundaries.

In the sequel we use the following notations to describe the problem. The boundary ∂T of the triangle T is split into the inflow boundary $\partial T_- := \{\boldsymbol{x} \in \partial T \mid \boldsymbol{n}(\boldsymbol{x}) \cdot \boldsymbol{b} < 0\}$ and an outflow part $\partial T_+ := \{\boldsymbol{x} \in \partial T \mid \boldsymbol{n}(\boldsymbol{x}) \cdot \boldsymbol{b} \geqslant 0\}$. An edge S is shared by the two triangles T and T'. We consider $v \in V_h$ which may have a jump discontinuity across S. The left hand limit is defined as $v^-(\boldsymbol{x}) := \lim_{s \to 0^-} v(\boldsymbol{x} + s\boldsymbol{b})$ and the right hand limit as $v^+(\boldsymbol{x}) := \lim_{s \to 0^+} v(\boldsymbol{x} + s\boldsymbol{b})$ for $\boldsymbol{x} \in S$. Finally the jump $[\![v]\!]$ across S is defined as $[\![v]\!] := v^+ - v^-$.

Using these definitions we can formulate the discontinuous Galerkin method for the hyperbolic problem Problem 5.4 as following.

For $T \in \mathcal{T}_h$, given u_h^- on ∂T_- find $u_h \in V_h$ with $u_h \equiv u_{h_{|_T}} \in \mathcal{P}^p(T)$ such that

$$\begin{aligned}(\boldsymbol{b} \cdot \nabla u_h + u_h, v_h)_T - \int_{\partial T_-} u_h^+ v_h^+ \boldsymbol{n} \cdot \boldsymbol{b}\, ds = \\ (f, v_h)_T - \int_{\partial T_-} u_h^- v_h^+ \boldsymbol{n} \cdot \boldsymbol{b}\, ds \qquad \text{for all } v_h \in \mathcal{P}^p(T)\end{aligned} \tag{5.28}$$

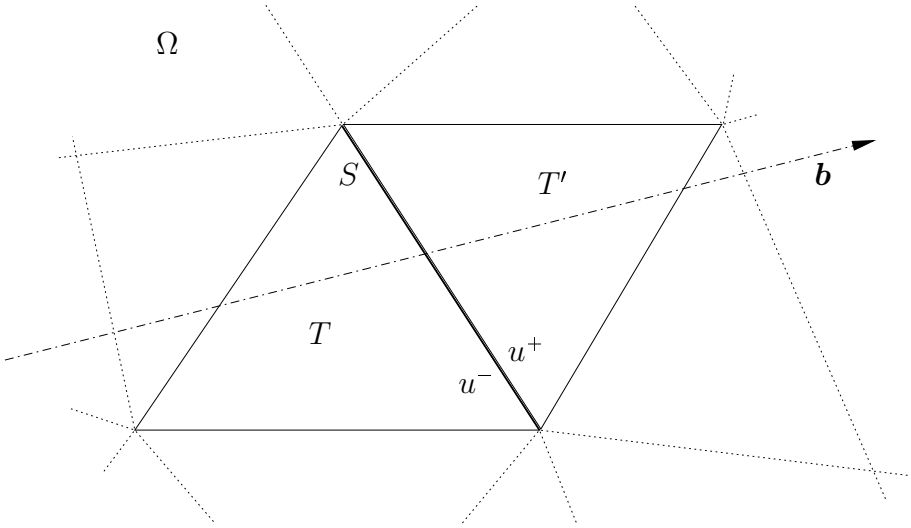

Figure 5.9: Flow across edge $S = \partial T_+$ in the direction of $\boldsymbol{b}$

where

$$(w, v)_T = \int_T w\, v\, dx, \quad u_h^- = g \text{ on } \Gamma_-.$$

This problem is just formed by a standard Galerkin method with weakly imposed boundary condition for one element. If $u_{h,-}$ is given on the inflow part of the element boundary it can be determined on the whole element. This allows the following strategy. Starting with the elements at the inflow boundary Γ_-, the solution can be extended triangle by triangle until the whole domain is covered.
In a more compact form we can write (5.28) as

$$B_T(u_h, v_h) = (f, v_h)_T \qquad \text{for all } v_h \in \mathcal{P}^p(T),$$

where

$$B_T(w, v) = (\boldsymbol{b} \cdot \nabla w + w, v)_T - \int_{\partial T_-} [\![w]\!] v^+ \boldsymbol{n} \cdot \boldsymbol{b}\, ds.$$

Now we can formulate the discontinuous Galerkin method in short.

Find $u_h \in V_h$ such that

$$B_{DG}(u_h, v_h) = (f, v_h) \qquad \text{for all } v_h \in V_h, \tag{5.29}$$

where

$$B_{DG}(w, v) = \sum_{T \in \mathcal{T}_h} B_T(w, v),$$

and $u_h^- = g$ on Γ_-. Note that for the exact solution $[\![u]\!]\, \boldsymbol{n} \cdot \boldsymbol{b} = 0$ is satisfied.

5.7 Standard Galerkin for mixed formulation

Now we tackle the convection-diffusion problem (5.4) in a slightly different way. Taking for simplicity the stationary problem with $c = 0$ and Dirichlet boundary conditions g on Γ we obtain

$$-\operatorname{div}(a\nabla u - \boldsymbol{b}\, u) = f \qquad \text{for } \boldsymbol{x} \in \Omega. \tag{5.30}$$

This equation can be reformulated as a mixed problem (see Section 3.2)

$$\begin{aligned} a^{-1}\,\boldsymbol{p} + \nabla u - a^{-1}\,\boldsymbol{b}\, u &= 0, & (5.31)\\ -\operatorname{div}\boldsymbol{p} &= -f. & (5.32) \end{aligned}$$

Multiplying with suitable test functions $\boldsymbol{q}$ and v followed by integration results in

$$\begin{aligned} (a^{-1}\,\boldsymbol{p}, \boldsymbol{q}) + (\nabla u, \boldsymbol{q}) - (a^{-1}\,\boldsymbol{b}\, u, \boldsymbol{q}) &= 0, & (5.33)\\ -(\operatorname{div}\boldsymbol{p}, v) &= -(f, v). & (5.34) \end{aligned}$$

Clearly, the integration by parts can be done in the first or in the second equation. Doing so in equation (5.34) leads to a mixed formulation with $u \in H^1(\Omega)$ and $\boldsymbol{p} \in [L^2(\Omega)]^d$, i. e., we obtain the same, function space as in the primal formulation. Therefore we can not expect a change in the performance of the standard Galerkin method. Performing the integration by parts in equation (5.33) yields the mixed problem

Find $(\boldsymbol{p}, u) \in H(\operatorname{div}, \Omega) \times L_2(\Omega)$ such that

$$\begin{aligned} (a^{-1}\,\boldsymbol{p}, \boldsymbol{q}) - (u, \operatorname{div}\boldsymbol{q}) - (a^{-1}\,\boldsymbol{b}\, u, \boldsymbol{q}) &= -\langle g, \boldsymbol{q}\cdot\boldsymbol{n}\rangle_\Gamma && \text{for all } \boldsymbol{q} \in H(\operatorname{div}, \Omega),\\ -(\operatorname{div}\boldsymbol{p}, v) &= -(f, v) && \text{for all } v \in L_2(\Omega), \end{aligned} \tag{5.35}$$

with the boundary term $\langle g, \boldsymbol{q}\cdot\boldsymbol{n}\rangle_\Gamma := \int_\Gamma g\, \boldsymbol{q}\cdot\boldsymbol{n}\, ds$. Note that essential boundary conditions g on Γ in the primal formulation become natural boundary conditions in the mixed formulation (5.35). In the case of homogeneous Dirichlet boundary conditions on Γ the boundary term vanishes.

We discretize the problem by choosing piecewise constant functions for u, i. e., $u_h, v_h \in \mathcal{M}_0(\mathcal{T}_h) \subset V$ and piecewise linear functions for $\boldsymbol{p}$, i. e., $\boldsymbol{p}_h, \boldsymbol{q}_h \in \mathcal{RT}_0(\mathcal{T}_h) \subset Q$.

The corresponding algebraic Galerkin system of (5.35) is of the general form

$$\begin{bmatrix} \underline{\underline{A}} & \underline{\underline{B}}_2^T \\ \underline{\underline{B}}_1 & \underline{\underline{0}} \end{bmatrix} \begin{bmatrix} \underline{p}_h \\ \underline{u}_h \end{bmatrix} = \begin{bmatrix} \underline{g}_h \\ \underline{f}_h \end{bmatrix} . \tag{5.36}$$

Example 5.13. *Transforming Example 5.2 into mixed form yields*

Find $(p, u) \in Q \times V$ *such that*

$$\begin{aligned} \frac{1}{a} p + u' - \frac{1}{a} b\, u &= 0 && \text{for } x \in (0,1), \\ -p' &= -f && \text{for } x \in (0,1), \\ u(0) &= 1, \\ u(1) &= 0. \end{aligned} \tag{5.37}$$

The variational formulation of Example 5.13 can be written as

Find $(p, u) \in Q \times V$ *such that*

$$\begin{aligned} (\frac{1}{a} p, q) - (u, q') - (\frac{1}{a} b\, u, q) &= q(0) && \text{for all } q \in Q, \\ -(p', v) &= -(f, v) && \text{for all } v \in V, \end{aligned} \tag{5.38}$$

with $V = L_2((0,1))$ *and* $Q = H(\mathrm{div}, (0,1)) = H^1((0,1))$.

In the case of Example 5.13 we discretize by choosing $p_h \in \mathcal{L}_1(\mathcal{T}_h) \subset Q$.

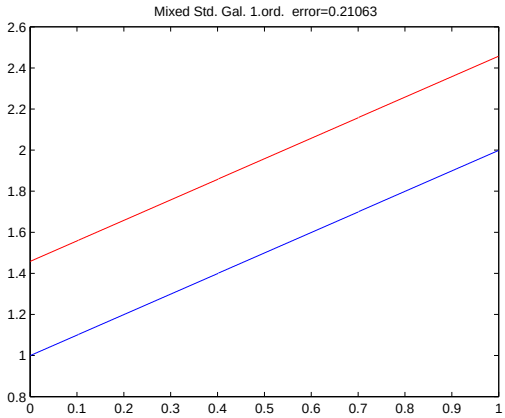

p for $a = 0.0005$ and $b = 1.0$ with $h = 0.0312$.

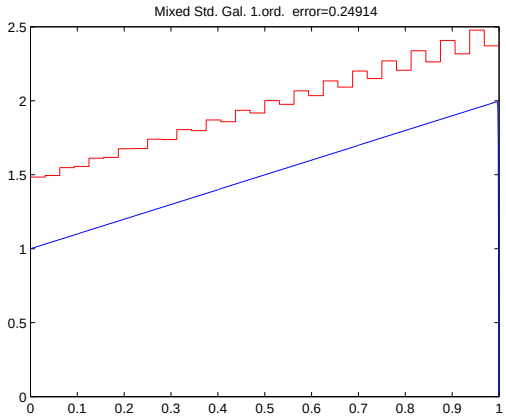

u for $a = 0.0005$ and $b = 1.0$ with $h = 0.0312$.

Figure 5.10: The exact (blue) and approximate (red) solutions of p (left) and u (right) for Example 5.13 applying standard Galerkin method using linear elements for p and constants for u.

The numerical results are presented in Figure 5.10. One can observe oscillations in a region of the boundary layer again. Due to the weak incorporation of the boundary conditions in the mixed problem, the approximate solution does not only show oscillations at the boundary layer, but also fail in fulfilling the boundary conditions (see Figure 5.10).

5.8 Streamline Edge-Upwind for mixed formulation

First we motivate the weighted stabilization term. Therefore we examine the system matrix in (5.36) for the Example 5.13.

$$\begin{bmatrix} \underline{\underline{A}} & \underline{\underline{B}}_2^T \\ \underline{\underline{B}}_1 & \underline{\underline{0}} \end{bmatrix} = \begin{bmatrix} 2\frac{h_k}{6a} & 1\frac{h_k}{6a} & 0 & \dots & 0 & 1-\frac{bh_k}{2a} & 0 & \dots & 0 \\ 1\frac{h_k}{6a} & 4\frac{h_k}{6a} & 1\frac{h_k}{6a} & \ddots & \vdots & -1-\frac{bh_k}{2a} & 1-\frac{bh_k}{2a} & \ddots & \vdots \\ 0 & 1\frac{h_k}{6a} & \ddots & \ddots & 0 & 0 & -1-\frac{bh_k}{2a} & \ddots & 0 \\ \vdots & \ddots & \ddots & 4\frac{h_k}{6a} & 1\frac{h_k}{6a} & \vdots & \ddots & \ddots & 1-\frac{bh_k}{2a} \\ 0 & \dots & 0 & 1\frac{h_k}{6a} & 2\frac{h_k}{6a} & 0 & \dots & 0 & -1-\frac{bh_k}{2a} \\ & & & & & & & & \\ 1 & -1 & 0 & \dots & 0 & 0 & \dots & \dots & 0 \\ 0 & 1 & -1 & \ddots & \vdots & \vdots & & & \vdots \\ \vdots & \ddots & \ddots & \ddots & 0 & \vdots & & & \vdots \\ 0 & \dots & 0 & 1 & -1 & 0 & \dots & \dots & 0 \end{bmatrix}.$$

In the stiffness matrix of the problem we observe that the off-diagonal term $-(\frac{1}{a}\,\boldsymbol{b}\,u, \boldsymbol{q})$ (contained in $\underline{\underline{B}}_2^T$) causes an essential unbalance for a small diffusion coefficient. Balancing this maladjustment introduces an upwind stabilization motivated by Discontinuous Galerkin methods as follows.

DG methods are designed for the convection dominated case. There, the numerical flux is often defined on the upwind triangle as

$$a^{-1}\boldsymbol{p}\cdot\boldsymbol{n} = -\nabla u_{up}\cdot\boldsymbol{n} + a^{-1}\,\boldsymbol{b}\,u_{up}\cdot\boldsymbol{n}.$$

We take this as a motivation and construct the following upwind stabilization.

Taking equation (5.31) and multiplying it with the normal vector $\boldsymbol{n}$ yields

$$a^{-1}\,\boldsymbol{p}\cdot\boldsymbol{n} + \nabla u\cdot\boldsymbol{n} - a^{-1}\,\boldsymbol{b}\,u\cdot\boldsymbol{n} = 0. \tag{5.39}$$

Multiplying this equation with $\boldsymbol{q}\cdot\boldsymbol{n}$ and integrating over the outflow boundary of each element gives

$$\sum_{T\in\mathcal{T}_h} Pe_h\,h\int_{out}(a^{-1}\,\boldsymbol{p} + \nabla u - a^{-1}\,\boldsymbol{b}\,u)\cdot\boldsymbol{n}\;\boldsymbol{q}\cdot\boldsymbol{n}\,ds = 0 \tag{5.40}$$

weighted with the dimensionless mesh Peclet number which is defined as $Pe_h = a^{-1}|\boldsymbol{b}|h$. The second factor h arises due to the different scaling of the volume and the boundary integrals. In the range $Pe_h \approx 1$, the stabilization term added to the upper left block is

of the same order as the original term. For large convection, the scheme is more a DG scheme, while for small convection, it approaches the standard mixed method.
In the following we will refer to this stabilization term by using the scalar product $\langle .,. \rangle_{out}$ defined on the skeleton $\partial\mathcal{T}_h$ of the triangulation $\mathcal{T}_h$

$$\langle v, w \rangle_{out} := \sum_{T \in \mathcal{T}_h} Pe_h \, h \int_{\partial T_{out}} v \, w \, ds. \tag{5.41}$$

Since (5.40) is fulfilled for the exact solutions $\boldsymbol{p}$ and u of the system of equations (5.31)-(5.32) adding this term to equation (5.31) gives a consistent problem formulation.

Find $(\boldsymbol{p}, u) \in H(\mathrm{div}, \Omega) \times L_2(\Omega)$ such that

$$\begin{array}{lll} (a^{-1}\,\boldsymbol{p}, \boldsymbol{q}) - (u, \mathrm{div}\,\boldsymbol{q}) - (a^{-1}\,\boldsymbol{b}\,u, \boldsymbol{q}) + & & \\ \langle (a^{-1}\,\boldsymbol{p} + \nabla u - a^{-1}\,\boldsymbol{b}\,u) \cdot \boldsymbol{n}, \boldsymbol{q} \cdot \boldsymbol{n} \rangle_{out} & = -\langle g, \boldsymbol{q} \cdot \boldsymbol{n} \rangle_{\Gamma} & \text{for all } \boldsymbol{q} \in H(\mathrm{div}, \Omega), \\ -(\mathrm{div}\,\boldsymbol{p}, v) & = -(f, v) & \text{for all } v \in L_2(\Omega). \end{array} \tag{5.42}$$

Next we incorporate the inflow given by the Dirichlet boundary condition. This is done by adding the integrals over the inflow boundary of elements T, where this coincides with the domain boundary, i. e., $\partial T_{in} \subset \partial\Omega$, to the stabilization term (5.40).

We discretize the problem by choosing $u_h, v_h \in \mathcal{M}_0(\mathcal{T}_h) \subset V$ and $\boldsymbol{p}_h, \boldsymbol{q}_h \in \mathcal{RT}_0(\mathcal{T}_h) \subset Q$. This yields the stabilized algebraic system which reads as

$$\begin{bmatrix} \underline{\underline{\tilde{A}}} & \underline{\underline{\tilde{B}}}_2^T \\ \underline{\underline{B}}_1 & \underline{\underline{0}} \end{bmatrix} \begin{bmatrix} \underline{\boldsymbol{p}}_h \\ \underline{u}_h \end{bmatrix} = \begin{bmatrix} \underline{\tilde{g}} \\ \underline{f} \end{bmatrix} . \tag{5.43}$$

with $\underline{\underline{\tilde{A}}} := \underline{\underline{A}} + \underline{\underline{A}}_{stab}$ and $\underline{\underline{\tilde{B}}}_2^T = \underline{\underline{B}}_2^T + \underline{\underline{B}}_{stab}$, where the stabilization matrices in the case of Example 5.13 are defined as

$$\underline{\underline{A}}_{stab} := \begin{bmatrix} \frac{|b|h_k^2}{a^2} & 0 & 0 & \dots & 0 \\ 0 & \frac{|b|h_k^2}{a^2} & 0 & \ddots & \vdots \\ 0 & 0 & \ddots & \ddots & 0 \\ \vdots & \ddots & \ddots & \frac{|b|h_k^2}{a^2} & 0 \\ 0 & \dots & 0 & 0 & \frac{|b|h_k^2}{a^2} \end{bmatrix}, \underline{\underline{B}}_{stab} := \begin{bmatrix} 0 & 0 & \dots & 0 \\ -\frac{|b|^2 h_k^2}{a^2} & 0 & \ddots & \vdots \\ 0 & -\frac{|b|^2 h_k^2}{a^2} & \ddots & 0 \\ \vdots & \ddots & \ddots & 0 \\ 0 & \dots & 0 & -\frac{|b|^2 h_k^2}{a^2} \end{bmatrix}.$$

where the upper left entry $\frac{|b|h_k^2}{a^2}$ of $\underline{\underline{A}}_{stab}$ is generated by the stabilization at the inflow boundary. The second part of the stabilization entry at $\partial\Omega_{in}$ moves to the right hand side of the equation, where $\tilde{g}$ then looks like

$$\underline{\tilde{g}} = \begin{bmatrix} 1 + \frac{|b|^2 h_k^2}{a^2} & 0 & \dots & 0 \end{bmatrix}^T$$

The numerical results for Example 5.13 can be observed in Figure 5.11. Already for a quite coarse discretization the approximate solution does not show any oscillations. The stabilization term at the inflow part of the Dirichlet boundary ensures that the boundary condition is fulfilled from the start in spite of its weak incorporation. Only on the outflow part of the Dirichlet boundary the boundary condition is not fulfilled for such a coarse grid and the boundary layer vanishes. Except for the boundary layer, the approximate solution matches the exact solution quite good (cf. Figure 5.11). The next step would be an adaptive refinement at the boundary layer.

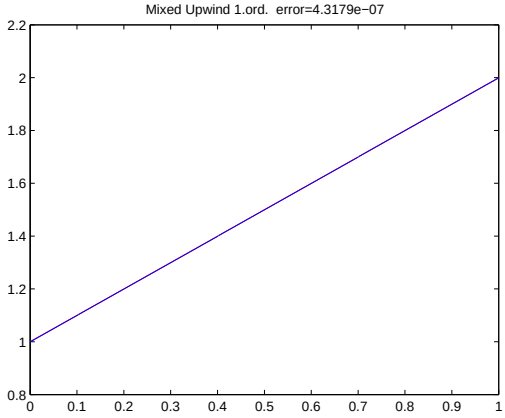

p for $a = 0.0005$ and $b = 1.0$ with $h = 0.0312$.

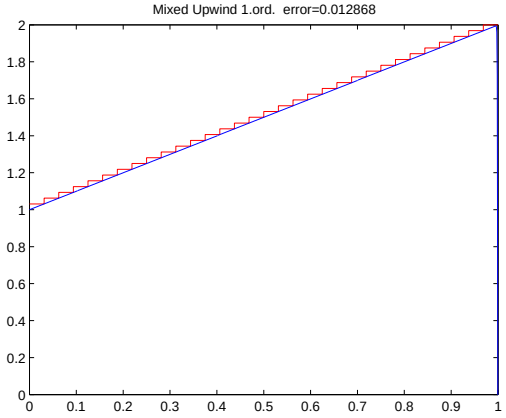

u for $a = 0.0005$ and $b = 1.0$ with $h = 0.0312$.

Figure 5.11: The exact (blue) and approximate (red) solutions p (left) and u (right) for Example 5.13 applying standard Galerkin method with upwind stabilization using linear elements for p and constants for u.

The results in Figure 5.11 are for the same discretization as in Figure 5.10 to simplify the comparison. The quality of this method for coarse grids can be seen in Figure 5.12.

Remark 5.14. *We gain higher regularity on the flux $\boldsymbol{p}$, but less for u. Knowing from* (5.31) *that $\boldsymbol{p}$ is something similar like the gradient field of u allows a post processing for the primal variable.*

If $a^{-1}\boldsymbol{b}$ is small, the off-diagonal block certainly will not destroy the order of convergence. But similar to the original problem, the mixed one suffers from large convective terms. We observe the effects on our example.

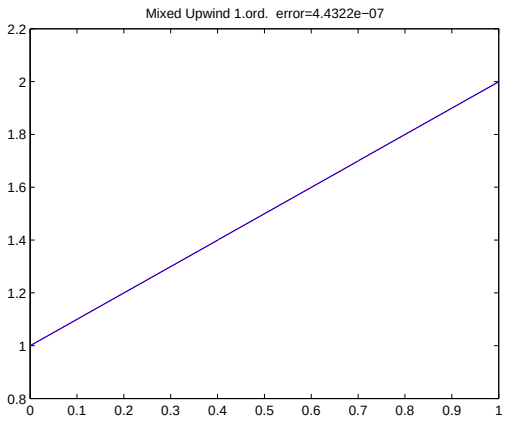

p for $a = 0.0005$ and $b = 1.0$ with $h = 0.25$.

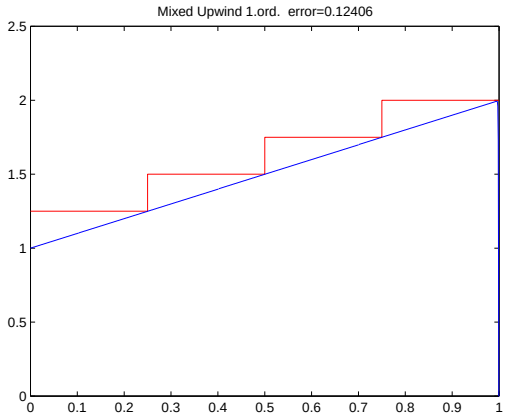

u for $a = 0.0005$ and $b = 1.0$ with $h = 0.25$.

Figure 5.12: The exact (blue) and approximate (red) solutions p (left) and u (right) for Example 5.13 applying standard Galerkin method with edge-upwind stabilization using linear elements for p and constants for u.

For the primal formulation of the problem we observe the SUPG method has the best performance results. In contrast for the mixed formulation the edge-upwind stabilization yields the best results. We compare the results of the SUPG method and the edge-upwind stabilization in mixed formulation. For a very coarse grid this is done in Figure 5.13.

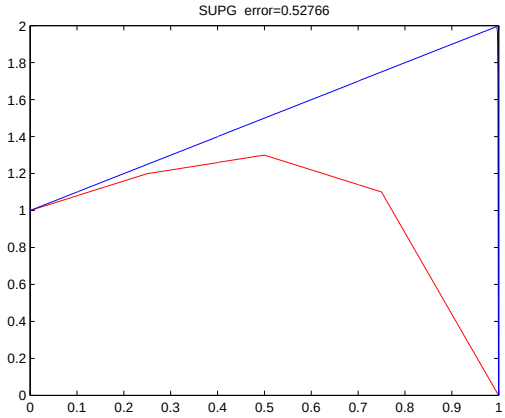

u for $a = 0.0005$ and $b = 1.0$ with $h = 0.25$.

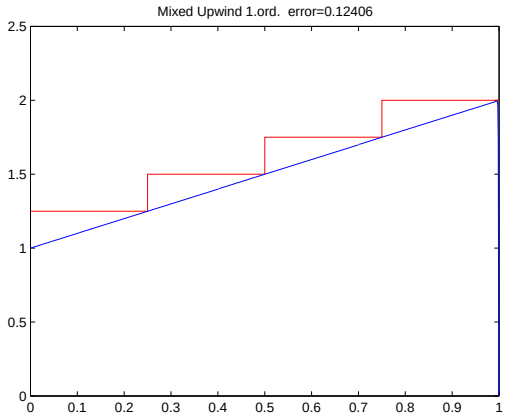

u for $a = 0.0005$ and $b = 1.0$ with $h = 0.25$.

Figure 5.13: The exact (blue) and approximate (red) solutions for u obtained with SUPG (left) – using linear elements – and edge-upwind stabilization in mixed formulation (right) – using constants – for Example 5.13.

In Figure 5.14 we compare the L_2-errors of the SUPG method in the primal formulation

with the L_2-errors of the streamline edge-upwind stabilization for mixed formulation. Until h is small enough to resolve the boundary layer, the streamline edge-upwind stabilization for mixed formulation gives better results, even without post processing.

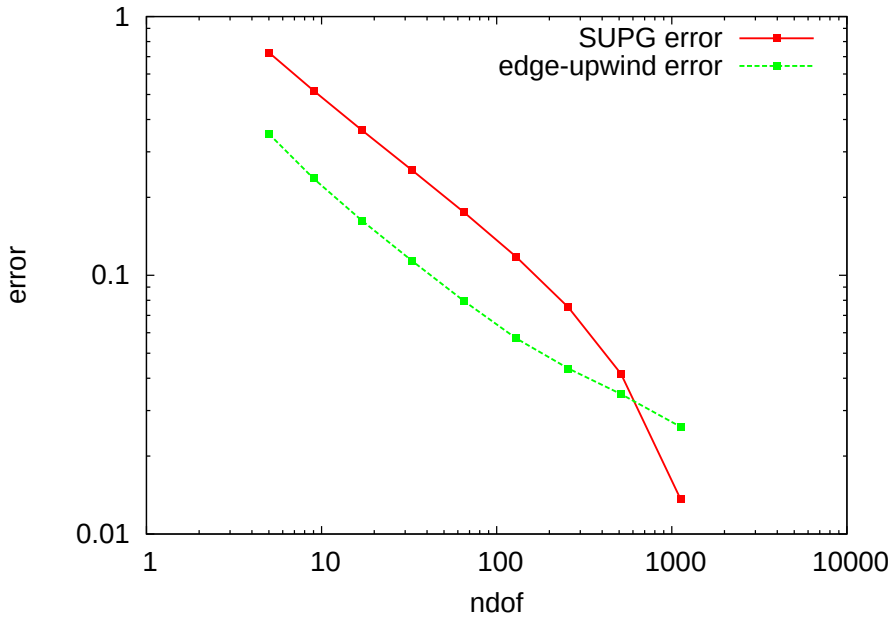

Figure 5.14: The L_2-errors of the SUPG method in the primal formulation versus the L_2-errors of the streamline edge-upwind stabilization for mixed formulation.

Chapter 6

The EHD Problem with Edge-Upwind Stabilization

We return to the full EHD problem described by the non-linear system of partial differential equations

$$-\operatorname{div}\varepsilon\,\nabla\Phi = \rho \tag{2.9}$$

$$\operatorname{div}\boldsymbol{j} + \frac{\partial\rho}{\partial t} = 0 \qquad \text{for } (x,t) \in \Omega \times (0,T) \tag{2.10}$$

$$\boldsymbol{j} = b\,\nabla\Phi\,\rho - d\,\nabla\rho, \tag{2.11}$$

with the boundary conditions

$$\begin{aligned} \varepsilon\nabla\Phi\cdot\boldsymbol{n} &= 0 \quad \wedge \quad \boldsymbol{j}\cdot\boldsymbol{n} = 0 && \text{on } \Gamma_{out}, && (2.13), (2.16)\\ \Phi &= 0 \quad \wedge \quad \rho = 0 && \text{on } \Gamma_{ta}, && (2.14)\\ \Phi &= \Phi_e \quad \wedge \quad \boldsymbol{j}\cdot\boldsymbol{n} = K_r(-\nabla\Phi\cdot\boldsymbol{n}) && \text{on } \Gamma_{el}, && (2.15), (4.12) \end{aligned}$$

where

$$K_r(E_n) = \begin{cases} \alpha_F(E_n - E_{co}) & \text{for } E_n \geqslant E_{co} \\ 0 & \text{else} \end{cases} \qquad \text{on } \Gamma_{el},$$

and the initial conditions

$$\Phi(x,0) = \Phi_0(x), \quad \rho(x,0) = \rho_0(x) \qquad \text{for } x \in \overline{\Omega}.$$

Our first strategy, the Fermi-potential approach in Chapter 4, turned out to be appropriate for the diffusion dominated case. But in the practically relevant case the convection dominates. With the attempt for solving also the physically relevant case, we concentrated on numerical methods for solving convection-diffusion equations in Chapter 5.
In the present chapter we apply our knowledge on numerical methods gained in Chapter 5 to the EHD problem. In the following section we derive the mixed variational formulation for the problem. Afterwards we consider the mixed formulation with edge-upwind stabilization analog to the one presented in Section 5.8.

6.1 The EHD problem in mixed formulation

First we reformulate the problem using the definition of the electric displacement $\boldsymbol{D} := \varepsilon \boldsymbol{E} = -\varepsilon \nabla \Phi$ and describe equation (2.9) in mixed formulation. The complete EHD problem in classical formulation from above can then be written in mixed formulation as follows. For $(\boldsymbol{x}, t) \in \Omega \times (0, T)$

$$\begin{aligned}
\varepsilon^{-1}\boldsymbol{D} + \nabla\Phi &= 0 && (6.1)\\
-\operatorname{div}\boldsymbol{D} + \rho &= 0 && (6.2)\\
\operatorname{div}\boldsymbol{j} + \frac{\partial \rho}{\partial t} &= 0 && (6.3)\\
\boldsymbol{j} + d\,\nabla\rho + \underbrace{b\,\varepsilon^{-1}\boldsymbol{D}}_{=:\hat{\boldsymbol{b}}(\boldsymbol{D})}\rho &= 0, && (6.4)
\end{aligned}$$

together with the boundary conditions of the previous page and the according initial conditions.
We first introduce the appropriate spaces for the variational framework and then derive a variational mixed formulation of our system. The natural function spaces are $Q = H(\operatorname{div}, \Omega)$ (for $\boldsymbol{D}$ and $\boldsymbol{j}$) and $V = L_2(\Omega)$ (for Φ and ρ) as already discussed in Chapter 3. The essential boundary conditions are incorporated in the test and ansatz spaces defined by

$$Q_{g,\Gamma} := \{\boldsymbol{p} \in H(\operatorname{div}, \Omega) \mid (\boldsymbol{p} \cdot \boldsymbol{n})_{|\Gamma} = g\}.$$

The required function spaces for the time dependent problem [13] are based on the following definition. Let $\boldsymbol{T} = (0, T)$ and W be a Banach space,

$$L_2(\boldsymbol{T}, W) := \{u : \boldsymbol{T} \to W \mid \|u\|_{L_2(\boldsymbol{T},W)} < \infty\},$$

where $\|u\|_{L_2(\boldsymbol{T},W)} := \left(\int_0^T \|u(t)\|_W^2\, dt\right)^{\frac{1}{2}}$.

Multiplying equations (6.1)-(6.4) by the appropriate test functions, integrating over the domain Ω and integrating by parts in the first and last equation yields for these two equations

$$\begin{aligned}
(\varepsilon^{-1}\boldsymbol{D}, \tilde{\boldsymbol{D}}) - (\Phi, \operatorname{div}\tilde{\boldsymbol{D}}) + \langle \Phi, \tilde{\boldsymbol{D}} \cdot \boldsymbol{n}\rangle_\Gamma &= 0 \qquad \forall\, \tilde{\boldsymbol{D}} \in Q_{0,\Gamma_{out}},\\
(d^{-1}\boldsymbol{j}, \tilde{\boldsymbol{j}}) - (\rho, \operatorname{div}\tilde{\boldsymbol{j}}) + (d^{-1}\hat{\boldsymbol{b}}(\boldsymbol{D})\rho, \tilde{\boldsymbol{j}}) + \langle \rho, \tilde{\boldsymbol{j}} \cdot \boldsymbol{n}\rangle_\Gamma &= 0 \qquad \forall\, \tilde{\boldsymbol{j}} \in Q_{0,\Gamma_{out}\cup\Gamma_{el}}.
\end{aligned}$$

The next step is to incorporate the boundary conditions. The boundary term of the first equation equals to

$$\langle \Phi, \tilde{\boldsymbol{D}} \cdot \boldsymbol{n}\rangle_\Gamma = \langle \underbrace{\Phi}_{=\Phi_e}, \tilde{\boldsymbol{D}} \cdot \boldsymbol{n}\rangle_{\Gamma_{el}} + \langle \underbrace{\Phi}_{=0}, \tilde{\boldsymbol{D}} \cdot \boldsymbol{n}\rangle_{\Gamma_{ta}} + \langle \Phi, \underbrace{\tilde{\boldsymbol{D}} \cdot \boldsymbol{n}}_{=0}\rangle_{\Gamma_{out}},$$

where only the term on Γ_{el} remains and can be moved to the right hand side (see system later). The second boundary term can be written as

$$\langle \rho, \tilde{\boldsymbol{j}} \cdot \boldsymbol{n} \rangle_{\Gamma} = \langle \rho, \underbrace{\tilde{\boldsymbol{j}} \cdot \boldsymbol{n}}_{=0} \rangle_{\Gamma_{el\setminus co}} + \langle \rho, \underbrace{\tilde{\boldsymbol{j}} \cdot \boldsymbol{n}}_{=0} \rangle_{\Gamma_{co}} + \langle \underbrace{\rho}_{=0}, \tilde{\boldsymbol{j}} \cdot \boldsymbol{n} \rangle_{\Gamma_{ta}} + \langle \rho, \underbrace{\tilde{\boldsymbol{j}} \cdot \boldsymbol{n}}_{=0} \rangle_{\Gamma_{out}} = 0.$$

Therefore the complete problem in mixed variational formulation reads as

Find $\boldsymbol{D} \in L_2(\boldsymbol{T}, Q_{0,\Gamma_{out}})$, $\Phi \in L_2(\boldsymbol{T}, V)$, $\boldsymbol{j} \in L_2(\boldsymbol{T}, Q_{g,\Gamma_{out}\cup\Gamma_{el}})$
with $g := \begin{cases} K_r(\varepsilon^{-1}\boldsymbol{D}\cdot\boldsymbol{n}) & \text{on } \Gamma_{el} \\ 0 & \text{on } \Gamma_{out} \end{cases}$, and $\rho \in L_2(\boldsymbol{T}, V)$ with $\frac{\partial \rho}{\partial t} \in L_2(\boldsymbol{T}, V^*)$ such that

$$\begin{aligned}
(\varepsilon^{-1}\boldsymbol{D}, \tilde{\boldsymbol{D}}) - (\Phi, \operatorname{div} \tilde{\boldsymbol{D}}) &= -\langle \Phi_e, \tilde{\boldsymbol{D}} \cdot \boldsymbol{n} \rangle_{\Gamma_{el}} && \forall\ \tilde{\boldsymbol{D}} \in Q_{0,\Gamma_{out}}, \\
-(\operatorname{div} \boldsymbol{D}, \tilde{\Phi}) + (\rho, \tilde{\Phi}) &= 0 && \forall\ \tilde{\Phi} \in V, \\
(d^{-1}\boldsymbol{j}, \tilde{\boldsymbol{j}}) - (\rho, \operatorname{div} \tilde{\boldsymbol{j}}) + (d^{-1}\,\hat{\boldsymbol{b}}(\boldsymbol{D})\rho, \tilde{\boldsymbol{j}}) &= 0 && \forall\ \tilde{\boldsymbol{j}} \in Q_{0,\Gamma_{out}\cup\Gamma_{el}}, \\
-(\operatorname{div} \boldsymbol{j}, \tilde{\rho}) - (\frac{\partial \rho}{\partial t}, \tilde{\rho}) &= 0 && \forall\ \tilde{\rho} \in V,
\end{aligned} \tag{6.5}$$

with the initial conditions

$$(\rho(0), \tilde{\rho}) = (\rho_0, \tilde{\rho}) \qquad \text{for all } \tilde{\rho} \in V.$$

In the sequel we discretize in space by using the finite element method. This yields the semi-discrete analogue of (6.5) which is an initial value problem for a system of ordinary differential equations.

6.2 Semi-discretization: the (vertical) method of lines

We do the spatial discretization first and replace the function spaces by $H(\mathrm{div})$- and L^2-conforming finite dimensional subspaces as described in Chapter 3.

Find $\boldsymbol{D}_h \in L_2(\boldsymbol{T}, Q_{h,0,\Gamma_{out}})$, $\Phi_h \in L_2(\boldsymbol{T}, V_h)$, $\boldsymbol{j}_h \in L_2(\boldsymbol{T}, Q_{h,g,\Gamma_{out}\cup\Gamma_{el}})$, and
$\rho_h \in L_2(\boldsymbol{T}, V_h)$ with $\frac{d}{dt}(\rho_h) \in L_2(\boldsymbol{T}, V_h^*)$ such that

$$\begin{aligned}
(\varepsilon^{-1}\boldsymbol{D}_h, \tilde{\boldsymbol{D}}_h) - (\Phi_h, \operatorname{div} \tilde{\boldsymbol{D}}_h) &= -\langle \Phi_e, \tilde{\boldsymbol{D}}_h \cdot \boldsymbol{n} \rangle_{\Gamma_{el}}, \\
-(\operatorname{div} \boldsymbol{D}_h, \tilde{\Phi}_h) + (\rho_h, \tilde{\Phi}_h) &= 0, \\
(d^{-1}\boldsymbol{j}_h, \tilde{\boldsymbol{j}}_h) - (\rho_h, \operatorname{div} \tilde{\boldsymbol{j}}_h) + (d^{-1}\,\hat{\boldsymbol{b}}(\boldsymbol{D}_h)\rho_h, \tilde{\boldsymbol{j}}_h) &= 0, \\
-(\operatorname{div} \boldsymbol{j}_h, \tilde{\rho}_h) - \frac{d}{dt}(\rho_h, \tilde{\rho}_h) &= 0,
\end{aligned} \tag{6.6}$$

for all $\tilde{\boldsymbol{D}}_h \in Q_{h,0,\Gamma_{out}}$, $\tilde{\Phi}_h \in V_h$, $\tilde{\boldsymbol{j}}_h \in Q_{h,0,\Gamma_{out}\cup\Gamma_{el}}$, and $\tilde{\rho}_h \in V_h$,
with the initial conditions

$$(\rho_h(0), \tilde{\rho}_h) = (\rho_0, \tilde{\rho}_h) \qquad \text{for all } \tilde{\rho}_h \in V_h.$$

For the L_2 discretization we consider piecewise constant functions, i. e., $V_h = \mathcal{M}_0(\mathcal{T}_h)$ and for the $H(\mathrm{div})$ discretization we use the Raviart-Thomas space of order 0, i. e., $Q_h = \mathcal{RT}_0(\mathcal{T}_h)$.
In the sequel let the basis functions for this problem be denoted by

function space	according basis	obtained representation
V_h	$\{\varphi_i^\Phi\}$	$\Phi_h(t)(x) = \sum_{j=0}^{N_h^\Phi} \Phi_j(t)\varphi_j^\Phi(x)$
V_h	$\{\varphi_i^\rho\}$	$\rho_h(t)(x) = \sum_{j=0}^{N_h^\rho} \rho_j(t)\varphi_j^\rho(x)$
$Q_{h,0,\Gamma_{out}}$	$\{\psi_i^{\boldsymbol{D}}\}$	$\boldsymbol{D}_h(t)(x) = \sum_{j=0}^{N_h^{\boldsymbol{D}}} \boldsymbol{D}_j(t)\psi_j^{\boldsymbol{D}}(x)$
$Q_{h,0,\Gamma_{out}\cup\Gamma_{el}}$	$\{\psi_i^{\boldsymbol{j}}\}$	$\boldsymbol{j}_h(t)(x) = \sum_{j=0}^{N_h^{\boldsymbol{j}}} \boldsymbol{j}_j(t)\psi_j^{\boldsymbol{j}}(x).$

Table 6.1: Basis functions and according representations.

Plugging the representations from Table 6.1 into (6.6) yields the algebraic system

$$\begin{aligned} \left[0,0,0,(\underline{\underline{M}}_h^\rho \underline{\rho}_h'(t))^T\right]^T + \underline{\underline{K}}_h \underline{u}_h(t) &= \underline{f}_h \\ \left[0,0,0,(\underline{\underline{M}}_h^\rho \underline{\rho}_h(0))^T\right]^T &= \underline{g}_h \end{aligned} \tag{6.7}$$

with the vectors

$$\underline{u}_h(t) = \left[\underline{\boldsymbol{D}}_h(t)^T, \underline{\Phi}_h(t)^T, \underline{\boldsymbol{j}}_h(t)^T, \underline{\rho}_h(t)^T\right]^T$$

where

$$\underline{\boldsymbol{D}}_h(t) = (\boldsymbol{D}_i(t))_{i=1..N_h^{\boldsymbol{D}}}, \quad \underline{\Phi}_h(t) = (\Phi_i(t))_{i=1..N_h^\Phi}, \tag{6.8}$$

$$\underline{\boldsymbol{j}}_h(t) = (\boldsymbol{j}_i(t))_{i=1..N_h^{\boldsymbol{j}}}, \quad \underline{\rho}_h(t) = (\rho_i(t))_{i=1..N_h^\rho} \tag{6.9}$$

using the coefficients from the table above, and

$$\underline{f}_h = \left[\underline{f}_{h,\boldsymbol{D}}^T, \underline{f}_{h,\Phi}^T, \underline{f}_{h,\boldsymbol{j}}^T, \underline{f}_{h,\rho}^T\right]^T,$$

where

$$\underline{f}_{h,\boldsymbol{D}} = (-\langle \Phi_e, \psi_i^{\boldsymbol{D}} \cdot \boldsymbol{n}\rangle_{\Gamma_{el}})_{i=1..N_h^{\boldsymbol{D}}}, \ \underline{f}_{h,\Phi} = \underline{f}_{h,\boldsymbol{j}} = \underline{f}_{h,\rho} = 0.$$

The involved matrices are the mass matrix $\underline{\underline{M}}_h^\rho$, where

$$(\underline{\underline{M}}_h^\rho)_{ij} = (\varphi_i^\rho, \varphi_j^\rho) \quad i,j = 1..N_h^\rho,$$

and the stiffness matrix $\underline{\underline{K}}_h$, which is built up like

$$\underline{\underline{K}}_h(\underline{\boldsymbol{D}}_h) = \begin{bmatrix} \underline{\underline{M}}_h^{\boldsymbol{D}} & -\underline{\underline{B}}_1^T & 0 & 0 \\ -\underline{\underline{B}}_1 & 0 & 0 & \underline{\underline{M}}_h^{\rho,\Phi} \\ 0 & 0 & \underline{\underline{M}}_h^{\boldsymbol{j}} & -\underline{\underline{B}}_2^T + \underline{\underline{M}}_h^{\rho,\boldsymbol{j}}(\underline{\boldsymbol{D}}_h) \\ -\underline{\underline{B}}_2 & 0 & 0 & 0 \end{bmatrix} \tag{6.10}$$

with the sub matrices

$$
\begin{array}{ll}
\underline{\underline{M}}_h^{\boldsymbol{D}} \text{ where } (\underline{\underline{M}}_h^{\boldsymbol{D}})_{ij} = (\varepsilon^{-1}\psi_j^{\boldsymbol{D}}, \psi_i^{\boldsymbol{D}}) & i,j = 1..N_h^{\boldsymbol{D}}, \\
\underline{\underline{B}}_1 \text{ where } (\underline{\underline{B}}_1)_{ij} = (\operatorname{div} \psi_j^{\boldsymbol{D}}, \varphi_i^{\Phi}) & i = 1..N_h^{\Phi},\ j = 1..N_h^{\boldsymbol{D}}, \\
\underline{\underline{M}}_h^{\rho,\Phi} \text{ where } (\underline{\underline{M}}_h^{\rho,\Phi})_{ij} = (\varphi_j^{\rho}, \varphi_i^{\Phi}) & i = 1..N_h^{\Phi},\ j = 1..N_h^{\rho}, \\
\underline{\underline{M}}_h^{\boldsymbol{j}} \text{ where } (\underline{\underline{M}}_h^{\boldsymbol{j}})_{ij} = (d^{-1}\psi_j^{\boldsymbol{j}}, \psi_i^{\boldsymbol{j}}) & i,j = 1..N_h^{\boldsymbol{j}}, \\
\underline{\underline{B}}_2 \text{ where } (\underline{\underline{B}}_2)_{ij} = (\operatorname{div} \psi_j^{\boldsymbol{j}}, \varphi_i^{\rho}) & i = 1..N_h^{\rho},\ j = 1..N_h^{\boldsymbol{j}}, \\
\underline{\underline{M}}_h^{\rho,\boldsymbol{j}}(\underline{\boldsymbol{D}}_h) \text{ where } (\underline{\underline{M}}_h^{\rho,\boldsymbol{j}}(\underline{\boldsymbol{D}}_h))_{ij} = (d^{-1}\,\hat{\boldsymbol{b}}(\underline{\boldsymbol{D}}_h)\varphi_j^{\rho}, \psi_i^{\boldsymbol{j}}) & i = 1..N_h^{\boldsymbol{j}},\ j = 1..N_h^{\rho}.
\end{array}
$$

The initial condition contains the mass matrices and the vector $\underline{g}_h$ with

$$\underline{g}_h = \left[0, 0, 0, \underline{g}_{h,\rho}^T\right]^T,$$

where

$$\underline{g}_{h,\rho} = (\rho_0, \varphi_i^{\rho})_{i=1..N_h^{\rho}}.$$

6.3 Time discretization

From the semi-discretization we obtained the initial value problem

$$
\begin{aligned}
\left[0, 0, 0, (\underline{\underline{M}}_h^{\rho}\, \underline{\rho}_h'(t))^T\right]^T &= \underline{f}_h - \underline{\underline{K}}_h \underline{u}_h(t), \\
\left[0, 0, 0, (\underline{\underline{M}}_h^{\rho}\, \underline{\rho}_h(0))^T\right]^T &= \underline{g}_h,
\end{aligned}
$$

with $\underline{u}_h(t) = \left[\underline{\boldsymbol{D}}_h(t)^T, \underline{\Phi}_h(t)^T, \underline{\boldsymbol{j}}_h(t)^T, \underline{\rho}_h(t)^T\right]^T$.

We solve this system of ordinary differential equations by using the implicit Euler method [20] for time discretization, where the time derivative $\frac{d}{dt}(\rho_h(t))$ is replaced by the forward difference quotient $\frac{1}{dt}(\rho_h^{k+1} - \rho_h^k)$ with k being the actual time step and $dt = t^{k+1} - t^k$. Within the time iteration the non-linear part of the stiffness matrix $\underline{\underline{M}}_h^{\rho,\boldsymbol{j}}(\underline{\boldsymbol{D}}_h)$ is in the $(k+1)$th step replaced by $\underline{\underline{M}}_h^{\rho,\boldsymbol{j}}(\underline{\boldsymbol{D}}_h^k)$. This linearization of the stiffness matrix $\underline{\underline{K}}_h(\underline{\boldsymbol{D}}_h)$ leads to

$$\frac{1}{dt}\operatorname{diag}(0, 0, 0, \underline{\underline{M}}_{h,\rho})(\underline{u}_h^{k+1} - \underline{u}_h^k) = \underline{f}_h - \underline{\underline{K}}_h^k \underline{u}_h^{k+1} \tag{6.11}$$

with $\underline{\underline{K}}_h^k = \underline{\underline{K}}_h(\underline{\boldsymbol{D}}_h^k)$.

The solution then is obtained by the iteration rule

$$\underline{u}_h^{k+1} = (\frac{1}{dt}\operatorname{diag}(0, 0, 0, \underline{\underline{M}}_{h,\rho}) + \underline{\underline{K}}_h^k)^{-1}(\frac{1}{dt}\operatorname{diag}(0, 0, 0, \underline{\underline{M}}_{h,\rho})\underline{u}_h^k + \underline{f}_h), \tag{6.12}$$

with the starting value

$$\underline{u}_h^0 = \underline{g}_h.$$

6.4 EHD in mixed form with edge-upwind stabilization

As observed in Chapter 5 this would not work for the convection dominant case. Therefore we construct an edge-upwind term as presented in Section 5.8.

Taking equation (6.4) and multiplying it with the normal vector $\boldsymbol{n}$ yields

$$(d^{-1}\boldsymbol{j} + \nabla\rho + d^{-1}\hat{\boldsymbol{b}}(\boldsymbol{D})\rho) \cdot \boldsymbol{n} = 0.$$

We plug this equation into the scalar product defined in (5.41) and get the stabilization term

$$\langle (d^{-1}\boldsymbol{j} + \nabla\rho + d^{-1}\hat{\boldsymbol{b}}(\boldsymbol{D})\rho) \cdot \boldsymbol{n}, \tilde{\boldsymbol{j}} \cdot \boldsymbol{n} \rangle_{out}.$$

Semi-discretization with finite elements yields

$$\langle (d^{-1}\boldsymbol{j}_h + \nabla\rho_h + d^{-1}\hat{\boldsymbol{b}}(\boldsymbol{D}_h)\rho_h) \cdot \boldsymbol{n}, \tilde{\boldsymbol{j}}_h \cdot \boldsymbol{n} \rangle_{out}. \tag{6.13}$$

Adding the edge-upwind term to (6.6) we obtain

Find $\boldsymbol{D}_h \in L_2(\boldsymbol{T}, Q_{h,0,\Gamma_{out}})$, $\Phi_h \in L_2(\boldsymbol{T}, V_h)$, $\boldsymbol{j}_h \in L_2(\boldsymbol{T}, Q_{h,g,\Gamma_{out}\cup\Gamma_{el}})$, and $\rho_h \in L_2(\boldsymbol{T}, V_h)$ with $\frac{d}{dt}(\rho_h) \in L_2(\boldsymbol{T}, V_h^*)$ such that

$$\begin{aligned}
&(\varepsilon^{-1}\boldsymbol{D}_h, \tilde{\boldsymbol{D}}_h) - (\Phi_h, \operatorname{div}\tilde{\boldsymbol{D}}_h) && = -\langle \Phi_e, \tilde{\boldsymbol{D}}_h \cdot \boldsymbol{n} \rangle_{\Gamma_{el}}, \\
-&(\operatorname{div}\boldsymbol{D}_h, \tilde{\Phi}_h) + (\rho_h, \tilde{\Phi}_h) && = 0, \\
&(d^{-1}\boldsymbol{j}_h, \tilde{\boldsymbol{j}}_h) - (\rho_h, \operatorname{div}\tilde{\boldsymbol{j}}_h) + (d^{-1}\hat{\boldsymbol{b}}(\boldsymbol{D}_h)\rho_h, \tilde{\boldsymbol{j}}_h) && \\
&\quad + \langle (d^{-1}\boldsymbol{j}_h + \nabla\rho_h + d^{-1}\hat{\boldsymbol{b}}(\boldsymbol{D}_h)\rho_h) \cdot \boldsymbol{n}, \tilde{\boldsymbol{j}}_h \cdot \boldsymbol{n} \rangle_{out} && = 0, \\
-&(\operatorname{div}\boldsymbol{j}_h, \tilde{\rho}_h) - \frac{d}{dt}(\rho_h, \tilde{\rho}_h) && = 0,
\end{aligned} \tag{6.14}$$

for all $\tilde{\boldsymbol{D}}_h \in Q_{h,0,\Gamma_{out}}$, $\tilde{\Phi}_h \in V_h$, $\tilde{\boldsymbol{j}}_h \in Q_{h,0,\Gamma_{out}\cup\Gamma_{el}}$, and $\tilde{\rho}_h \in V_h$, with the initial conditions

$$\begin{aligned}
(\Phi_h(0), \tilde{\Phi}_h) &= (\Phi_0, \tilde{\Phi}_h) \qquad \text{for all } \tilde{\Phi}_h \in V_h, \\
(\rho_h(0), \tilde{\rho}_h) &= (\rho_0, \tilde{\rho}_h) \qquad \text{for all } \tilde{\rho}_h \in V_h.
\end{aligned}$$

The edge-upwind term (6.13) equals according to definition (5.41)

$$\sum_{T\in\mathcal{T}_h} Pe_h\, h \,\langle (d^{-1}\boldsymbol{j}_h + \nabla\rho_h + d^{-1}\hat{\boldsymbol{b}}(\boldsymbol{D}_h)\rho_h) \cdot \boldsymbol{n}, \tilde{\boldsymbol{j}}_h \cdot \boldsymbol{n} \rangle_{\partial T_{out}}, \tag{6.15}$$

where $Pe_h = d^{-1}\|\hat{\boldsymbol{b}}(\boldsymbol{D}_h)\|_0 h$.

Using the representations from Table 6.1 yields the following stiffness matrix of the stabilized EHD system

$$\underline{\underline{K}}_h(\underline{\boldsymbol{D}}_h) = \begin{bmatrix} \underline{\underline{M}}_h^{\boldsymbol{D}} & -\underline{\underline{B}}_1^T & 0 & 0 \\ -\underline{\underline{B}}_1 & 0 & 0 & \underline{\underline{M}}_h^{\rho,\Phi} \\ 0 & 0 & \underline{\underline{M}}_h^{\boldsymbol{j}} + \underline{\underline{A}}_{stab} & -\underline{\underline{B}}_2^T + \underline{\underline{M}}_h^{\rho,\boldsymbol{j}}(\underline{\boldsymbol{D}}_h) + \underline{\underline{B}}_{stab} \\ -\underline{\underline{B}}_2 & 0 & 0 & 0 \end{bmatrix} \tag{6.16}$$

with

$$\begin{aligned} (\underline{\underline{A}}_{stab})_{ij} &= Pe_h\, h \langle d^{-1}\psi_j^{\boldsymbol{j}}, \psi_i^{\boldsymbol{j}} \rangle_{\partial T_{out}}, \\ (\underline{\underline{B}}_{stab})_{ij} &= Pe_h\, h \left(\langle \nabla\varphi_j^{\rho} \cdot \boldsymbol{n}, \psi_i^{\boldsymbol{j}} \rangle_{\partial T_{out}} + \langle d^{-1}\hat{\boldsymbol{b}}(\underline{\boldsymbol{D}}_h) \cdot \boldsymbol{n}\, \varphi_j^{\rho}, \psi_i^{\boldsymbol{j}} \rangle_{\partial T_{out}} \right) \end{aligned}$$

for $h = |\partial T_{out}|$.

6.5 Numerical Results

6.5.1 Parameters

We set the required parameters to the values of a convection dominated case:

- the permittivity of the ambient gas $\varepsilon = 1\ As/Vm$,
- the mobility of ions $b = 3 \cdot 10^4\ m^2/Vs$ and
- the ions diffusion coefficient $d = 1\ m^2/s$.
- the potential at the electrode $\Phi_e = 1\ V$ and
- the threshold strength of the electric field $E_{co} = 0.3\ V/m$.

Further parameters needed for the computation are

- the slope of $K_r(E_n)$, i. e., $\alpha_F = 10^3$ and finally
- the initial conditions $\rho_0 = \Phi_0 = 0$.

The Fermi-potential approach from Chapter 4 turned out to be appropriate for the diffusion dominant case. We use the ratio of convection b to diffusion d as indicator for the dominance of the convection. The highest ratio which could be solved by the Fermi-potential approach was $\frac{b}{d} = 0.002$, which means a diffusion dominant case. For the following calculations the ratio is $\frac{b}{d} = 30000$. Also the mesh can be chosen coarser than for the Fermi-potential approach.

6.5.2 Computations

The following details are for a calculation done with an Dual Intel Xeon, 2.8 GHz processor.

We solve for the time interval $[0, 1]$ and choose the step width $dt = 0.01$. The iteration process in time converges towards a stationary equilibrium. The results for Φ and ρ of the calculations with the mentioned time interval are presented in Figure 6.1 and Figure 6.2 respectively.

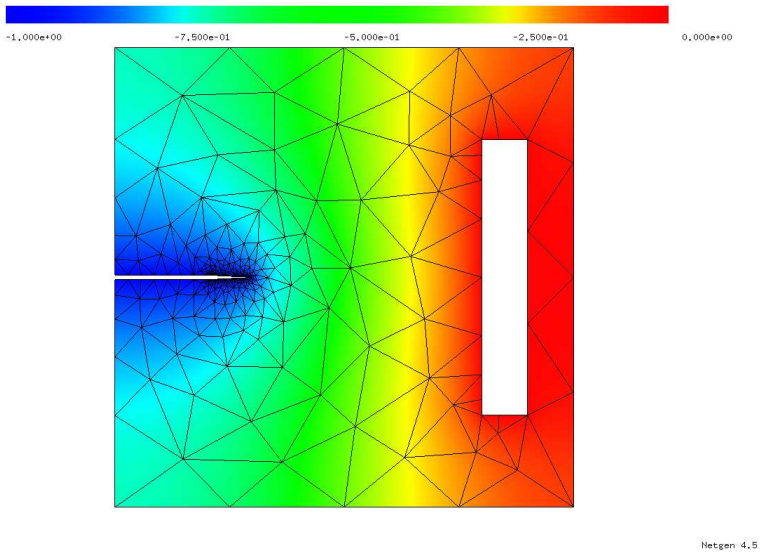

Figure 6.1: The electric potential Φ at time $t = 1$.

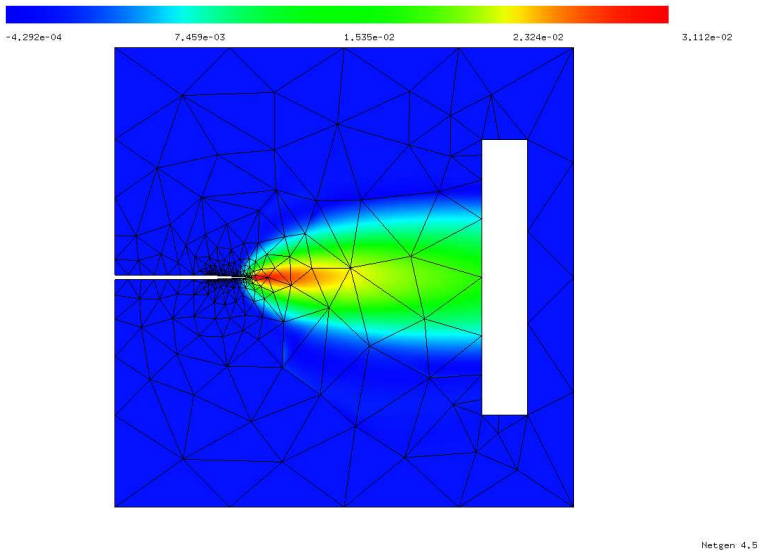

Figure 6.2: The space charge density ρ at time $t = 1$.

The evolution of the space charge density ρ in time ($t = 0.0001$ until $t = 0.0012$ in steps of $dt = 0.0001$) is displayed in Figure 6.3.

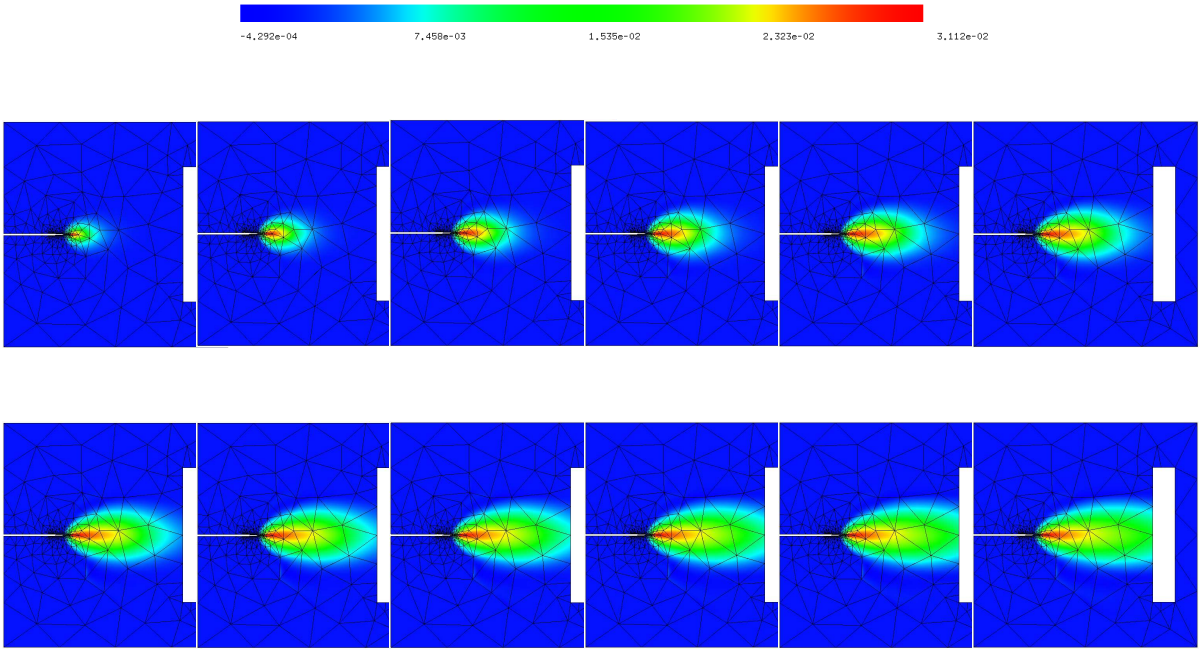

Figure 6.3: The evolution of the space charge density ρ from $t = 0.0001$ to $t = 0.0012$ with time step $dt = 0.0001$

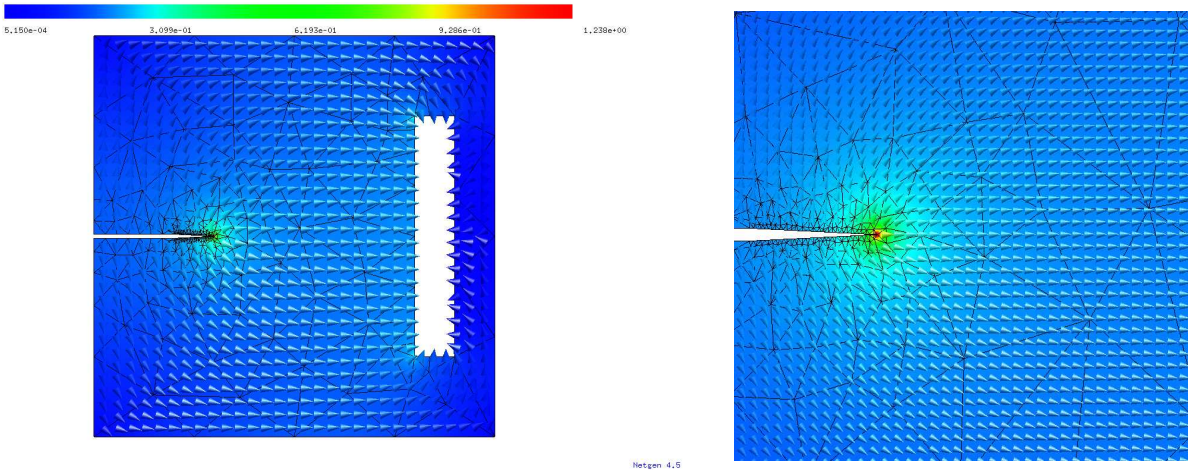

Figure 6.4: The electric field $\boldsymbol{E}$ at time $t = 1$ on the whole domain (left) and zoomed onto the peak of the needle (right).

The electric field and the current density for $t = 1$ are presented in Figure 6.4 and Figure 6.5 accordingly.

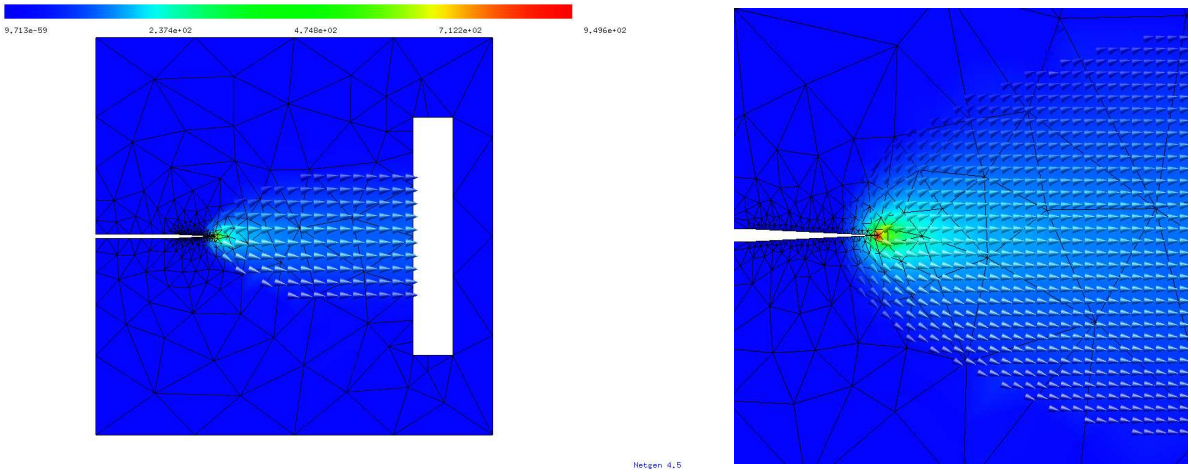

Figure 6.5: The current density $\boldsymbol{j}$ at time $t = 1$ on the whole domain (left) and zoomed onto the peak of the needle (right).

Bibliography

[1] R.A. Adams. *Sobolev spaces*. Acad. Press, New York, 1975.

[2] P. Atten, K. Adamiak, B. Khaddour, and J.-L. Coulomb. Simulation of corona discharge in configurations with a sharp electrode. *Journal of Optoelectronics and Advanced Materials*, 2004.

[3] D. Braess. *Finite Elemente: Theorie, schnelle Löser und Anwendungen in der Elastizitätstheorie*. Springer Verlag, Berlin, Heidelberg, 3rd edition, 2003.

[4] S.C. Brenner and L.R. Scott. *The Mathematical Theory of Finite Element Methods*, volume 15 of *Texts in Applied Mathematics*. Springer Verlag, New York, 2nd edition, 2002.

[5] F. Brezzi and M. Fortin. *Mixed and Hybrid Finite Element Methods*. Springer-Verlag, New York, Berlin, Heidelberg, 1991.

[6] P.G. Ciarlet. *The Finite Element Method for Elliptic Problems*. North Holland, Amsterdam, 1978.

[7] B. Cockburn, G.E. Karniadakis, and C.-W. Shu (Eds.). *Discontinuous Galerkin Methods: Theory, Compuration and Applications*. Number 11 in Lecture Notes in Computational Science and Engineering. Springer Verlag, New York, Berlin, Heidelberg, 1st edition, 2000.

[8] C. Johnson. *Numerical solution of partial differential equations by the finite element method*. Cambridge University Press, Lund, Sweden, 1987.

[9] N.A. Kaptzov. *Elektricheskiye Yavleniya v Gazakh i Vacuume*. OGIZ, Moscow, 1947.

[10] H. Krenn and L. Palmetshofer. *Halbleiterphysik I, Lecture Notes*. Institut für Halbleiter- und Festkörperphysik, JKU Linz.

[11] L.B. Loeb. *Electrical Coronas*. University of California Press, London, England, 1965.

[12] O. Madelung. *Grundlagen der Halbleiterphysik*. Springer-Verlag, Berlin, Heidelberg, New York, 1970.

[13] C. Großmann and H.-G. Roos. *Numerik partieller Differentialgleichungen*. B.G. Teubner, Stuttgart, 1994.

[14] P.A. Markowich. *The Stationary Semiconductor Device Equations*. Springer-Verlag, Wien, New York, 1986.

[15] P.A. Markowich, C.A. Ringhofer, and C. Schmeiser. *Semiconductor Equations*. Springer-Verlag, Wien, New York, 1990.

[16] A. Neubauer. *Mathematische Methoden der Elektrotechnik, Lecture Notes*. Institut für Industriemathematik, JKU Linz.

[17] J.E. Roberts and J.-M. Thomas. Mixed and hybrid methods. In *Handbook of Numerical Analysis, Vol. II*, Handb. Numer. Anal., II, pages 523–639. North-Holland, Amsterdam, 1991.

[18] H.R. Schwarz. *Numerische Mathematik*. B.G. Teubner, Stuttgart, 4th edition, 1997.

[19] J. Stoer. *Einführung in die Numerische Mathematik 1*. Springer-Verlag, Berlin-Heidelberg-New York-Tokyo, 4th edition, 1983.

[20] J. Stoer and R. Bulirsch. *Numerische Mathematik 2*. Springer-Verlag, Berlin-Heidelberg-New York-Tokyo, 4th edition, 1983.

[21] S.M. Sze and K.K. Ng. *Physics of semiconductor devices*. Wiley-Intersience, Hoboken, N.J., 2007.

[22] D. Werner. *Funktionalanalysis*. Springer-Verlag, Berlin-Heidelberg-New York, 4th edition, 2002.

[23] P.Y. Yu and M. Cordona. *Fundamentals of semiconductors - physics and materials properties*. Springer-Verlag, Berlin, 1999.

[24] S. Zaglmayr. *High Order Finite Element Methods for Electromagnetic Field Computation*. PhD thesis, Institute for Computational Mathematics, J.K.University Linz, 2006.

[25] L. Zhao and K. Adamiak. Ehd flow in air produced by electric corona discharge in pin-plate configuration. *Journal of Electrostatics*, 63:337–350, 2005.

[26] L. Zhao, G.S.P. Castle, and K. Adamiak. The effect of space charge on the performance of an electrostatic induction charging spray nozzle. *Journal of Electrostatics*, 63:261–272, 2005.

Eidesstattliche Erklärung

Ich, Larissa G. Vorhauer, erkläre an Eides statt, dass ich die vorliegende Diplomarbeit selbstständig und ohne fremde Hilfe verfasst, andere als die angegebenen Quellen und Hilfsmittel nicht benutzt bzw. die wörtlich oder sinngemäß entnommenen Stellen als solche kenntlich gemacht habe.

Linz, Dezember 2007

Larissa G. Vorhauer

Curriculum Vitae

Personal Data

Name:	Larissa G. Vorhauer
Nationality:	Austria
Date of Birth:	28. 5. 1981
Place of Birth:	Ried i. Innkreis, Austria

Education

1987 - 1991	Elementary School Altheim
1991 - 1995	Comprehensive Secondary School Braunau
1995 - 2000	Bakip Ried
2000 - 2007	Studies in Technical Mathemtics, Branch of study: Industrial Mathematics, Johannes Kepler University Linz

Special Activities

Aug. 2004 - Feb. 2005	Studies at DTU / Technical University of Denmark